SCUOLA DI DOTTORATO

UNIVERSITÀ DEGLI STUDI DI MILANO-BICOCCA

Department of:

School of medicine and school of science

PhD program: Translational and Molecular Medicine
Cycle: XXIX

MALDI-MSI in the study of glomerulonephritis: Possible molecular indicators of CKD progression

Surname: Smith **Nome / Name:** Andrew

Registration number: 788433

Tutor: Prof. Fulvio Magni

Co-tutor: Dr. Antonia Vlahou

Coordinator: Prof. Andrea Biondi

ACADEMIC YEAR: 2015-2016

“When we strive to become better than we are, everything around us becomes better, too”

TABLE OF CONTENTS

Chapter 1

Introduction

1 INTRODUCTION

Mass spectrometry (MS) is one of the most important tools for the characterisation and identification of a wide range of biomolecules, including metabolites, lipids and proteins. The study of such molecules constitutes the major –omics disciplines studied using MS techniques. In MS, analyte molecules are first ionised in the source and can be present in solid, liquid or gaseous form, depending upon the type of ion source employed. The ionised analytes are then separated in the mass analyser according to their physical properties, with the corresponding electrical signals then recorded by a detector. These detected signals are correlated with a particular mass-to-charge ratio (*m/z*). Results are then displayed in the form of a mass spectrum, with the relative intensity of each signal presented as a function of its *m/z*.

The concept of Mass Spectrometry Imaging (MSI) first came to the fore nearly 50 years ago, representing a technique suitable for the analysis of elements and other small molecules. In first instances, MSI instruments employed secondary ion mass spectrometry (SIMS) technology, which was then shortly followed by the laser microprobe analyser. Both of these techniques were capable of performing high spatial resolution surface analysis of small organic and inorganic molecules. However, it wasn't until the late 1990's when the research of Richard Caprioli and co-workers led to the introduction of MSI into a clinical setting, employing Matrix Assisted Laser Desorption Ionisation (MALDI) as a means of analysing a wider range of biomolecules, including proteins, directly on intact tissue[1]. In this early body of work, Caprioli *et al.* were able to demonstrate the ability of MSI to localise the distribution of biomarkers within tissue, without the need for labelling. This early research subsequently led to an explosion of MSI based studies, having a substantial impact on clinical and pharmacological research.

Currently, there are a number of MSI techniques employed in clinical studies, including SIMS, desorption electrospray ionisation (DESI), laser ablation electrospray ionisation (LAESI) and rapid evaporative ionisation mass spectrometry (REIMS) (Table 1). In addition to this, there are a number of newly emerging MSI techniques that have shown promise for employment in this field of research,

including liquid junction surface sampling and mass cytometry[2]. However, as a result of its widespread availability, ability to analyse proteins and numerous other advantages (Table 2), MALDI remains the most commonly applied MSI technique. Given that proteins play a significant role in a large number of pathways involved in defective cellular signalling cascades, the ability to spatially resolve the localisation of a number of proteins concurrently within the same section of pathological tissue can enable the detection of pathological processes, and, ultimately, disease candidates. Additionally, it has also become increasingly common for lipids and metabolites to be analysed in order to study disease mechanisms, provide complimentary information that can be integrated with proteomic findings. Since its inception, MALDI-MSI has been used in a plethora of clinical based studies, covering the fields of oncology, pathology, diagnostics and surgery[3]. Furthermore, it has been regularly used to monitor the distribution of xenobiotics and their metabolites, establishing itself as an invaluable tool in drug distribution studies[4]. This chapter will focus on the methodological aspects underpinning on-tissue MALDI-MSI and proceed to discuss its application and relevance in clinical-based studies.

Table 1. An overview of the most commonly used ionisation sources for Mass Spectrometry Imaging experiments.

Source	Ionisation	Pre-treatment	Analyte class	Mass Range	Spatial Resolution
MALDI	Laser ablation of the surface sample and desorption/ionisation of analytes	Coating of the sample with a MALDI matrix solution	Metabolites, lipids, peptides or proteins (matrix dependent)	1 Da - 500 kDa	<5-10µm (commercial instruments)
SIMS	The sample surface is sputtered with a primary ion beam, generating secondary ions	Not required. However, a matrix/metal coating can be used to increase the yield of generated ions	Static SIMS: Elements, fatty acids and lipids Dynamic SIMS: Elements	1 Da - 10 kDa	Static SIMS: >1µm Dynamic SIMS: <1µm
DESI	Droplets are generated via an electrospray mechanism and directed towards the surface sample	None	Small metabolites (from tissue)	1 Da- 2 kDa	>100µm
Nano-DESI	A liquid bridge samples the surface molecules which are are then ionised by nanoESI	None	Metabolites, peptides and proteins (solvent combination dependent)	1 Da – 2 kDa	<10µm (dependent upon the size of liquid bridge)
LAESI	Generation of gas-phase particles by laser ablation and ionised by electrospray	None	Metabolites, peptides and proteins	50 Da – 100kDa	MSI: <200µm Cell-by-cell analysis: <50µm
REIMS	Rapid evaporation of analyte molecules generating gas-phase ions	None	Metabolites and lipids	150 Da – 2 kDa	<500µm
Mass Cytometry	Functionalised antibodies bound to polymers containing lanthanide	Addition of functionalised antibodies	Proteins	50 Da to 250 Da	<1µm (when coupled with a SIMS instrument)

Table 2. Advantages and disadvantages of MALDI-MSI.

Advantages	Disadvantages
High-throughput	No intracellular information
Label-free	Matrix application can be tissue dependent, yielding variable results
Relative quantitation	Difficulty in identifying peptides directly on tissue
Applicable to a wide range of analytes	
Maintains morphological structure	
Maintains spatial localisation of analytes	
Well-established	

1.1 MALDI-MSI: General Principles

MALDI-MSI was formally introduced in 1997 by Richard Caprioli and its use has increased exponentially in recent years to become the most widely employed MSI technique. This technique relies on the use of a MALDI matrix, which consists of small organic molecules that are designed to absorb the energy of a pulsed laser beam. These molecules commonly possess a suitable chromophore, usually in the form of an aromatic core, and it is this property of the matrix that facilitates the absorption of the UV laser energy. When this matrix is applied to the surface of a sample it promotes the formation of a ubiquitous layer of co-crystals, which incorporates both matrix and analyte molecules in its network. This co-crystallisation process, which occurs on the surface of the sample, is characterized by significant variability and is related to a number of different parameters including the choice of solvent, time of incubation and matrix concentration[5]. When the laser beam is applied to the surface of the sample, the absorbed energy leads to rapid desorption of both

the matrix and analyte crystals and subsequent ionisation (Figure 1). This ionisation process is similar to electrospray ionisation (ESI) in the aspect that both techniques are capable of generating large gaseous phase ions without extensive fragmentation occurring during the procedure. This is termed "soft" ionisation. The most significant difference between MALDI and ESI is that MALDI produces far fewer multiply charged ions, leading to less complex spectra, which are, ultimately, easier to interpret.

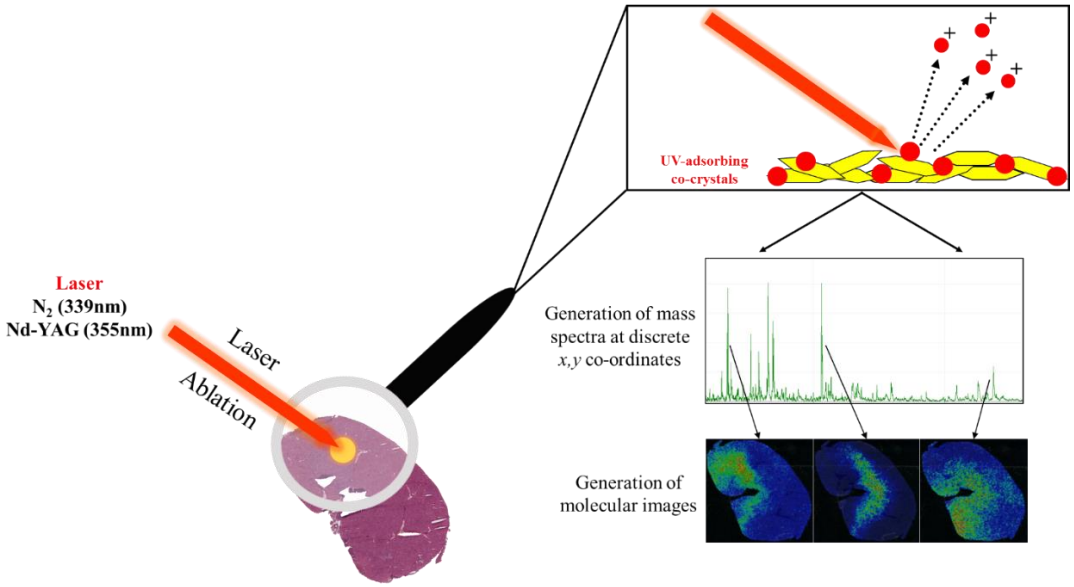

Figure 1. The general principles of MALDI-MS Imaging. Laser ablation leads to the desorption and ionisation of matrix and analyte ions. The detected ions yield the generation of mass spectra at discrete spatial co-ordinates and the spatial distribution of any of the ions present in these spectra can be visualised following the generation of a molecular image.

MALDI sources can be combined with a wide array of mass analysers, including time-of-flight (TOF) and Fourier transfer ion cyclotron resonance (FT-ICR), which are commonly employed for the analysis of intact proteins due to the wide mass range that they cover. Alternatively, multiple stage quadropole time-of-flight and various forms of ion traps can be used for the analysis of smaller molecules, including metabolites, lipids and peptides. However, coupling MALDI with TOF mass

analysers appears to be the most common approach for MALDI-MSI studies. This combination enables the analysis over a large mass range (50Da to upwards of 150 kDa), spatial resolutions higher than 20µm and the possibility of performing MS/MS experiments directly on tissue when TOF/TOF is employed. The ability to identify proteins of interest, by utilising MS/MS fragmentation directly on tissue, is of paramount importance when considering the progression of this MSI technique in terms of facilitating the translation of these findings into tests that are suitable for use in a routine clinical setting.

In MALDI-Imaging, a mass spectrum is acquired at each desired *x*,*y* co-ordinate within a defined measurement region, which is usually related to an entire section or particular regions of interest present within a tissue section. Using the acquired mass spectra, the spatial distribution of any of the biomolecules present can be visualised and a molecular image of the tissue reconstructed. These molecular images can then be correlated with tissue images obtained using histological techniques. The distance between spectral acquisitions in MALDI-MSI analysis is referred the *rastering*, which is inversely proportional to the *spatial resolution* (ie. the smaller the distance between the two raster positions, the higher the spatial resolution). MALDI-TOF instruments are capable of high-throughput MSI analysis with spatial resolutions higher than 20µm. Although other instruments, such as TOF-SIMS, are capable of acquiring images with a higher spatial resolution (as high as 1.5µm), they are unable to do so in the same high-throughput manner and the mass range is more limited in comparison.

Notwithstanding the rapid evolution of MALDI mass spectrometry instrumentation and sample preparation protocols[6], several technical issues related to MALDI-MSI still need to be improved, such as increased spatial resolution and sensitivity. However, next generation instruments are beginning to address these limiting factors, not only improving spatial resolution and sensitivity, but also increasing the spectral acquisition rate as well as minimising pixel-to-pixel variability, facilitating higher quality and more robust analysis. Perhaps of greater importance is the imaging and visualisation of single cells and, in fact, when using the correct cell fixation protocols

and a laser with a smaller diameter (<7μm) this has already been shown to be possible with currently available MALDI-MSI instrumentation[7]. Continuing in this vein, MALDI-MSI will be able to not only analyse single cells, but also potentially delve deeper and analyse at a subcellular level. Furthermore, it will also be possible to routinely generate three-dimensional MALDI images in order to obtain a snapshot of the pathological state of an entire organ by combining MALDI-MS images of consecutive tissue sections and reconstructing a three-dimensional representation using the appropriate (and currently available) software[8].

1.2 Experimental Procedures in MALDI-MS Imaging

1.2.1 Sample Handling: Storage, Embedding and Sectioning

Sample handling is arguably the most critical aspect for obtaining satisfactory results from MALDI-MSI experiments, with sample collection, storage, embedding and sectioning all to be carefully considered. The first challenging aspect is related to how the sample is treated following collection. At this initial phase, it is imperative that protein degradation is minimised and the analyte molecules are stabilised in a consistent manner. This insures that chemical integrity of biomolecules and spatial organisation of tissue structure is maintained.

Fresh samples represent the primary source of tissue for MALDI-MSI experiments and are routinely collected for this type of analysis. However, fresh samples need to be frozen directly after collection in order to stabilise the proteome by inhibiting enzymatic proteolysis. The major advantage of using fresh-frozen (FF) tissue is that it closely mimics the native state of the tissue, preserving its morphology and integrity. The freezing process here must be gentle and homogenous in order to avoid different parts of the tissue from cooling at different rates, which can lead to the formation of ice crystals, and, ultimately, tissue cracking. The most common approach involves loosely wrapping the tissue in aluminium foil and freezing in liquid nitrogen or cooled alcohol (to approximately -70^{o}C) for approximately one minute. Alternatively, the tissue can also be cooled in isopentane dry ice. One final solution to avoid protein degradation can be through the use of conductive heat

transfer. However, it is important to check the compatibility of each tissue with this treatment, as, in some cases, tissue morphology can be altered during the process. Once stabilisation has been performed, the tissue is stored at -80^{o}C prior to MALDI-MSI analysis.

More recently, and of perhaps greater importance to employing MALDI-MSI in a clinical setting, protocols have been developed in order to facilitate the analysis of formalin-fixed paraffin-embedded (FFPE) tissue. FFPE tissue represents a large percentage of the patient samples collected and stored in hospitals and other medical centres, thus representing potential gold-mines of information for histopathological studies involving MALDI-MSI[9]. Ultimately, the analysis of FFPE tissue enables retrospective studies with much larger cohorts of patients. This can be of particular importance when attempting to collect samples of particularly rare diseases, which would take a considerably longer period of time if attempting to obtain an appropriate number using FF specimens. In terms of sample storage, FFPE tissue can also be stored for up to 10 years at room temperature (RT).

Upon treatment with formalin, a reaction occurs between formaldehyde and the amine groups of the tissue proteins promoting the formation of methylene bridges between amino acids. This ultimately leads to the formation of inter- and intra-molecular cross-links in proteins. While at RT, lipids, nucleic acids and molecules not cross-linked to formaldehyde can degrade, the formed cross-links promote the stability of the proteins present in the tissue and preserve the morphological structures present. However, as a result of this extensive cross-linking, specific sample preparation steps are required in order to facilitate the MALDI-MSI analysis of FFPE samples. Firstly, the paraffin in which the sample is embedded needs to be removed as it acts as a strong ion suppressant. Secondly, antigen retrieval is required in order to unmask the epitopes in order to allow for the enzymatic digestion to occur, most commonly using trypsin. This protein digestion can be completed *in situ* using a number of automated devices, which keep the localisation of the peptides intact and produce highly reproducible results. The peptides generated from this enzymatic

digestion can be submitted for MALDI-MSI analysis but also for direct MS/MS analysis when using a TOF/TOF instrument, facilitating protein identification.

The sectioning of FFPE samples is usually performed at RT, with the thickness of the sections commonly being 5µm. Sections are then transferred into a water bath at 37^{o}C and mounted onto a conductive surface compatible with MALDI-MSI instruments, such as indium titanium oxide (ITO) glass slides. Once the sections are mounted, excess water is removed and the slides are gently warmed at 30-37^{o}C for a few minutes in order to ensure proper adhesion. Following this step, the sections mounted onto the ITO glasses can be stored at RT for up to ten years prior to the MALDI-MSI preparation process, however it is preferable to analyse within the first two years[10].

On the contrary, the sectioning of FF tissue is usually performed in a cryostat set to approximately -20^{o}C. Additionally, the tissue requires an embedding medium in order to ensure proper attachment of the tissue to the stage of the cryostat, improve the ease of cutting and avoid tissue damage. However, embedding the tissue entirely in this medium should be avoided because it leads to ion suppression. Therefore, it is recommended to add only a very small amount of the cutting medium to the bottom of the organ in order for it to adhere correctly to the stage whilst the major proportion of the tissue remains uncovered for the purpose of sectioning for MALDI-MSI experiments. Optimal Cutting Temperature (OCT) compound is the most common polymer used in standard histological applications but, like other polymer-based embedding media, it has been shown to be a strong ion suppressant[11]. Therefore, once the FF tissue sections have been cut and mounted onto glass slides, any remaining OCT that surrounds on and around the tissue has to be carefully and efficiently removed. Alternatively, the sample can also be embedded in gelatin or in 15% poly[*N*-(2-hydroxypropyl)methacrylamide] (pHPMA)[12], with both of these compounds being reportedly more compatible with MALDI-MSI analysis. Once the section has been mounted onto the glass slide it is also recommended to assist the adhesion of the tissue to the slide by placing a finger on the back of the slide, in the location where the tissue section is mounted, and this is known as *thaw mounting*.

The thickness of the section is often set to between 10 and 12µm, representing a balance between tissue conductivity and robustness. For example, the rate of moisture evaporation is accelerated when the thickness of the section is reduced. This can be an important factor that limits proteolysis and other enzymatic activities. However, thin sections are also more fragile and more difficult to manipulate onto the slide. Once the section has been mounted onto the slide, it is recommended to dry it under vacuum in order to remove condensation from the surface of the tissue and minimise protein diffusion. At this time, if the cutting of the sections is done outside of the routine clinical workflow (where the following steps are always performed), it is advised to cut some additional consecutive sections to which immune-histological staining is applied, in order to combine molecular and histological findings[13].

Prior to MALDI-MSI analysis, it is highly recommended to wash the tissue in order to remove any molecules that may interfere with the ionisation of proteins (eg. salts, lipids). Standard protocols recommend washing the tissue sequentially in increasing concentrations of EtOH, commencing with a short wash (~30 sec) in 70% EtOH in order to remove cell debris and salts followed by 95 and 100% EtOH in order to fix the tissue. A solvent such as EtOH is recommended for this step as it does not promote the diffusion of proteins. However, it has been widely reported that optimisation of the washing steps, based upon the chemical composition of the tissue, can lead to enhanced sensitivity of the MALDI-MSI analysis. For example, brain tissue is often associated with a high content of lipids, a strong protein ion suppressant, and washing this tissue with chloroform or xylene can improve protein detection. Conversely, a different washing protocols should be used if the intended analytes are not proteins, for example, EtOH (70%) with the addition of ammonium acetate (NH_4Ac) is recommended for the desalting of tissue prior to tissue lipidomic analysis[14].

Following these washing steps, it is again recommended to perform an additional drying step under vacuum. However, the drying time should be selected carefully based upon the thickness of the tissue and the type/percentage of solvents used in the

washing procedure. Once this additional drying phase has been performed, the FF tissue is then ready for matrix application.

1.2.2 Matrix Application

Matrix deposition plays a critical role in MALDI-MSI experiments, being a major limiting factor in the lateral resolution that can be achieved. The general aim of the matrix deposition is to achieve an optimal balance between crystal dimension/shape (homogenous and small) and maximal analyte extraction, whilst at the same time avoiding diffusion. Thus, matrix deposition represents arguably the most crucial step in the sample preparation phase. Depending upon the target analyte of choice, a number of different matrices can be used. For example, sinapinic acid (SA; 3, 5-dimethoxy-4-hydroxycinnamic acid) and α-CHCA (α-cyano-4-hydroxycinnamic acid) are most commonly the matrices of choice for the extraction of proteins, peptides and lipids (1-20kDa). Furthermore, ferulic acid (3-(4-hydroxy-3-methoxy-phenyl)-prop-2-enoic acid) has also been reported for the extraction of high molecular weight proteins (up to 140kDa). For MALDI-MSP purposes, DHB (2, 5-Dihydroxybenzoic acid) is also commonly used for the extraction of low molecular weight proteins. However, due to the large crystal size, it is unsuitable for modern imaging applications as this large crystal size severely hampers the spatial resolution achievable. Additionally, ionic matrices, such as CHCA/aniline (CHCA/ANI) and CHCA/N,N-dimethylaniline (CHCA/DANI), have also been employed alone or in combination with other matrices in order to improve the homogeneity of the crystallisation and the detection of protein signals[15]. It is also important to note the increased prevalence of metabolomic targeted MSI analysis in clinical studies. In these instances, the matrix9AA (9-aminoacridine) is often employed and the mass spectrometer is set in negative-ion mode[16].

It is also important to note that with the increased demand for higher spatial resolution images and the rapid evolution in instrument technology, new matrices have been explored. For example, Garate et al[17] demonstrated the use of MBT (2-mercaptobenzothiazole) and DAN (2, 5-diaminonapthalene) as MALDI matrices that

can enable the acquisition of higher spatial resolution images (with pixel sizes as low as 5µm), both in positive and negative? ion mode. Furthermore, it stressed the importance of the correct choice of matrix and crystal size with regards to the spatial resolution achievable in MALDI-MSI experiments, suggesting that higher spatial resolutions can yet be obtained with the instrumentation currently in place in many research laboratories.

Focusing on the most commonly employed matrices, the matrix concentration for SA is usually between 10-30 mg/mL and 7-20 mg/mL for CHCA. The choice of concentration is dependent upon the choice of deposition, ensuring the correct balance between minimising analyte diffusion and maximising analyte inclusion into the matrix co-crystal network. For example, low matrix concentration can lead to analyte diffusion, whereas high matrix concentration induces rapid crystal formation and prevents proper incorporation of the analyte into the crystals.

Matrices such as SA and CHCA are dissolved in a solution containing organic solvents, water and trifluoroacetic acid (TFA). TFA is added to the matrix solution is order to assist in the MALDI ionisation process while the organic solvents facilitate optimal crystal formation. The balance between the rate of solvent evaporation and time of incubation of the analytes is highly important in order to achieve the optimal analyte extraction, and this is directly related to the ratio between the organic solvent and water. Usually, a good balance between solvent evaporation and crystal formation can be obtained with the use of a 1:1 ratio between solvent and water. The choice of organic solvent is dependent upon the physical properties of the analyte molecule. However, 50% acetonitrile (ACN) and 50% ethanol (EtOH) are most commonly employed, with a higher ratio of solvents, such as methanol (MeOH) or isopropanol, been employed to extract more hydrophobic molecules from tissue.

It is also important to note that this crystallisation process can also be affected by the particular type of tissue used, with the surfaces of some sample types not being conducive to optimal and homogenous crystal formation. Therefore, it is imperative that the protocol for matrix deposition is optimised for each type of tissue used.

Furthermore, the presence of salts, lipids and other compounds (eg. Haemoglobin) can also impact upon the crystallisation process, thus affecting spectral quality. The impact of these interfering molecules can be minimised by performing washing steps prior to matrix deposition. Additionally, other strategies can be used in order to improve spectral quality, with the addition of detergents to the matrix solution being a successful method to obtain increased sensitivity of proteins. For example, the addition of 0.05% Triton X-100 to a SA solution deposited onto brain tissue, a tissue with a high abundance of lipids, which can often lead to ion suppression of protein signals, led to an increase in intensity of 42% of the peaks present in the average spectrum compared with the deposition of SA without the detergent[18].

The choice of method for matrix deposition is dependent upon the spatial resolution desired in the MALDI-MSI experiment. However, there are a number of methods, both manual and automated, that can be employed for various purposes. For tissue profiling, manual spotting can be performed by pipetting the matrix solution directly onto the tissue region of interest. This approach deposits large droplets onto the surface of the sample (a few µL), extracting analytes from a region which is a few millimetres in diameter. However, there are devices that can be used to spot matrix in an automated fashion across the entire surface of the sample or in specific regions of the tissue. Quite commonly, the droplet area is reduced to below 200µm in diameter, thus leading to less efficient analyte extraction but enabling higher spatial resolution images (Figure 2). Deposition using an automated spotter offers the advantage of the droplets generally being deposited in discrete positions. Thus, if any diffusion of the analyte occurs then it is limited to a relatively small region and the spatial localisation of the analyte is maintained. However, the disadvantage of this approach means that it can be quite difficult to obtain a completely homogenous layer of matrix. Automated matrix spotters are often associated with piezoelectric nozzles and acoustic wave transfer. In these instances, the dimension of the droplets depends on the following factors: solvent composition and surface tension, the number of layers deposited, tissue structure and the chemical composition of the analytes.

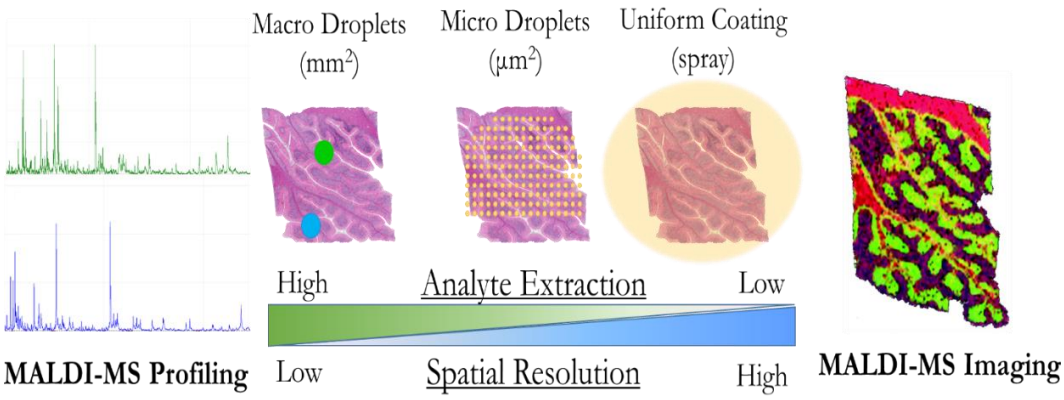

Figure 2. The different approaches in matrix deposition for MALDI-MS Profiling and MALDI-MS Imaging.

In order to achieve a more homogenous coating of matrix, automated spraying of the matrix solution onto the surface of the sample is performed. In these instances, the spraying devices produce very small droplets which, after drying, produce a very homogenous and thin layer of solid matrix crystals which are less than 20µm in diameter. A homogenous layer of small matrix crystals offers the possibility for higher spatial resolution MALDI-MS images (<100µm) compared to automated spotting. Additionally, spraying of the matrix is faster than automated spotting, thus reducing the sample preparation time and increasing sample throughput. In contrast to spotting, matrix spraying forms a layer of liquid on the tissue. Thus, the method must be optimized in order to avoid analyte diffusion. Automated spraying devices are commonly based upon vibrational, pneumatic or electrospray mechanisms, providing depositions in a highly controlled and reproducible manner. More recently, Gou et al. introduced the concept of Electric Field-Assisted Matrix Coating, which employs the use of a uniform static electric field can enhance the detection of positively or negatively charged small molecule metabolites in the MALDI matrix layer[19]. Manual spraying of matrix can also be accomplished using a TLC (Thin Layer Chromatography) sprayer, airbrush or pneumatic sprayer. However, these approaches are certainly less reproducible, with the crystallisation being dependent upon the surrounding environment (ie. temperature and humidity)[20].

A sublimation-based approach can also be employed in order to generate the smallest matrix crystal size possible, and ultimately acquire higher spatial resolution images when using the appropriate instrumentation. Generally, this approach involves two steps; 1) the sublimation of matrix onto the surface of the sample and 2) a rehydration/recrystallization step[21].

Depending upon the properties of the particular matrix used, the slide is heated under vacuum (approximately 145^{o}C at 25mTorr for SA), which promotes sublimation onto the surface of the tissue. Then, the slide containing the tissue is placed in a petri dish containing a piece of filter paper soaked in aqueous TFA (commonly a 5% TFA solution) and the petri dish is sealed in order to create a hydration chamber. In order to achieve tissue rehydration, the petri dish is placed in an oven at 85^{o}C for 3.5 minutes. However, in the case of sublimation, protein extraction is not as efficient compared to other matrix deposition techniques. An additional rehydration phase can increase analyte extraction. It is challenging to optimize sublimation protocols in order to obtain a good balance between matrix crystal size and analyte extraction.

Finally, the same automated devices that are used for matrix deposition can also be used for the deposition of other solutions and derivatizing agents employed for some specific MALDI-MSI experiments[22]. Most importantly, they can also be used for the application of enzymes for on-tissue digestion in a highly homogenous manner and in some instances, the enzyme application and sample incubation can also be performed using the same device.

Following MALDI-MSI analysis, the matrix can be removed from the tissue by washing sequentially in increasing concentrations of EtOH (70, 95 and 100%) for short periods of time. Once the washes have been performed, the tissue can be observed under a microscope in order to ascertain if the matrix has been entirely removed. Following this step, the tissue sections can be subjected to histological staining if desired.

1.3 Spectral Processing

A MALDI-MSI dataset can be visualized as a Data Cube in which the three dimensions are represented by: *m/z* values, signal intensity and spatial co-ordinates. Since a single MALDI-MSI analysis is composed from thousands of spectra topologically positioned in a 2D array, the output file of an MSI analysis can range from several gigabytes in size to up to more than one terabyte. This high dimensionality of the data is a challenge since it makes data management and elaboration time-consuming. Data processing requires significant computer resources.

Pre-processing steps, applied to raw data, are employed in order to remove sources of variation or noise that could lead to artefacts in the data elaboration phase and to enhance the biologically relevant information in the MALDI Spectra. Pre-processing steps include Baseline Correction, Smoothing, Normalisation, Alignment and Calibration, Smoothing and Peak detection.

1.3.1 Baseline Removal

The baseline of a spectrum is the connecting line between the data points with the lowest intensity values, on which the entire spectrum lays. Shin proposed that MALDI analyses may contain three discrete sources of noise[23]:

Electrical noise from the MS components

Shot noise due to the discrete nature of ion detection

Chemical background generated by impurities (matrix clusters, fragments)

Since the baseline originates from fluctuations in the background signal of the instrument it has no biological meaning and needs to be removed. Many algorithms are employed in order to remove this contribution; the most widely used being Iterative Convolution and TopHat.

Iterative Convolution:

Baseline Removal through Iterative Convolution applies a Gaussian filter multiple times, removing spectral features (ie. the peaks). The algorithm requires the Sigma parameter, σ, in order to control the width of this Gaussian filter. The filtering iteration yields a spectrum without peaks, i.e. just the baseline. The next step is to take the pointwise minimum of the trend as an estimation of the baseline, subtracting it to the spectrum. The method converges very quickly, meaning that after 15-30 iterations the output does not change.

TopHat operation:

The TopHat operator was derived from the theory of Mathematical Morphology and allows the "extraction" of peaks from an image. Itis based on the principle that features of interest should stand out in a complex environment (i.e. the noise). This algorithm computes the so-called morphological opening, which in this instance are the background signals, of the spectrum and then subtracts the result from the original spectrum.

1.3.2 Smoothing

Signal smoothing aims to alleviate the spectral noise. It aids interpretation and the visualization of the single spectrum and can be performed using two common algorithms; Savitzky Golay and Gaussian smoothing.

Savitzky Golay:

Savitzky-Golay is a digital filter that can be applied to a set of data points. It is known to be an almost universal method to improve the signal-to-noise ratio. It achieves smoothing by fitting adjacent data points with a low-degree polynomial taking the central point of the fitted polynomial curve as output. Since it does not distort the essential features in the spectrum this filter tends to preserve the peak waveform and does not shift the peak positions.

Savitzky-Golay filter is very slow but intensity loss is much lower; and should be preferentially used to smooth low-mass spectra where peaks are sharp.

Gaussian Smoothing:

The degree of smoothing is again determined by the standard deviation, σ, of the spread parameter, with a larger σ implying a wider Gaussian filter, and thus a greater degree of smoothing. It is a fast method but it may cause significant intensity loss for sharp peaks. Due to these characteristics, it is usually employed to smooth high-mass spectra where peaks are broader.

1.3.3 Spectral Normalisation

A MALDI imaging data set can be considered as a collection of independently measured spectra; for this reason, a normalisation step is a crucial task in the pre-processing phase in order to compensate for the chemical and analytical differences, facilitating a fair comparison between spectra. It is an indispensable step if several sets of spectra have to be compared with each other, not only intra-analysis but, and more importantly, inter-analysis.

Normalisation is the process of multiplying a mass spectrum with an intensity-scaling factor, *f,* in order to expand or reduce the range of the intensity axis. It is able to project spectra of varying intensity onto a common intensity scale, removing variations in pixel-to-pixel intensity due to uneven matrix deposition, ion suppression or other factors that can alter the intensity of peaks not strictly due to the actual analyte composition present at a specific spot.

Each normalisation method is based on certain assumptions regarding the data and it is necessary to carefully choose the most appropriate algorithm for a particular dataset in order to avoid generation of artefacts that do not correspond to significant biologial information. There are many algorithms employed for spectra normalisation, such as Total Ion Current (TIC), Root Mean Square (RMS) and Median.

Total Ion Current (TIC):

The TIC normalisation method divides all spectra by their total ion current (i.e. the sum of the intensities of all the peaks), yielding spectra with a common area under the curve. The assumption on which this normalisation is based on is that all spectra have a similar area, defined largely by the chemical noise and only to a small extent by the peak intensities. This normalisation is the most widely used and can be applied to the majority of MALDI-MSI datasets.

It is important to stress that artefacts may be created in spectra containing a single high intensity ion (e.g. Insulin or haemoglobin). This peak would significantly suppress the intensity of every other peak in the spectrum after normalisation. It is possible, however, to exclude such peaks from the normalisation calculation, potentially solving this problem.

Root Mean Square (RMS):

The RMS normalisation method divides all spectra by the root mean square of all data points. This method is most appropriate for use with datasets containing spectra that are expected to have small variations in the peak intensities. The RMS normalisation method usually leads to a very uniform distribution of intense signals.

Median:

This normalisation method divides all spectra in the data set by the median of all data points. Median normalisation is not significantly affected by the intensity or area of signals in the spectra, and can therefore be used if the RMS or TIC normalisation methods lead to artefacts.

Median normalisation results depend on the type of noise in the spectra. If spectra do not contain a fully symmetrical noise profile, this method will generate significant artefacts.

1.3.4 Spectral Realignment

Spectral alignment is an optional step during the pre-processing phase of mass spectra. It is used to account for the slight shifts in the output *m/z* of peaks as a result of chemical noise and instrument accuracy. Spectral realignment ensures that all of these peaks are realigned to a common mass, and thus enable correct spectral comparisons. Most commonly, spectra are realigned by considering the peaks of the mean spectrum as a reference, covering the entire mass range of the analysis, and by then adjusting the spectra by linear or non-linear interpolation.

1.3.5 Generating an overview spectrum

It is useful to evaluate peaks obtained in the entire section or in specific areas. The generation of a single spectrum that efficiently represents the molecular composition of the region of interest helps in achieving this goal. There are two main types of overview spectra that can be generated, Average and Skyline:

Average Spectrum:

The average spectrum is obtained simply by averaging all the intensities for each data point. This is the most used approach in the data mining performed after MALDI-MSI analyses, but it can potentially yield artefacts since it can reduce the contribution of ions that are present only in small and specific regions of the tissue.

Skyline Spectrum:

The Skyline spectrum is obtained by picking the highest value of intensity for each data point: regiospecific peaks are well represented in the total spectrum and are not eliminated as in the case of the average spectrum approach.

This method should be applied only to well-calibrated, aligned, low-noise spectra in order to avoid peak broadening and a loss of accuracy.

1.3.6 Peak Picking

This process detects a representative set of *m/z* values in a group of mass spectra that significantly rise above the noise level (i.e. above a certain S/N threshold). The aim

of the peak picking is to reduce the number of *m/z* values by discarding those values corresponding to noise signals or to non-specific baseline. Various peak picking methods for MALDI mass spectra are available and are implemented in mass spectrometry software packages: the most used algorithms are Orthogonal Matching Pursuit and Local Maximum.

Applying this process in MSI spectra containing large amounts of data takes a lot of time and uses significant computing resources. The simplest approach would be to apply the algorithm on the single mean spectrum. However, this approach results in elimination of peaks with high intensity in very discrete areas of tissue.

Orthogonal Matching Pursuit:

OMP is a signal processing application that models each spectrum as a sum of Gaussian-shaped functions (peaks). The parameter, Sigma, determines the width of the Gaussian peaks (can also be estimated automatically based on the mean spectrum). For each single spectra, OMP selects *m/z* peaks that fit the Gaussian shape. This algorithm allows the user to manually set a maximum number of possible peaks.

Local Maxima:

This approach identifies all the local maxima in the spectra and marks them as peak positions (it assumes that a peak should differentiate itself from the background noise). It is the simplest approach but the most prone to yield false positive peaks positions that are in fact correlated with the background noise.

1.4 Data elaboration

On order to analyse MALDI-MSI data, conventional statistical tests can be applied (such as ANOVA, t-test and z-test). For example, ANOVA is commonly used to detect differences between groups (ie. Peaks, and therefore proteins), a typical task in research and clinical diagnosis. However, the inherent variability in MALDI spectra due to anatomically and biologically distinct regions may hinder significant conclusions. In order to improve the reliability of the statistical analysis, *regions of*

interest (ROI) in spectra, which correlate with histopathological features, can be defined. Following this, both unsupervised and supervised data mining approaches can be undertaken as a means of finding biologically significant information within the dataset.

1.4.1 Unsupervised Data Mining

Unsupervised methods aim at revealing hidden structures in unlabelled data and can be applied without any prior knowledge of the data structure[24].

Examples of unsupervised analysis are Hierarchical Clustering, Principal Component Analysis and Bisecting K-Mean.

Hierarchical Clustering:

Hierarchical clustering is a data mining method which consists in grouping several data subsets into clusters based on their similarity and then building a hierarchy, exploiting intra-cluster differences. The algorithm is able to evaluate dissimilarities by calculating the actual distance between two spectra according to different metrics (Euclidian distance, Manhattan distance)

The output is a dendrogram representing a hierarchical tree in which similar spectra are clustered under a single node. In a MALDI-MSI dataset, it is possible to plot the spatial distribution of the clusters identified by this analysis which can then be correlated with the histological image.

It can be performed in a bottom-up approach (each observation starts in its own cluster) or top-down (all observations start in one cluster). The only downside is that this approach may use significant computer resources since it requires the creation of a distance matrix of size n^2 (where n is the number of spectra).

Bisecting K-Means:

Bisecting k-Means is a divisive clustering algorithm that combines k-Means and Hierarchical Clustering: it iteratively splits the data into two maximally different clusters (bi-sectioning) which are then further separated into sub-clusters according

to similarities in their data points (k-mean). The sub-clustering is achieved by selecting K points as the initial centroids, assigning spectra to the closest centroid and then computing the centroid of each cluster again until a convergence is reached.

Principal Component Analysis (PCA):

Principal Component Analysis (PCA) is the most commonly used component analysis method for MALDI Imaging data representation. Due to the complexity of the information (i.e. the number of variables) enclosed in a single mass spectrum it is impossible to visualize the entire dataset in an N-dimensional space.

PCA is capable of reducing the dimensionality of a dataset whilst retaining the majority of the information contained in the data. Since many variables often contain redundant information it is possible to replace a group of variables with a single, more informative, variable (Component) by a linear combination of the single variables. PCA differs from the other variable transformations employed in statistics since the data itself determines the transformation vectors.

From a technical standpoint this analysis employs an orthogonal transformation to convert a set of observations into a set of values of linearly uncorrelated variables (Principal Component). Orthogonal means that every component is uncorrelated with the preceding components and these new variables are used to plot the data distribution. The variables are ordered by their variance (with the first component accounting for the highest possible variance).

Using PCA, one can represent the full dataset with a few score images corresponding to first principal components. These score images reveal spatial structures hidden in the dataset by showing prominent spatial patterns (high intensity regions)[25].

1.4.2 Supervised Data Mining

Receiver operating characteristic (ROC):

A receiver operating characteristic (ROC) curve illustrates the performance of a binary classifier system as its discrimination threshold is varied. The curve is created

by plotting the true positive rate (sensitivity) against the false positive rate (1-specificity) at various threshold settings.

It is a univariate measurement used to assess the ability of a single peak or of a classifier based on several peaks to differentiate between two populations.

The area under the ROC curve (AUC) measures the discrimination quality in the interval between 0.5 and 1.0. A perfect discrimination would yield an AUC equal to 1 or 0. The closer the AUC to 0.5, the less useful the m/z value, and the closer it is to 1.0, the more suitable the *m/z* value is to be used as a univariate criterion[26].

1.5 Correlating MALDI-MS images with pathology

Particular pathological regions of interest (ROI) present within the tissue can be well defined using traditional histopathology stains, with the most widely used being hematoxylin & eosin (H & E), cresyl violet, methylene blue, toluidine blue, DAPI and/or immunohistochemistry, directing the analysis towards obtaining region-specific molecular signatures. There are two different staining approaches which can be currently used: staining on the same section of tissue used for MALDI-MSI analysis, both pre and post-analysis, or staining on consecutive tissue sections. While performing staining on the same tissue used for MALDI-MSI analysis enables unambiguous correlation of MALDI-MS images with histological images, it can be potentially hampered by a loss in integrity of the tissue following analysis and/or removal of the MALDI matrix. Conversely, correlating with consecutive tissue sections can avoid the aforementioned issue; however, it is not always certain that the adjacent tissue sections will be identical. If histological staining is to be performed prior to MALDI-MSI analysis, dyes such as cresyl violet or methylene blue are preferable since HE dyes interfere with the analysis and affect spectral quality[27]. The resulting histological images can then later be scanned with an optical scanner and stored in a database. Optimal results can be achieved in microscopic resolution with an MSI compatible MIRAX SCAN instrument (Carl Zeiss); however, other scanners that achieve image resolutions greater than 10,000 dpi can also be used. It is also important to note that using the appropriate digital platforms, such as

Aperio Spectrum, which are now becoming commonplace in clinical centres in order to facilitate the sharing of digital slides, a pathologist can annotate these scanned images electronically in order to highlight regions of interest[28]. This can enable the correct interpretation of the slides by individuals who are not experts in the field of histopathology and, ultimately, increase the throughput of the analysis.

Various software packages are currently available and can be used to exploit the unique capability to correlate molecular and histological images. SCils Lab 2014 software enables the importation of histological images and can automatically search for particular *m/z* markers that are co-localised with the histopathological annotations. Furthermore, recent developments in instrumentation have further facilitated the correlation of MALDI-MS images with histology. For example, Shimadzu Corporation has recently introduced a novel imaging mass microscope (*iMScope*) that combines an optical microscope for the visualisation of high-resolution images with a hybrid ion trap TOF-mass spectrometer with a MALDI source. This novel instrument visualises the distribution of molecules in a scanned tissue sample at atmospheric pressure.

1.6 Applications of MALDI-MS Imaging in Clinical Research

MALDI-MSI is a highly flexible platform and has been successfully employed in numerous studies, ranging all the way from the study of human diseases to forensic science. Furthermore, there has been an emerging trend towards combining MALDI-MSI with clinical imaging techniques, such as Magnetic Resonance Imaging (MRI)[29], in a multi-modal manner, highlighting the rapidly evolving nature of this approach. However, perhaps of greatest clinical relevance is the role of MALDI-MSI in the study of cancer biology, with studies targeting breast[30], colon[31,] lung, ovarian[32], prostate[33] and thyroid cancer[34] being widely published. Furthermore, MALDI-MSI approaches in cancer biology have also been applied to novel sample types, such as cytological smears taken from thyroid via fine-needle aspiration biopsy (FNAB)[34,35], further highlighting the flexibility of this technique. In all of these studies, the primary objective has been to discriminate cancer tissue from the normal and/or

tumour margin regions and to classify different grades of cancer at a molecular level. Of particular note, Balluff and colleagues studied tissue taken from gastric and breast carcinoma patients[30]. They were able to study phenotypic intratumour heterogeneity, identifying different regions within tumour tissue that appeared homogenous using traditional histological techniques. Using elegant spatial segmentation and multivariate analysis methods, they were able to identify tumour sub-populations, within histologically homogenous regions, that were associated with changes in the levels of DEFA-1 and Histone H2A. Moreover, by combining this information with clinical data obtained from the patients studied, they were able to predict the survival rate of patients based upon the number of observed phenotypic tumour sub-populations. This is a powerful example of how MALDI-MSI can not only support traditional histological analyses, but also potentially provide additional, and clinically significant, information that was previously not possible.

The combination of MSI and histology is now extensively used for pharmacological research, due to the capability of this technique to simultaneously monitor the distribution of a drug and its metabolites[36]. In addition, with suitable calibration curves, it is possible to obtain semi-quantitative measurements of drug compound concentrations[37]. Such studies can be used in the pre-clinical phase, filtering out lead compounds that are shown to accumulate in non-specific regions of tissue and/or generate toxic metabolites[38]. Furthermore, MALDI-MSI techniques are now being applied in order to image the spatial localisation of drugs and their metabolites within 3D cell-cultures, enabling more detailed information related to the site of action[39].

As with proteomic applications, studies are increasingly correlating MALDI-MSI with traditional histology, focusing on the accumulation of cancer drugs in heterogeneous tumour tissue environments. One example of this approach was the study of microvascularization effects of numerous anti-cancer drugs in tumour tissue[40]. In another example, MALDI-MSI was used to monitor the distribution of a targeted medicine, vemurafenib, for malignant melanoma to metastatic lymph nodes tumours. The study provided evidence that the drug specifically targeted proto-oncogene BRAF sites, a gene that promotes an expression of the serine/threonine-

protein kinase B-Raf, that is ultimately responsible for sending signals that are related to cell growth, and mutations of this gene have been shown to be implicated in cancer. The ability to monitor the distribution of a drug to histologically specific regions provides a greater understanding of the mode of action of drugs within particular disease environments whilst highlighting whether or not a drug targets the intended site. This can provide an insight into the potential success, or failure, of a developing drug and help drive the pharmaceutical industry towards the development of personalised drug therapies.

1.7 Chronic Kidney Disease

The main function of the kidneys is to remove excess fluids and various types of waste products from the body (e.g. protein degradation products - urea, creatinine and other metabolites) by naturally filtering the blood. They also help to maintain homeostasis and regulate blood pressure, electrolytes and pH. Chronic Kidney Disease (CKD) is a progressive loss in renal function that occurs over a period of time and develops as a result of organ damage. This damage leads to subsequent reduction in the number of nephrons, the functional units of the kidney, during the course of various renal diseases. Clinical guidelines classify the severity of CKD in five stages, based upon the Glomerular Filtration Rate (GFR), with Stage 1 being the mildest and stage 5, also called *End-Stage Renal Disease* (ESRD), being the most severe.

Table 3. The five stages of Chronic Kidney Disease, as classified based upon the Glomerular Filtration Rate.

Stage	Description	GFR(mL/min/1.73)
I	Kidney damage with a normal/increased GFR	≥90
II	Kidney damage with a mild reduction of GFR	60-89
III	Moderate reduction in GFR	30-59
IV	Severe reduction of GFR	15-29
V	Full-blown Kidney Insufficiency (ESRD)	<15 or Dialysis

CKD is a worldwide public health problem. In the United States alone, the number of patients enrolled in the ESRD Medicare-funded program has increased from 10 000 beneficiaries in 1973 to 616 000 as of December 2011[41]; this increase in the incidence is due to the exposure to many risk factors, coupled with expansion in life expectancy. Furthermore, CKD is characterized by a high probability of comorbidities (e.g. cardiovascular disease, obesity, diabetes, and hypertension) and many of these conditions can be both a cause, or consequence, of the renal disease.

1.8 Proteomics and Glomerulonephritis

Glomerulonephritis (GNs), or Glomerular Kidney Diseases (GKDs) are one of the most frequent causes of chronic kidney disease (CKD) and a careful assessment of these diseases is essential for prognostic and therapeutic purposes[41]. The renal biopsy is still playing a crucial role for the distinction among the various types of glomerular diseases (Table 1)[42,43]. However, it is an invasive procedure affected by complications[44,45]. Therefore, in recent decades, many efforts have been made in order to identify biomarkers able to discriminate among CKDs using less invasive and easy-to-collect samples, such as urine and blood. In this context, various proteomic techniques have played a crucial role in determining the molecular changes related to disease progression and early pathological glomerular

modifications[46,47]. Moreover, the direct analysis of renal tissue aimed at highlighting differences in protein expression among a wide range of glomerular conditions, entirely *in situ*, represents a new stimulating perspective. The very recent introduction of MALDI-MS Imaging (MALDI-MSI) of fresh frozen tissue and also of Formalin Fixed Paraffin Embedded (FFPE) renal biopsies unlocks new technical opportunities in biomarker discovery.

Table 4. Most relevant types of glomerulonephritis with clinico-pathological features and treatment options.

Type of GN	Clinical picture	Laboratory tests	Pathological findings	Therapy
IgA Nephropathy	Nephrotic syndrome Hematuria 1 or 2 days after a sore throat	- Urinalysis - proteinuria and hematuria - U+Es - renal impairment - Raised serum IgA is present in 50% - Confirmational renal biopsy needed	- Light microscopy shows mesangial expansion, mesangial cell proliferation and also thickening of the glomerular basement membrane - IgA and C3 deposition	- No specific treatment - Statins - ACE inhibitors
Membranous Nephropathy	Nephrotic syndrome Hypertension and chronic renal impairment	- Urinalysis - proteinuria and hematuria - U+Es, lipid profile and albumin - Consider hepatitis screen and autoantibodies - Renal biopsy needed for definitive diagnosis	- Light microscopy shows diffuse thickening of the glomerular basement membrane and subepitelial deposits - Diffuse deposition of IgM and C3	- No specific treatment - Diuretics - Statins - ACE inhibitors
Focal Segmental Glomerulosclerosis (FSGS)	Nephrotic syndrome Foamy urine due to high levels of protein, hypertension and chronic renal impairment	- Urinalysis - proteinuria +/- hematuria - U+Es, lipid profile and albumin - Protein/Creatinine ratio - Renal biopsy needed for definitive diagnosis	- Light microscopy shows focal and segmental glomerular sclerosis - Electron microscopy shows fusion of the epithelial podocyte foot processes - IgM and C3 in a segmental distribution	- Steroids - Diuretics - Statins - ACE inhibitors

1.8.1 IgA Nephropathy

IgA nephropathy (IgAN) is the most common GN worldwide[48] and may present in an isolated manner or in the context of other clinical conditions (e.g. Henoch-Schoenlein purpura-HSPN- and HCV infection[49-51]. Studies investigating the molecular and cellular interactions involved in the pathogenesis of IgA nephropathy have highlighted the abnormal production, and consequent handling, of IgA1. The pathogenesis of this disease has been further reviewed by Wyatt et al and noted an unusual secretion of a particular polymeric form of IgA1 (pIgA1) with a structural alteration related to the O-glycosilation process[52]. As a result, circulating nephritogenic immune complexes form and are deposited in the glomerular mesangium. These deposits of immune complexes promote the proliferation of resident mesangial cells, which ultimately leads to an increased production of extracellular matrix proteins. Additionally, a number of inflammatory cytokines that are produced by the mesangial cells damage the filtration barrier, which results in hematuria, proteinuria, and, ultimately, progressive renal damage.Although the levels of galactose-lacking pIgA1 are often high in the sera of IgAN patients[53], and could be used to detect individuals affected by IgA Nephropathy, the low sensitivity/specificity of this test does not enable the replacement of the more invasive renal biopsy in the assessment of these cases[54]. However, many proteomic techniques have been employed for detecting alternative diagnostic biomarkers both in urine and serum samples. Those proteins found to be differentially expressed in IgAN patients, detected by using MS-based proteomic approaches, are summarised in Table 5.

Table 5. Summary of the differentially expressed proteins detected in IgA Nephropathy through the use of MS-based proteomics.

Study	Disease	Marker	Sample Type
Park (2005)	IgAN	Thirty-five polypeptides including those derived from: zinc finger proteins 324 and 155, GRFB2-related protein 2, phosphatidylinositol 3-kinase	Urine
Park (2005)	IgAN	Twenty-seven polypeptides including those derived from: signal-induced proliferation-associated protein 1, insulin receptor precursor, NADH-ubiquinone oxidoreductase	Urine
Julian (2007)	IgAN	Ninety-five polypeptides including those derived from: collagen alpha-1 (I) and (III), alpha-1-antitrypsin, uromodulin, membrane-associated progesterone receptor component, apolipoprotein A-I	Urine
Julian (2007)	IgAN	Twenty-five polypeptides including those derived from: collagen alpha-1 (I)	Urine
Kaneshiro (2009)	IgAN	92 peptides, among which: fragments of fibrinogen alpha chain, complement C3f and kininogen-1 light chain	Serum
Kalantari (2013)	IgAN	afamin, leucine-rich alpha-2-glycoprotein, ceruloplasmin, alpha-1-microgolbulin, hemopexin, apolipoprotein A-I, complement C3, vitamin D-binding protein, beta-2-microglobulin, and retinol-binding protein 4	Urine
Graterol (2013)	IgAN	Bradykinin, uromodulin, and alpha-1-antitrypsin	Urine Serum
Sui (2014)	IgAN	β-2-microglobulin, annexin A1, complement C5, retinol-binding protein 4 (RBP4) and argininosuccinate synthase	Tissue

1.8.2 Membranous Nephropathy

Membranous Nephropathy (MN) is an immunocomplex mediated renal disease that represents the leading cause of nephrotic syndrome in adults and is one of the most frequent glomerulopathies worldwide[55,56]. Notwithstanding its relatively low incidence rate, many cases of MN progress to end-stage renal disease (ESRD),

having a clear negative impact upon the patients' quality of life and healthcare costs[57-59]. This glomerular disease can manifest as primary (idiopathic)[60] or secondary[61-64] and in the latter occurs as a result of underlying systemic conditions which can be brought about due to treatment with therapeutic agents (eg. NSAIDs), malignancies or autoimmune rheumatologic conditions. This distinction is crucial when choosing the most appropriate approach for MN patients. In secondary cases, the best strategy consists in treating the underlying disease[65,66], which results in a consequent improvement of the patient's renal condition. On the contrary, in primary forms clinicians would desire a final confirmation of the idiopathic origin of the disease to avoid improper medical investigations and to manage the more correct protocols[65-71]. For these reasons, the discovery of useful biomarkers seems mandatory[72,73]. An important step in this field has been reached by Beck et al. with the identification of circulating auto-antibodies directed against a normally expressed podocyte membrane antigen, the M-type phospholipase A2 receptor (PLA2R), which is present in at least 70% of patients with idiopathic (iMN)[74]. Recently, a further contribution to this field was provided by Tomas et al. with the description of another podocyte membrane antigen, termed thrombospondin type-1 domain-containing 7A (TSHD7A), which was able to account for a further 5% of iMN cases[72]. Alternatively, the evidence of restriction to a particular subtype of immunoglobulins (IgG4) in the context of iMN immunocomplexes and the relative absence of these antibodies in secondary forms may represent another crucial element for the discrimination of iMN subtypes[73].

1.8.3 Focal Segmental Glomerulosclerosis

Focal segmental glomerulosclerosis (FSGS) is characterized by sclerotic processes that affect a partial number of glomeruli (focal) with a limited extension among the glomerular structures (segmental)[75]. These sclerotic processes lead to the destruction of glomerular capillary tufts and increased matrix. Primary, or idiopathic, FSGS is considered to be associated with podocyte injury and the mechanisms underlying this podocyte damage have been extensively investigated. A number of circulating factors that could affect the permeability barrier of the podocyte have been proposed,

but not proven to cause FSGS. Furthermore, FSGS may also be caused by genetic alterations that affect those genes that are responsible for regulating and maintaining the actin cytoskeleton of podocytes, as well as the foot process structure. A wide range of MS-based proteomic approaches have been employed in order to detect diagnostic markers of FSGS, and are summarised in Table 6.

Table 6. Summary of the differentially expressed proteins detected in IgA Nephropathy through the use of MS-based proteomics.

Study	Disease	Marker	Sample Type
Shui (2008)	FSGS	Extracellular matrix protein 1, cerberus, ADAM 32, kininogen-1 precursor, GST, apoptosis-inducing factor-2, annexin A1, albumin, serotransferrin, carboxylesterase N, cysteine sulfinic acid decarboxylase, tropomodulin-4, sorbitol dehydrogenase 1, protein-b-aspartate methyltransferase, and Rab GDP dissociation inhibitor	Urine
Hellin (2009)	FSGS	Fragments of albumin, 2 of them apparently containing peptides from both C- and N-terminal parts of the whole protein.	Serum
Kalantari (2014)	FSGS	Apolipoprotein A-1, Matrix-remodeling protein 8, Ribonuclease 2 and haptoglobin	Urine
Nafar (2014)	FSGS	CD59, CD44, IBP7, Robo4, and DPEP1	Urine

1.9 MALDI-MS Imaging and Glomerulonephritis

MALDI-MSI has also become an important tool in the investigation of renal diseases, studying proteins/peptides, lipids and drugs in both animals and humans. One approach involved the isolation of glomeruli from rats with focal segmental glomerulosclerosis (FSGS) via laser capture microdissection (LCM) and analysed using MALDI-MSP[76]. The authors demonstrated that they were able to generate proteomic patterns of sclerotic and nonscleoritc gomeurli within FSGS. However,

they also noted that the proteomic patterns of nonsclerotic glomeruli were more similar to sclerotic glomeruli than to completely healthy glomeruli, postulating that that there is an early activation of sclerotic processes occurring at the molecular level.

Furthermore, the pathogenesis of IgA nephropathy (IgAN) was investigated in a mouse model that spontaneously develops mesangioproliferative lesions with IgA deposition, comparable to the human disease[77]. The molecular distribution of a number of lipids was mapped in the hyper-IgA (HIGA) murine kidneys using MALDI-MSI. Interestingly, a number of lipids were found to be over-expressed in the cortical region of the HIGA kidney, with respect to controls; for example O-phosphatidylcholine, PC(O-16:0/22:6) and PC(O-18:1/22:6).

The application of MALDI-MSI directly on bioptic renal tissue in order to highlight differences in protein expression among a wide range of glomerular conditions represents a new stimulating perspective[8]. Through the correlation of molecular with histological information, along with the direct collaboration with nephropathologists, facilitates the detection of specific proteomic indicators that are directly correlated with the pathological alterations that occur within the glomeruli, or tubules, during the development of glomerulonephritis. Given the small amount of tissue made available through the bioptic procedure (renal biopsies are commonly ~10mm in length and ~3mm in diameter), correlation with the histological features represents a crucial step in the study of glomerular diseases.

Mainini et al. first applied MALDI-MSI to human renal tissue obtained by biopsy in order to evaluate the feasibility of this modern proteomic approach, analysing renal biopsies from patients with MN (Stages I and II, n=12), Minimal Change Disease (MCD, n=3) and normal cortical biopsies (Controls, n=3)[25]. Interestingly, it was determined that the glomeruli and tubules of healthy tissue presented similar proteomic profiles. However, in the case of primary glomerulonephritis, glomeruli and tubules presented different protein profiles. Furthermore, altered protein expression compared to controls was evident between different types of primary glomerulonephritis, such as MN and MCD. Finally, tubules affected by GN, even

without morphological evidence of the disease, showed a different protein profile compared to controls. Thus, it is possible to detect early molecular alterations of the disease that are not accessible by traditional histological methods. This feasibility study highlighted the potential role that MALDI-MSI could play in the detection of diagnostic biomarkers associated with primary glomerulonephritis[9].

2 SCOPE OF THE THESIS

The body of work enclosed in this thesis follows the application of MALDI-MS Imaging to fresh-frozen and formalin-fixed paraffin-embedded renal biopsies in order to detect diagnostic and prognostic molecular markers associated with the most common forms of glomerulonephritis.

Chapter two: development and optimisation of a protocol for the analysis of formalin-fixed paraffin-embedded tissue samples that is compatible with the routine clinical workflow.

Chapter three: analysis of fresh-frozen renal biopsies in order to detect proteomic signatures of the most common forms of glomerulonephritis as well as potential markers associated with chronic kidney disease progression.

Chapter four: analysis of formalin-fixed paraffin-embedded renal biopsies in order to generate proteomic signatures of primary and secondary Membranous Nephropathy from which potential molecular markers that can discriminate between these two forms of Membranous Nephropathy can be obtained.

REFERENCES

1. Caprioli RM, Farmer TB, Gile J. Molecular Imaging of Biological Samples: Localization of Peptides and Proteins Using MALDI-TOF MS. *Anal Chem*. 1997;69(23):4751-4760.

2. Bandura DR, Baranov VI, Ornatsky OI, et al. Mass Cytometry: Technique for Real Time Single Cell Multitarget Immunoassay Based on Inductively Coupled Plasma Time-of-Flight Mass Spectrometry. *Anal Chem*. 2009;81(16):6813-6822.

3. Chughtai K, Heeren RMA. Mass spectrometric imaging for biomedical tissue analysis. *Chem Rev*. 2010;110(5):3237-3277.

4. Cornett DS, Frappier SL, Caprioli RM. MALDI-FTICR imaging mass spectrometry of drugs and metabolites in tissue. *Anal Chem*. 2008;80(14):5648-5653. doi:10.1021/ac800617s.

5. Mainini V, Lalowski M, Gotsopoulos A,et al. MALDI-Imaging Mass Spectrometry on Tissues. In: Vlahou A, Makridakis M, eds.; 2015:139-164. doi:10.1007/978-1-4939-1872-0_8.

6. Thomas A, Chaurand P. Advances in tissue section preparation for MALDI imaging MS. *Bioanalysis*. 2014;6(7):967-982.

7. Boggio KJ, Obasuyi E, Sugino K, et al. Recent advances in single-cell MALDI mass spectrometry imaging and potential clinical impact. *Expert Rev Proteomics*. 2011;8(5):591-604.

8. Römpp A, Spengler B. Mass spectrometry imaging with high resolution in mass and space. *Histochem Cell Biol*. 2013; 139(6):759-83.

9. Longuespée R, Fléron M, Pottier C, et al. Tissue proteomics for the next decade Towards a molecular dimention in histology. *OMICS*. 2014;18(9):539-552.

10. Lemaire R, Desmons A, Tabet JC, et al. Direct analysis and MALDI imaging of formalin-fixed, paraffin-embedded tissue sections. *J Proteome Res*. 2007; 6(4):1295-1305.

11. Norris JL, Caprioli RM. Analysis of tissue specimens by matrix-assisted laser desorption/ionization imaging mass spectrometry in biological and clinical research. *Chem Rev*. 2013;113(4):2309-2342.

12. Zaima N, Hayasaka T, Goto-Inoue N, et al. Matrix-assisted Laser Desorption/Ionization Imaging Masss Spectrometry. *Int J Mol Sci*. 2010; 11(12):5040-5055.

13. Schwartz SA, Reyzer ML, Caprioli RM. Direct tissue analysis using matrix-assisted laser desorption/ionization mass spectrometry: Practical aspects of sample preparation. *J Mass Spectrom*. 2003;38(7):699-708.

14. Wang H-YJ, Liu C Bin, Wu H-W. A simple desalting method for direct MALDI mass spectrometry profiling of tissue lipids. *J Lipid Res*. 2011;52(4):840-849.

15. Calvano CD, Carulli S, Palmisano F. Aniline/alpha-cyano-4-hydroxycinnamic acid is a highly versatile ionic liquid for matrix-assisted laser desorption/ionization mass spectrometry. *Rapid Commun Mass Spectrom*. 2009; 23(11):1659-1668.

16. Fagerer SR, Nielsen S, Ibánez A, et al. Matrix-assisted laser desorption/ionization matrices for negative mode metabolomics. *Eur J Mass Spectrom*. 2013; 19(1):39-47.

17. Garate J, Fernández R, Lage S, et al. Imaging mass spectrometry increased resolution using 2-mercaptobenzothiazole and 2,5-diaminonaphtalene matrices: application to lipid distribution in human colon. *Anal Bioanal Chem*. 2015;407(16):4697-4708.

18. Leinweber BD, Tsaprailis G, Monks TJ, et al. Improved MALDI-TOF imaging yields increased protein signals at high molecular mass. *J Am Soc Mass Spectrom*. 2009;20(1):89-95.

19. Guo S, Yammin W, Zhou D, et al. Electric Field-Assisted Matrix Coating Method Enhances the Detection of Small Molecule Metabolites for Mass Spectrometry Imaging. *Anal Chem*. 2015; 87(12):5860-5965.

20. Chughtai K, Hereen RM. Mass spectrometric imaging for biomedical tissue analysis. *Chem Rev*. 2010; 110(5):3237-3277. doi: 10.1021/cr100012c.

21. Yang J, Caprioli RM. Matrix Sublimation/Recrystallization for Imaging Proteins by Mass Spectrometry at High Spatial Resolution. *Anal Chem*. 2011; 83(14):5728-5734.

22. Flinders B, Morrell J, Marshall P et al. The use of hydrazine-based derivatizaion reagents for improved sensitivity and detection of carbonyl containing compounds using MALDI-MSI. *Anal Bioanal Chem*. 2015; 407:2085-2094.

23. Shin H, Mutlu M, Koomen JM, et al. Parametric power spectral density analysis of noise from instrumentation in MALDI TOF mass spectrometry. *Cancer Inform*. 2007; 3:219–230.

24. Dziuda DM. *Data Mining for Genomics and Proteomics*. First Edit. Wiley-Interscience; 2010.

25. Mainini V, Pagni F, Ferrario F, et al. MALDI imaging mass spectrometry in glomerulonephritis: Feasibility study. *Histopathology*. 2014;64(6):901-906.

26. Swets JA. Measuring the accuracy of diagnostic systems. *Science*. 1998; 240(4857):1285-1293.

27. Chaurand P, Schwartz SA, Billheimer D, et al. Integrating Histology and Imaging Mass Spectrometry. *Anal Chem*. 2004;76(4):1145-1155..

28. Krishnamurthy S, Mathews K, McClure S, et al. Multi-Institutional Comparison of Whole Slide Digital Imaging and Optical Microscopy for Interpretation of Hematoxylin-Eosin-Stained Breast Tissue Sections. *Arch Pathol Lab Med*. 2013; 137(12):1733-1739.

29. Attia AS, Schroeder KA, Seeley EH, et al. Monitoring the Inflammatory Response to Infection trhough Integration of MALDI-MSI and MRI. *Cell Host Microbe*. 2012;11(6):664-673.

30. Balluff B, Frese CK, Maier SK, et al. De novo discovery of phenotypic intratumour heterogeneity using imaging mass spectrometry. *J Pathol*. 2015;235(1):3-13.

31. Mirnezami R, Spagou K, Vorkas PA, et al. Chemical mapping of the colorectal cancer microenvironment via MALDI imaging mass spectrometry (MALDI-MSI) reveals novel cancer-associated field effects. *Mol Oncol*. 2014;8(1):39-49.

32. Kang S, Shim HS, Lee JS, et al. Molecular proteomics imaging of tumor interfaces by mass spectrometry. *J Proteome Res*. 2010;9(2):1157-1164.

33. Steurer S, Borkowski C, Odinga S, et al. MALDI mass spectrometric imaging based identification of clinically relevant signals in prostate cancer using large-scale tissue microarrays. *Int J Cancer*. 2013;133(4):920-928.

34. Pagni F, Mainini V, Garancini M, et al. Proteomics for the diagnosis of thyroid lesions: preliminary report. *Cytopathology*. 2014:n/a - n/a. doi:10.1111/cyt.12166.

35. Mainini V, Pagni F, Garancini M, et al. An Alternative Approach in Endocrine Pathology Research: MALDI-IMS in Papillary Thyroid Carcinoma. *Endocr Pathol*. 2013;24(4):250-253.

36. Ait-Belkacem R, Sellami L, Villard C, et al. Mass spectrometry imaging is moving toward drug protein co-localizaiton. *Trends Biotechnol*. 2012;30(9):466-474.

37. Reyzer ML, Hsieh Y, Ng K, et al. Direct analysis of drug candidates in tissue by matrix-assisted laser desorption/ionization mass spectrometry. *J Mass Spectrom*. 2003;38(10):1081-1092.

38. Aichler M, Walch A. MALDI Imaging mass spectrometry: current frontiers and perspectives in pathology research and practice. *Lab Invest*. 2015;95(4):422-431.

39. Liu X, Hummon AB. Mass Spectrometry Imaging of Therapeutics from Animal Models to Three-Dimensional Cell Cultures. *Anal Chem.* 2015;87(19):9508-9519.

40. Buck A, Halbritter S, Späth C, et al. Distribution and quantification of irinotecan and its active metabolite SN-38 in colon cancer murine model systems using MALDI MSI. *Anal Bioanal Chem*. 2015;407(8):2107-2116.

41. U.S. Renal Data System. USRDS 2013 Annual Data Report: Atlas of Chronic Kidney Disease and End-Stage Renal Disease in the United States. *National Institutes of Health, National Institute of Diabetes and Digestive and Kidney Diseases*. Bethesda, MD. 2013.

42. Cameron JS, Hicks J. The introduction of renal biopsy into nephrology from 1901 to 1961: a paradigm of the forming of nephrology by technology. *Am. J. Nephrol.* 1997; *17*: 347–358.

43. Korbet SM. Percutaneous renal biopsy. *Semin. Nephrol.*2002; *22*: 254–267.

44. Walker PD, Cavallo T, Bonsib SM. Practice guidelines for the renal biopsy. *Mod. Pathol.* 2004; *17*: 1555–1563.

45. Hergesell O, Felten, H, Andrassy K., Kuhn K, Ritz E. Safety of ultrasound-guided percutaneous renal biopsy retrospective analysis of 1090 consecutive cases. *Nephrol. Dial. Transplant.* 1998; *13*:975–977.

46. Wilkey DW, Merchant ML. Proteomic methods for biomarker discovery in urine. *Semin. Nephrol.* 2007; *27*: 584–596.

47. Thongboonkerd V, Biomarker discovery in glomerular diseases using urinary proteomics. *Proteomics Clin. Appl.* 2008; *2*: 1413–1421.

48. D'Amico G. The commonest glomerulonephritis in the world: IgA nephropathy. *Q. J. Med.* 1987; *6:*, 709–727.

49. Haas M. IgA Nephropathy and Henoch-Schonlein purpura nephritis, in: Jennette J. C., Schwartz,M.M., Silva F. G. (Eds.), *Heptinstall's pathology of the kidney*. Vol 1. 6th ed. Lippincott Williams & Wilkins, Philadelphia 2007, pp. 423–486.

50. Davin JC, Ten Berge IJ, Weening JJ. What is the difference between IgA nephropathy and Henoch-Schonlein purpura nephritis? *Kidney Int*. 2001; *59*: 823–834.

51. Ozkok, A., Yildiz, A., Hepatitis C virus associated glomerulopathies. *World J. Gastroenterol.* 2014; *20*: 7544–7554.

52. Wyatt RJ, Julian BA. IgA nephropathy. *N. Engl. J. Med.* 2013; *36:*, 2402–2414.

53. Moldoveanu Z, Wyatt RJ, Lee JY, Tomana M, et al. Patients with IgA nephropathy have increased serum galactose-deficient IgA1 levels. *Kidney Int*. 2007; *71*: 1148–

1154.

54. Julian BA, Wittke S, Haubitz M, Zurbig, P, et al. Urinary biomarkers of IgA nephropathy and other IgA-associated renal diseases. *World J. Urol.* 2007; *25*: 467–476.

55. Black DA, Rose G, Brewer DB. Controlled trial of prednisone in adult patients with the nephrotic syndrome. *Br Med*. 1970;3:421-426.

56. Medawar W, Green A, Campbell E, et al. Clinical and histopathologic findings in adults with the nephrotic syndrome. *Ir J Med Sci*. 1990;159(5):137-140.

57. Falagas ME, Vardakas KZ, Vergidis PI. Under-diagnosis of common chronic diseases: prevalence and impact on human health. *Int J Clin Pr*. 2007;61:1659-1579.

58. Bethesda M. *United States Renal Data System. USRDS 2013 Annual Data Report: Atlas of Chronic Kidney Disease and End-Stage Renal Disease in the United States. National Institutes of Health. National Institute of Diabetes and Digestive and Kidney Diseases. 2013*. 2013.

59. Obrador GT, Pereira BJG, Kausz AT. Chronic kidney disease in the United States: an underrecognized problem. *Semin Nephrol*. 2002;22(6):441-448.

60. Ronco P, Debiec H. Anti-phospholipase A2 receptor antibodies and the pathogenesis of membranous nephropathy. *Nephron Clin Pract*. 2014;128(3-4):232-237. doi:10.1159/000368588.

61. Hsu HC, Lin GH, Chang MH, Chen CH. Association of hepatitis B surface (HBs) antigenemia and membranous nephropathy in children in Taiwan. *Clin Nephrol*. 1983;20:121-129.

62. Slusarczyk J, Michalak T, Nazarewicz-de Mezer T, Krawczyński K, Nowosławski A. Membranous glomerulopathy associated with hepatitis B core antigen immune complexes in children. *Am J Pathol*. 1980;98:29-43.

63. Takekoshi Y, Tanaka M, Shida, N, Satake Y, Saheki Y, Matsumoto S. Strong association between membranous nephropathy and hepatitis-B surface antigenaemia in Japanese children. *Lancet*. 1978;2:1065-1068.

64. Kleinknecht C, Levy M, Gagnadoux MF, Habib R. Membranous glomerulonephritis with extra-renal disorders in children. *Med*. 1979;58:219-228.

65. Matsui S, Tsuji H, Takimoto Y, Ono S. Clinical improvement of membranous nephropathy after endoscopic resection of double early gastrointestinal cancers. *Clin Exp Nephrol*. 2011;15(2):285-288. doi:10.1007/s10157-010-0389-6.

66. Zheng XY, Wei RB, Tang L, Li P, Zheng XD. Meta-analysis of combined therapy for adult hepatitis B virus-associated glomerulonephritis. *World J Gastroenterol WJG*. 2012;18(8):821-832. doi:10.3748/wjg.v18.i8.821.

67. Ponticelli C, Zucchelli P, Passerini P, Cagnoli L, Cesana B, Pozzi C, Pasquali S, Imbasciati E, Grassi C, Redaelli B, et al. A randomized trial of methylprednisolone and chlorambucil in idiopathic membranous nephropathy. *N Engl J Med*. 1989;320:8-13.

68. Ponticelli C, Zucchelli P, Imbasciati E, Cagnoli L, Pozzi C, Passerini P, Grassi C, Limido, D, Pasquali S, Volpini T et al. Controlled trial of methylprednisolone and

chlorambucil in idiopathic membranous nephropathy. *N Engl J Med*. 1984;310:946-950.

69. Ponticelli C, Zucchelli P, Passerini P, Cesana, B, Locatelli F, Pasquali S, Sasdelli M, Redaelli B, Grassi C, Pozzi C, et al. A 10-year follow-up of a randomized study with methylprednisolone and chlorambucil in membranous nephropathy. *Kidney Int*. 1995;48:1600-1604.

70. Ponticelli C, Zucchelli P, Passerini P, Cesana B. Methylprednisolone plus chlorambucil as compared with methylprednisolone alone for the treatment of idiopathic membranous nephropathy. The Italian Idiopathic Membranous Nephropathy Treatment Study Group. *Engl J Med*. 1992;327:599-603.

71. Branten AJ, Reichert LJ, Koene RA, Wetzels JF. ral cyclophosphamide versus chlorambucil in the treatment of patients with membranous nephropathy and renal insufficiency. *QJM Mon J Assoc Physicians*. 1998:359-366.

72. Tomas NM, Beck LH, Meyer-Schwesinger C, et al. Thrombospondin type-1 domain-containing 7A in idiopathic membranous nephropathy. *N Engl J Med*. 2014;371(24):2277-2287. doi:10.1056/NEJMoa1409354.

73. Debiec H, Ronco P. Immunopathogenesis of membranous nephropathy: an update. *Semin Immunopathol*. 2014;36(4):381-397. doi:10.1007/s00281-014-0423-y.

74. Beck LH, Bonegio RGB, Lambeau G, et al. M-type phospholipase A2 receptor as target antigen in idiopathic membranous nephropathy. *N Engl J Med*. 2009;361(1):11-21. doi:10.1056/NEJMoa0810457.

75. D'Agati VD, Kaskel FJ, Falk RJ. Focal segmental glomerulosclerosis. *N. Engl. J. Med.* 2011; *365*: 2398–2411.

76. Xu BJ, Shyr Y, Liang X, et al. Proteomic patterns and prediction of glomerulosclerosis and its mechanisms. *J Am Soc Nephrol*. 2005;16(10):2967-2975.

77. Kaneko Y, Obata Y, Nishino T, et al. Imaging mass spectrometry analysis reveals an altered lipid distribution pattern in the tubular areas of hyper-IgA murine kidneys. *Exp Mol Pathol*. 2011;91(2):614-621.

Chapter 2

MALDI-Mass Spectrometry Imaging method applicable to different formalin-fixed paraffin-embedded human tissues

Gabriele De Sio MS†#, Andrew James Smith MS†#, Manuel Galli MS†#, Mattia Garancini MD*, Clizia Chinello PhD†, Francesca Bono MD**, Fabio Pagni MD** and Fulvio Magni PhD†

†Department of Health Sciences, Clinical Proteomics Unit, University Milan-Bicocca, Milan, Italy

* Department of Surgery, San Gerardo Hospital, Monza, Italy

**Department of Surgery and Translational Medicine, Pathology, University Milan-Bicocca, Monza, Italy,

# equally contributor authors

Published: *Molecular Biosystems*. 2015. Jun;11(6):1507-14

ABSTRACT

Recent advancements in Matrix Assisted Laser Desorption/Ionisation (MALDI) Mass Spectrometry Imaging (MSI) technology have enabled the analysis of formalin-fixed paraffin-embedded (FFPE) tissue samples, unlocking a wealth of new proteomic information and facilitating the possibility of performing studies with higher statistical power as well as multi-centric collaborations within the field of proteomics research. However, current methods used to analyse these specimens are often time-consuming and they need to be modified when applied to human tissue of different origin. Here we present a reproducible and time-effective method that could address these aforementioned issues and widen the applicability of this technology to a number of challenging tissue types. Additionally, tissue molecular images show high spatial resolution and a strong correlation with the morphological features, enabling the identification of tissue morphology using statistically derived visualisation, without any prior knowledge.

Keywords: *Proteomics; MALDI-MSI, Imaging Mass Spectrometry; FFPE*

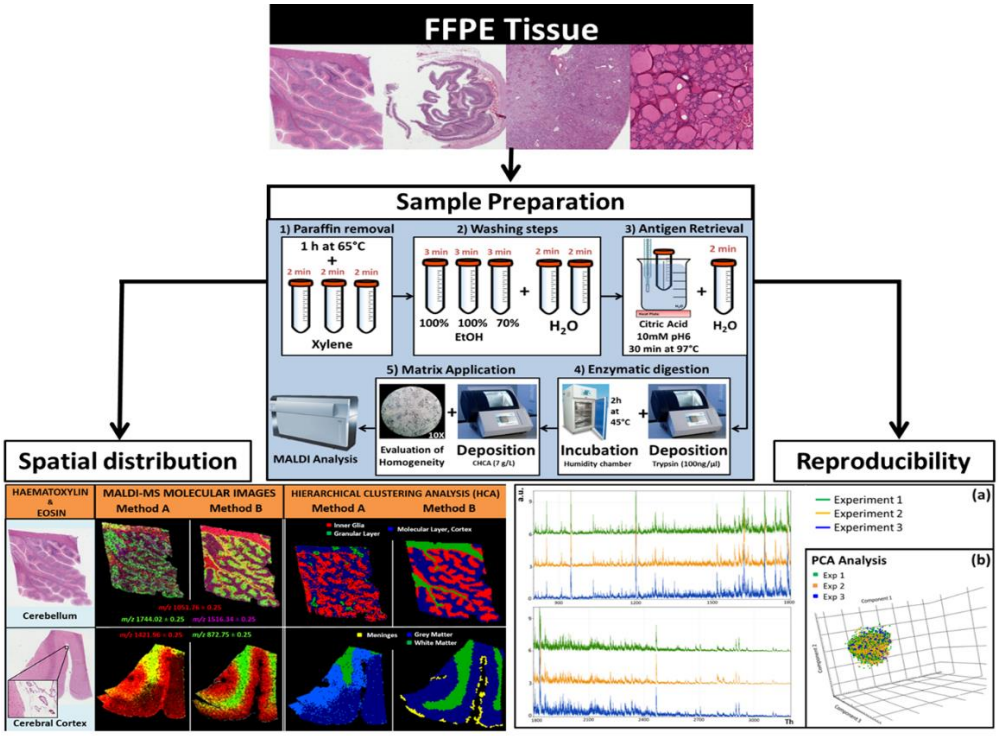

1 INTRODUCTION

Matrix Assisted Laser Desorption/Ionisation Mass Spectrometry Imaging (MALDI-MSI) has high potential in providing clinical translational applications for disease-related protein identification, especially in histopathology. Indeed, MALDI-MSI is commonly used to visualise the spatial distribution of proteins and peptides in pathological tissue sections directly in situ, matching specific morphological criteria with exact localisation. It can also target a number of other analytes including lipids, metabolites and xenobiotics.

This proteomic technique was traditionally developed for the analysis of fresh-frozen tissue sections[1,2] and it has been successfully used in preclinical and clinical investigations showing a variety of applications in several fields such as oncology,[3] degenerative disorders[4] and immunological diseases.[5,6] Different types of tissues have been used in these studies, including brain, breast, ovarian, prostate, gastrointestinal and kidney tissues. Interestingly, recent pilot studies have also applied this methodology to samples different from fresh-frozen tissues, such as cytological smears,[7,8] widening the scope of this type of analysis. However, since all these specimens require fresh material, MALDI-MSI has been limited to centres containing both MALDI mass spectrometers as well as their own pathology department, which are required in order to avoid the sample degradation that may occur during shipment unless very stringent and expensive methods are followed. Consequently, the recruitment of a number of patients sufficient to increase the robustness of the outcome has become a challenging aspect of clinical studies focused on MALDI MSI.[9]

The most promising strategy for overcoming these limitations for proteomic analyses could be represented by formalin-fixed paraffin-embedded (FFPE) tissues, allowing access to large collections of clinically annotated samples and enabling the tissue preservation of samples when stored at room temperature for long periods. Despite these advantages, the application of MALDI-MSI is much more troublesome than with fresh-frozen tissues. More specifically, the analysis of FFPE tissues requires a

more complex and time-consuming sample preparation, limiting the widespread use of this methodology in proteomic research, with deparaffinisation, rehydration, antigen retrieval and enzymatic digestion representing the most important FFPE tissue-specific issues.[10] Although general methods applicable to different tissue types have been suggested,[11] several parameters should often be optimised specifically for each different tissue in order to achieve usable results.[12–14]

Therefore, we propose a reproducible and easy-to-perform strategy that fulfils the requirement of a generic method for the MALDI-MSI analysis of human FFPE specimens and performs optimally with tissues of different origin.

2 MATERIALS AND METHODS

The study was conducted on the left-over material according to the local Ethics Board rules; FFPE blocks of different human tissues were taken from the archive of the Department of Pathology, San Gerardo Hospital, Monza, Italy. The tissues were fixed according to standard routine methods, with a timing of 24 to 48 hours for surgical specimens. For autoptic samples, no rigorous standardisation was applied and the fixation time ranged between 24 hours and 5 days. After the fixation phase, inclusion was performed using an automatic Tissue Processing Centre (TPC 15 Duo/Trio, Medite, MeBurgdorf, Germany). Different human tissue specimens were chosen to evaluate the analytical method. The specimens selected included the human brain, cerebellum and cerebral cortex, from autopsy; normal kidney from nephrectomy specimens performed for neoplasia; normal thyroid residual from multinodular goiter and normal small bowel from pancreatectomy for ductal adenocarcinoma. For each block, 5 micron thick sections were cut and mounted on conductive Indium Tin Oxide (ITO)-glass. The slides were stocked at room temperature until the day of the analysis. Each slide was treated using method (A) derived from published studies[15,16] and with our method (B).

Method A: the slides were washed twice for 5 min with high performance liquid chromatography (HPLC) grade xylene; then for 5 min with EtOH (90–70–50–30%)

followed by 10 mM ammonium bicarbonate buffer (twice for 3 min); the antigen retrieval was performed in a bath of 20 mM Tris-HCl buffer, pH 9 at 97 °C for 30 min.

Method B: the slides were first left in the oven for 1 hour at 65 °C then washed three times for 2 min with high performance liquid chromatography (HPLC) grade xylene; then with 100% EtOH (twice for 3 min); with 70% EtOH (once for 3 min); and with HPLC grade H2O (twice for 2 min); the antigen retrieval was performed in a bath of 10 mM citric acid buffer at 97 °C for 30 min followed by 2 min in a histology glass container with HPLC grade H2O.

Afterwards, trypsin deposition (Sigma-Aldrich, Chemie Gmbh, Steinheim, Germany, 100 ng μl^{-1}) was performed using the ImagePrep (Bruker Daltonics, Bremen, Germany) automated spraying system and then left in a humid chamber for 2 hours at 45 °C for method B instead of the approximate 3 hours at 37 °C used for method A. Finally, matrix deposition for MALDI analysis was performed by spraying cyano-4-hydroxycinnamic acid (7 mg ml^{-1}) using the ImagePrep (Bruker Daltonics, Bremen, Germany).

All the mass spectra were acquired in reflectron positive mode in the mass range of *m/z* 800 to 4000 (approximately 9000 spectra per tissue section) using an UltrafleXtreme mass spectrometer (Bruker Daltonics, Bremen, Germany). The spectra were collected with a laser diameter of 50 microns and 80 micron raster. After MALDI analysis, the matrix was removed with increasing concentrations of EtOH (70% and 100%) and the slides were stained using haematoxylin & eosin. The slides were converted to digital format by scanning using a ScanScope CS digital scanner (Aperio, Park Center Dr., Vista, CA, USA), thus allowing the direct overlap of images and the integration of proteomic and morphologic data. FlexImaging 3.0 (Bruker Daltonics, Bremen, Germany) data, containing spectra of each entire measurement region, were imported into SCiLS Lab 2014 software (http://scils.de/; Bremen, Germany) after the acquisition. SCiLS was used to perform a series of pre-processing steps on the loaded spectra: baseline subtraction (TopHat algorithm[17]) and

normalisation (total ion current algorithm[18]). A series of further steps were performed in order to generate an average (avg.) spectrum representative of the whole measurement region: peak picking (orthogonal matching pursuit algorithm[19]), peak alignment (to align the detected ions with peak maxima[20,21]) and spatial denoising (http://scils.de/; SCiLS Lab; 8.8 Spatial Denoising). Reproducibility of methods was evaluated based on the number of ions, variance and standard deviation of their intensity. Moreover, Principal Component Analysis (PCA) and Hierarchical Clustering (HC), in particular using the bisecting K-means algorithm, were also performed. The spectra showing comparable features were grouped under the same node and then selected and assigned a specific colour based upon their similarity. Each colour was assigned to a group of pixels and used to generate an image representative of the tissue sections.

3 RESULTS

The main aim of the study was to set up a reproducible and easy-to-perform method useable with different human tissues of different origin, process (autopsy and surgery) and fixation time. Firstly, the proposed method (B) was compared to the one derived from the literature (method A) using human brain and thyroid specimens. Then, the analytical features of the proposed method were evaluated in order to ensure the robustness of the method with other human tissues: kidney and small bowel.

3.1 Comparison of methods

The method derived from published studies (method A) and the modified version (method B) were initially compared using human brain sections, one of the most heterogeneous and challenging samples, and then using thyroid tissues. The average spectra of the two different areas of human brain, cerebellum and cortex, showed a remarkable difference between the two methods, as visualised in Fig. 1 (left and middle panels).

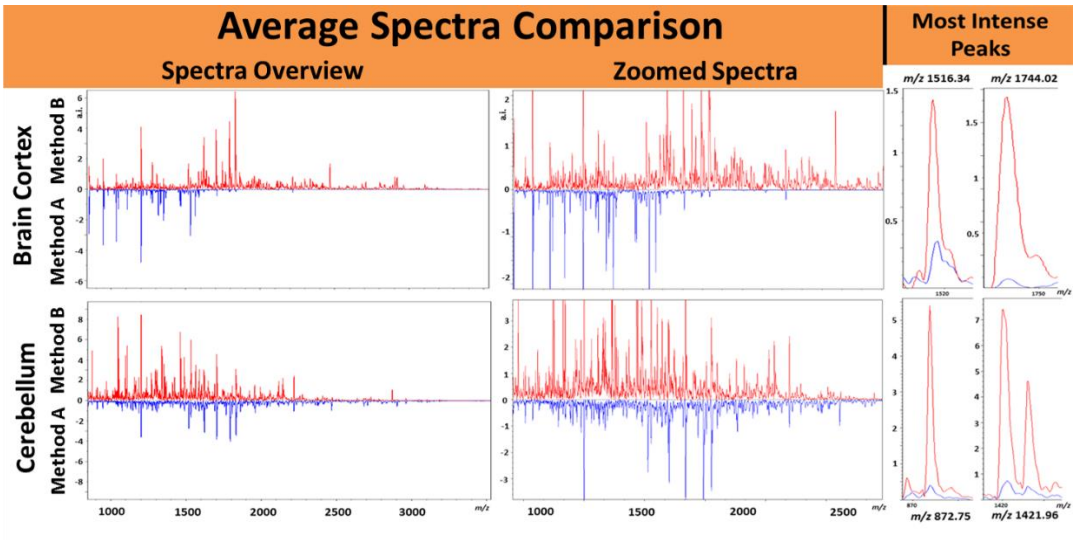

Figure 1. Comparison of method A (blue) and method B (red) using average spectra obtained from the brain cortex (top) and cerebellum (bottom). The differences are highlighted using the overview spectra (left panel), the zoomed spectra (central panel) and ions with a particular spatial localisation in the cerebral cortex (m/z 1516, m/z 1744) and cerebellum (m/z 872, m/z 1421), respectively (right panel).

The majority of the ions (*m/z*) had an enhanced intensity when using method B in comparison with method A. These differences can be better evaluated in the zoomed spectra (Fig. 1; middle panels). For most of the signals (*m/z*), such as those shown in Fig. 1 (right panels), the low intensity observed in samples prepared with method A could hamper the acquisition of the MS/MS spectra. The number of signals in the average mass spectrum of the whole sections and different histological areas within the cerebral cortex and cerebellum (inner glia, granular layer, molecular layer, white and grey matter and meninges) was always higher with method B than with method A (Table 1), independently from the considered mass range (Fig. 2).

Table 1. Overview of the number of ions (peaks; m/z) detected in the average spectrum of the cerebellum, brain cortex and their sub-regions and thyroid using method A (A) and method B (B) along with the signal-to-noise ratio and intensity (expressed as arbitrary intensity, a.i.) ranges of the five most intense ions detected in the average spectrum of the cerebellum, brain cortex and thyroid

Tissue	n° of peaks in the Avg. Spectrum		S/N range of the five most intense peaks		Intensity range of the five most intense peaks	
	A	B	A	B	A	B
Cerebellum	155	292	23 - 33	32 - 60	1.8 - 4.9	4.2 - 8.6
Inner glia	128	286				
Granular layer	136	291				
Molecular layer	129	282				
Brain Cortex	160	289	15 - 29	45 - 62	2.7 - 3.9	4.9 - 7.5
White matter	185	316				
Grey matter	171	301				
Meninges	0	310				
Thyroid	256	570	20 – 26	30 – 69	3.7 – 5.1	7.4 – 9.2

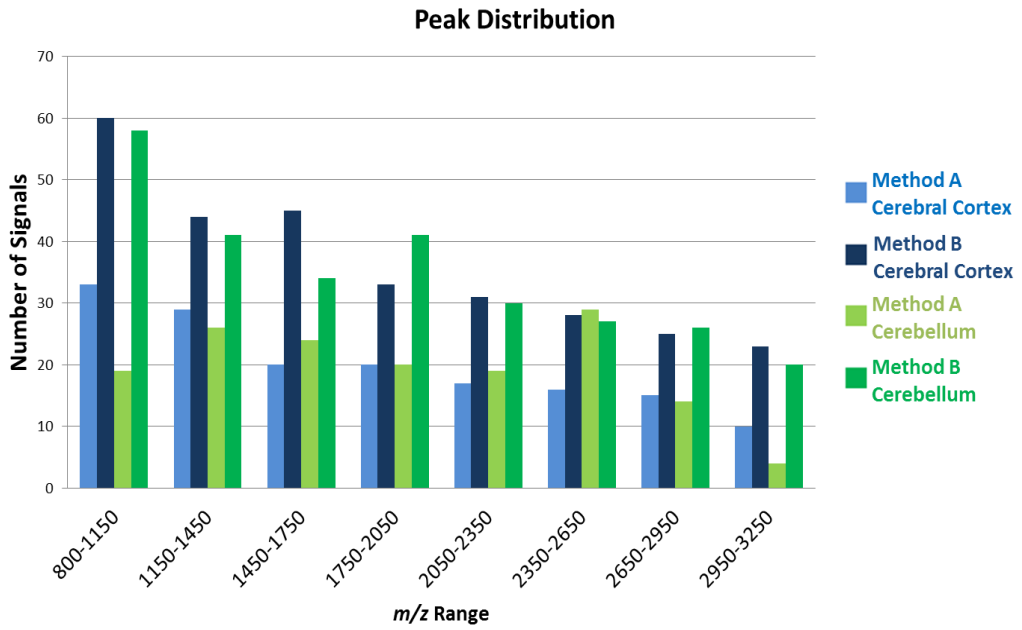

Figure 2. Distribution of the number of ions detected in different mass ranges across the average mass spectra obtained from the cerebral cortex and cerebellum, comparing method A with method B.

Indeed, not only was the signal intensity higher with method B than with method A but also the signal-to-noise ratios were better, as shown by using the five most intense signals (Table 1).

Similarly, in thyroid specimens, we detected more than 500 signals with method B and approximately 250 with method A. Additionally, the signals detected with method B also had a higher intensity and signal-to-noise ratio (Table 1).

3.2 Spatial distribution

To investigate whether method B does not promote protein/peptide delocalisation, molecular images of the human cerebellum were generated using peptides with different localisation, but specific for particular morphological regions, and compared with those derived from method A, as shown in Fig. 3 (MALDI-MS molecular images). The spatial distribution of peptides at *m/z* 872, 1051, 1421 and 1744 in the cerebellum and cerebral cortex enables the generation of well-defined molecular images that correlate with areas of specific morphology using method B but not with method A, as highlighted in Fig. 3.

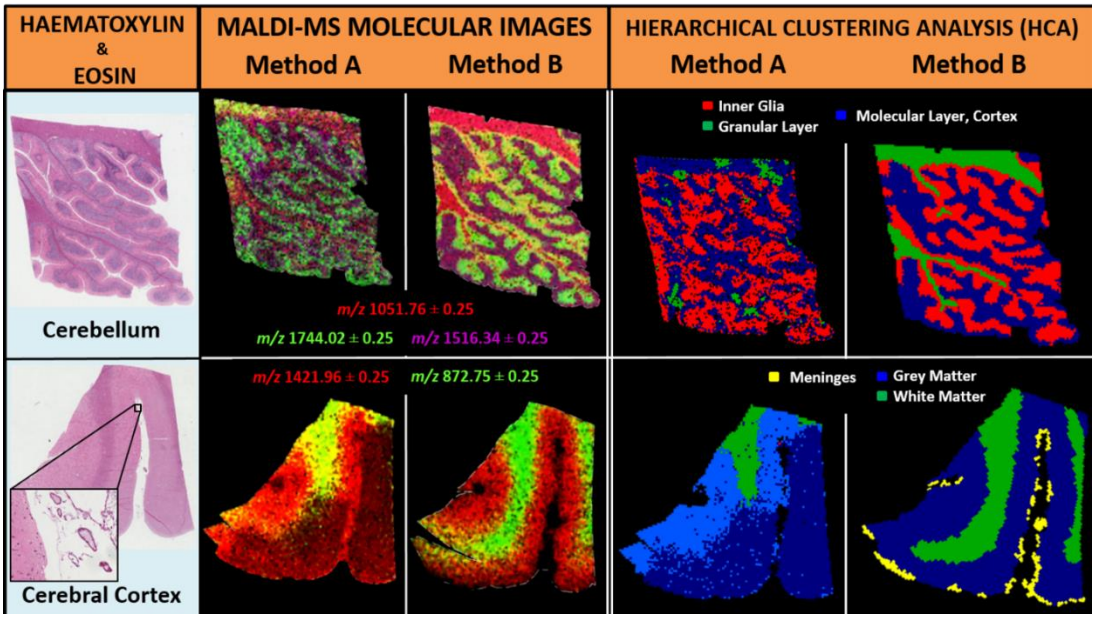

Fig. 3. MALDI-MSI analysis of human brain FFPE tissues. Hematoxylin & eosin stained images of tissue sections taken from human cerebellum and cerebral cortex (left). Examples of MALDI-MS images of peptides localised to distinct morphological regions of the brain, shown as an overlay, and used to visualise the entire section (centre). Visualisation of the hierarchical clustering analysis, indicating the spectral similarities (represented as colour-coded pixels) are correlated with morphological regions of the brain (right): the molecular layer, cortex (blue), the granular layer (green) and the inner glia (red) for the cerebellum and grey matter (blue) and

white matter (green) for the cerebral cortex. In the specimens taken from the cerebral cortex, a cluster of spectra is associated with the meninges (yellow).

To further investigate the potentiality of method B, we submitted the entire dataset of mass spectra of these two tissues to Hierarchical Cluster Analysis (HCA) in blind mode. The HCA classified spectra are based upon their similarities, under specific nodes, and generated a colour-coded image correlating with these nodes (Fig. 3, right column, HCA). The generated clusters of spectra successfully classified regions of the external molecular layer of the cerebellum cortex, the granular layer and the inner glia with a notable improvement in image resolution using data belonging to method B compared with method A. These findings were also confirmed in the cerebral cortex. Additionally, in specimens analysed with the proposed method, a cluster of spectra that could be associated with the meninges was also observed.

3.3 MALDI-Imaging with different human tissues

Based on the encouraging results obtained with brain (cerebellum and cortex) and thyroid tissues using the modified method (B), we investigated its performance with other tissues with different cellular composition: normal kidney and duodenum. For this purpose, three sections of each specimen were prepared using method B and analysed. Average spectra obtained from each of the different tissue types by the application of this method are shown in Fig. 4. A high number of signals (approximately 300 per each specimen, similar to brain tissue) of high relative intensity were also obtained for these tissues (Table 2). Additionally, almost all of the ions present in the spectra were within the *m/z* 800–2500 range with only a few signals above *m/z* 3000, thus suggesting that complete digestion had occurred within the 2-hour incubation period. Finally, different proteomic profiles were observed for each tissue type.

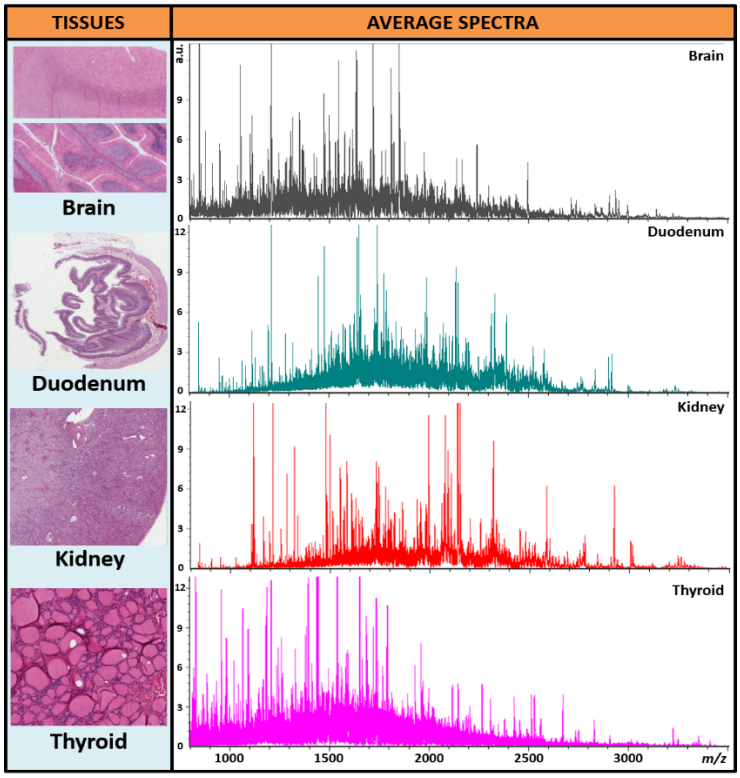

Figure 4. Comparison of the average spectra of human brain, duodenum, kidney and thyroid samples. On the left, hematoxylin & eosin staining of the aforementioned tissue sections derived from FFPE blocks is shown. On the right, average spectra obtained from each tissue type are shown in the mass range of m/z 800 to 3500. The intensity of the signals is expressed in arbitrary units (a.u.).

Table 2. The number of ions (peaks; m/z) detected, the average number and the standard deviation of their intensity in different sections of human FFPE tissues obtained from the three different analytical assays.

Tissue	Experiment 1 n° of Peaks	Experiment 2 n° of Peaks	Experiment 3 n° of Peaks	Avg n° of Peaks	StDev (% peak intensity)
Cerebellum	314	299	295	303	<7%
Cerebral Cortex	315	282	296	298	<10%
Thyroid	577	552	596	575	<8%
Kidney	283	264	268	272	<3%
Cortex	344	360	317	340	<9%
Medulla	328	349	356	344	<3%
Duodenum	320	296	286	301	<4%

3.4 Reproducibility

The analytical variability of method B was evaluated by analysing three consecutive sections of each tissue type in three different days and by three different operators. The results showed a reproducible number of ions detected for all specimens in the three analytical sections with an average number of approximately 300 signals for all specimens, and with a standard deviation of the intensity for all ions present in the mass spectra always below 10%. (Table 2). A particularly higher number (more than 500 ions) was obtained for the thyroid tissues.

An example of results obtained in the three consecutive days of analysis of normal human cerebellum is shown in Fig. 5. The average number of signals present in the three spectra was 303 ± 10, with all the standard deviations of their intensity below 7%, underlining a good level of reproducibility (Fig. 5a). To further strengthen these findings, PCA was performed on the entire dataset (∼25 000 spectra), with each point on the PCA score chart representing an individual spectrum (Fig. 5b). The homogeneous and concentric distribution, along with the absence of isolated clusters within the dataset emphasises the low variability between the three experiments.

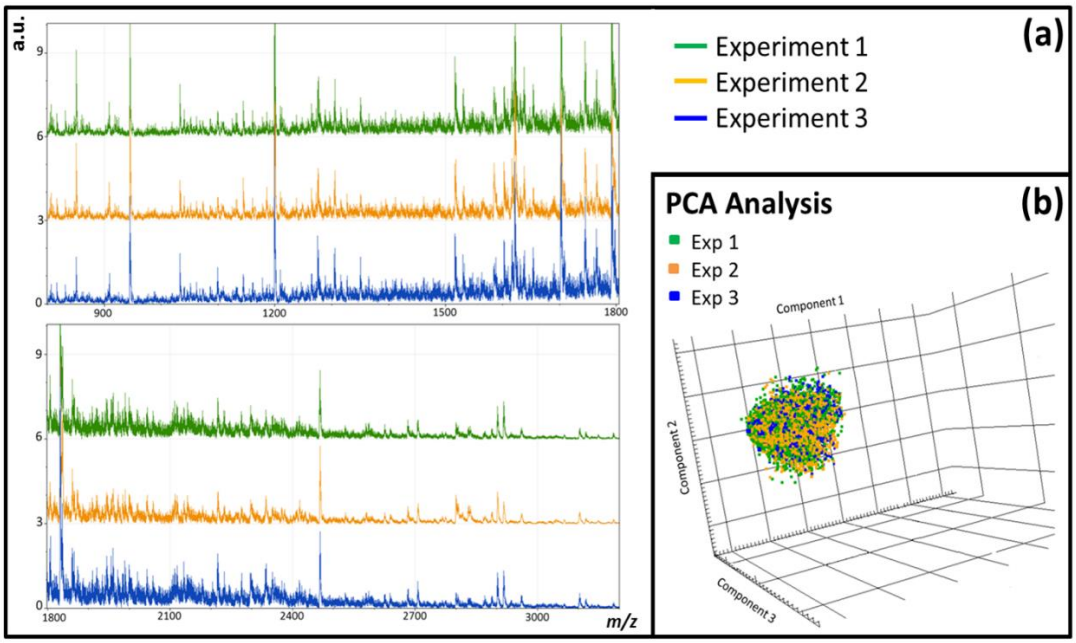

Figure 5. Average mass spectra obtained by analysing three consecutive sections of the human cerebellum independently. (a) Zoomed regions of spectra in the mass range of m/z 800 to 1800 (top) and m/z 1800 to 3500 (bottom). (b) Variability present within the data as represented by a three-dimensional PCA score chart incorporating the entire dataset, with each pixel representing an individual spectrum (green: experiment 1; orange experiment 2, blue: experiment 3).

4 DISCUSSION

Recently, numerous groups have published successful methods for the management of FFPE tissues for MALDI-MSI analysis[11–17] and several reviews have outlined the challenging points of these procedures.[16,22] However, these methods are generally evaluated using only one type of tissue sample, with no comparison between different biological specimens, and they usually require further specific optimisation depending upon the tissue type. The method described here is easy-to-perform, reproducible and could be useful in the analysis of different FFPE tissues. Moreover, the method is more time-effective, taking on average no longer than 4–5 hours to prepare a tissue section for MALDI-MSI. The performance of this method was evaluated, using features such as the number of signals, the signal-to-noise ratio, the

intensity of the five most abundant ions and molecular images, and was shown to be enhanced when compared to the method derived from previous studies (Table 1).

Some modifications to the recently published methods[4–6] seem to be relevant in order to widen its application. Three critical steps were addressed in this method: paraffin removal, antigen retrieval and on-tissue digestion with trypsin. Firstly, more efficient deparaffinisation and tissue adhesion could be achieved by placing the glass slides in an oven at 65 °C for an hour prior to washing with xylene. As a result, the total washing time with xylene is greatly diminished and the efficacy enhanced, also preventing tissue distortion due to long-term xylene immersion. The second crucial step regards the fixation. Although the reaction of formaldehyde with basic amino acid residues, such as arginine or lysine, preserves tissue integrity and cellular constituents, the formation of these methylene bridges alters the three-dimensional configuration of the proteins and leads to inefficient protein recovery.[11] This protein cross-linking can be overcome by the process of antigen retrieval, resulting in the unmasking of epitopes and partial unfolding of proteins. During the antigen retrieval phase, the combination of citric acid buffer with a gradual increase and decrease in temperature at the start and end of the phase avoids thermal shock and damage to the tissue structure. Moreover, we examined tissues of different origin using our method (both autoptic and bioptic specimens). The results obtained with all the investigated specimens highlighted that the proposed method is reproducible, irrespective of the origin of the tissue (Table 2). In order to be detectable via MALDI-MSI, proteins present in FFPE tissues must be digested, most commonly enzymatically using trypsin. Our incubation step during tryptic digestion has been reduced to only 2 hours and was shown to be sufficient for use with tissues of varying origin and fixation time (Fig. 4). Moreover, one of the major problems attributed to trypsin deposition is the delocalisation of peptides, being a strong aqueous based step. The results highlighted that our protocol well preserved the spatial distribution of the analytes, enabling the visualisation of different peptides with localisation related to different morphological features (Fig. 3). This could potentially be a result of the reduced incubation time for tryptic digestion, ensuring that the tissue remains in a humid

atmosphere for the minimum amount of time possible, along with a successful enzymatic process. Generally, the proposed method is both time- (4 hours for a complete experiment) and cost-effective as well as being able to provide mass spectra of high quality with different specimens prepared with different fixation times (Fig. 4). In particular, we chose tissue types that are particularly challenging for proteomic analysis, such as lipid-rich nervous tissues of cerebellum and cerebral cortex, highly hemoglobin-rich kidney sections, colloid-embedded thyroid follicles and visceral organs with a succession of overlapping layers such as mucosa, submucosa, muscularis and peritoneum.

In each of these cases, the mass spectra were of the same high quality (high number of ions with a higher relative intensity) and displayed significantly different proteomic profiles which could potentially be used to classify sub-areas of tissue of pathological interest. Additionally, we have also highlighted that our protocol is highly reproducible, even when performed by different operators (Fig. 5). More interestingly, by submitting the raw data on the entire dataset in blind mode to HCA, it was possible to successfully distinguish regions of tissue based upon their spectral differences, even in instances where these regions are very small but also potentially significant (Fig. 4, yellow spots on the meninx vessels). Additionally, great benefits could be derived from the application of our method to other proteomic strategies such as on-tissue MS/MS, due to the higher ion intensity (Fig. 1, right panel), and nanoLC-ESI-MS/MS with a micro-extraction strategy[23] due to the peptide localisation within the tissue being preserved. These techniques could enable the attainment of information regarding the identity of proteins detected in FFPE tissues which can act as biological markers of disease, providing diagnostic, prognostic and potentially therapeutic significance.

CONFLICT OF INTEREST STATEMENT

The authors declare that there are no conflicts of interest.

ACKNOWLEDGEMENTS

This work was supported by grants from the MIUR: FIRB 2007 (RBRN07BMCT_11), FAR 2010–2013; from i-MODE-CKD (FP7-PEOPLE-2013-ITN) and in part by the EuroKUP COST Action (BM1104) Mass Spectrometry Imaging: New Tools for Healthcare Research.

REFERENCES

1. Caprioli RM, Fermer TB, Gile J. Molecular imaging of biological samples: localization of peptides and proteins using MALDI-TOF MS, *Anal. Chem*., 1997, **69**,4751–4760.

2. Mainini V, Pagni F, Ferrario F, et al. MALDI imaging mass spectrometry in glomerulonephritis: feasibility study, *Histopathology*, 2014, **64**(6), 901–906.

3. Gemoll T, Roblick UJ, Habermann JK. MALDI mass spectrometry imaging in oncology, *Mol. Med. Rep*., 2011, **4**(6), 1045–1051.

4. Hanrieder J, Phan NT, Kurczy ME, Ewing AG. Imaging mass spectrometry in neuroscience, *ACS Chem. Neurosci*., 2013, **4**(5), 666–679.

5. Lalowski M, Magni F, Mainini V, et al. Imaging mass spectrometry: a new tool for kidney disease investigations, *Nephrol., Dial., Transplant*., 2013, **28**(7), 1648–1656.

6. Neubert P, Walch A. Current frontiers in clinical research application of MALDI imaging mass spectrometry, *Expert Rev. Proteomics*, 2013, **10**(3), 259–273.

7. Pagni F, Mainini V, Garancini M, et al. Proteomics for the diagnosis of thyroid lesions: preliminary report, *Cytopathology*, 2014, DOI: 10.1111/cyt.12166.

8. Mainini V, Pagni F, Garancini M, et al. An alternative approach in endocrine pathology research: MALDI-IMS in papillary thyroid carcinoma, *Endocr. Pathol*., 2013, **24**(4), 250–253.

9. Dekker TJ, Balluff BD, Jones EA, et al. Multicenter Matrix-Assisted Laser Desorption/Ionization Mass Spectrometry Imaging (MALDI MSI) Identifies Proteomic Differences in Breast-Cancer-Associated Stroma, *J. Proteome Res.*, 2014, **13**(11), 4730–4738.

10. Gorzolka K and Walch A. MALDI mass spectrometry imaging of formalin-fixed paraffin-embedded tissues in clinical research, *Histol. Histopathol*., 2014, **29**(11), 1365–1376.

11. Casadonte R and Caprioli RM. Proteomic analysis of formalin-fixed paraffin-embedded tissue by MALDI imaging mass spectrometry, *Nat. Protoc.*, 2011, **6**(11), 1695–1709.

12. Ronci M, Bonanno E, Colantoni A, et al. Protein unlocking procedures of formalin-fixed paraffin-embedded tissues: application to MALDI-TOF imaging MS investigations, *Proteomics*, 2008, **8**(18), 3702–3714.

13. Franck J, Arafah K, Elayed M, et al. MALDI imaging mass spectrometry: state of the art technology in clinical proteomics, *Mol. Cell. Proteomics*, 2009, **8**, 2023–2033.

14. Casadonte R, Kriegsmann M, Zweynert F, et al. Imaging mass spectrometry to discriminate breast from pancreatic cancer metastasis in formalin-fixed paraffin embedded tissues, *Proteomics*, 2014, **14**(7–8), 956–964.

15. Lemaire R, Desmons A, Tabet JC, Day R, Salzet M, Fournier I. Direct Analysis and MALDI Imaging of Formalin-Fixed, Paraffin-Embedded Tissue Sections, *J. Proteome Res.*, 2007, **6**, 1295.

16. Fowler CB, O'Leary TJ, Mason JT, Toward improving the proteomic analysis of formalin-fixed, paraffin-embedded tissue, *Expert Rev. Proteomics*, 2013, **10**, 389.

17. Powers TW, Neely BA, Shao Y. MALDI Imaging Mass Spectrometry Profiling of N-Glycans in Formalin-Fixed Paraffin Embedded Clinical Tissue Blocks and Tissue Microarrays, *PLoS One*, 2014, **9**(9), e106255.

18. Deininger SO, Cornett D, Paape R, et al. Normalization in MALDI-TOF imaging data sets of proteins: practical considerations, *Anal. Bioanal. Chem.*, 2011, **401**, 167–181.

19. Alexandrov T, Becker M, Deininger SO, et al. Spatial segmentation of imaging mass spectrometry data with edgepreserving image denoising and clustering, *J. Proteome Res.*, 2010, **9**, 6535–6546.

20. Alexandrov T and Kobarg JH. Efficient spatial segmentation of large imaging mass spectrometry data sets with spatially aware clustering, *Bioinformatics*, 2011, **27**(13), i230–i238.

21. Alexandrov T, Meding S, Trede D, et al. Super-resolution segmentation of imaging mass spectrometry data: Solving the issue of low lateral resolution, *J. Proteomics*, 2011, **75**, 237–245.

22. Hood BL, Conrads TP, Veenstra TD. Mass spectrometric analysis of formalin-fixed paraffin-embedded tissue: unlocking the proteome within, *Proteomics*, 2006, **6**(14), 4106–4114.

23. Quanico J, Franck J, Dauly C, Strupat K, Dupuy J, Day R, Salzet M, Fournier I, Wisztorski M. Development of liquid microjunction extraction strategy for improving protein identification from tissue sections, *J. Proteomics*, 2013,**79**, 200–218.

Chapter 3

α-1-antitrypsin detected by MALDI-Imaging in the study of glomerulonephritis: its relevance in chronic kidney disease progression

#Andrew Smith BSc*, #Vincenzo L'Imperio MD**, Gabriele De Sio MSc*, Franco Ferrario MD**, Carla Scalia**, Giacomo Dell'Antonio MD***, Federico Pieruzzi MD****, Claudia Pontillo MSc[#^], Szymon Filip MSc[##,^], K aterina Markoska MSc[▪], Antonio Granata MD[^^], Goce Spasovski MD[▪], Joachim Jankowski PhD[^^^], Giovambattista Capasso MD[###], Fabio Pagni MD** and Fulvio Magni PhD*

# Equally contributing authors

* Department of Health Sciences, Proteomics, University of Milano-Bicocca, Monza, Italy

** Department of Surgery and Translational Medicine, Pathology, University of Milano-Bicocca, Monza, Italy

*** Department of Pathology, San Raffaele Hospital, Milan, Italy

**** Department of Health Sciences, Nephrology, University of Milano-Bicocca, Milan, Italy

Mosaiques diagnostics GmbH, Hannover, Germany

Biomedical Research Foundation Academy of Athens, Athens, Greece

Department of Cardio-Thoracic and Respiratory Science, Second University of Naples, Naples, Italy

^ Charité – Universitätsmedizin Berlin, Berlin, Germany

^^ Department of Nephrology, Ospedale San Giovanni di Dio, Agrigento, Italy

^^^ University Hospital RWTH Aachen, Institute for Molecular Cardiovascular Research, Aachen, Germany

▪ Department of Nephrology, Medical Faculty, University of Skopje, Skopje, Macedonia

Published: *Proteomics*. 2016. Jun;16(11-12):1759-66.

ABSTRACT

Idiopathic glomerulonephritis (GN), such as membranous glomerulonephritis (MGN), focal segmental glomerulosclerosis (FSGS) and IgA nephropathy (IgAN), represent the most frequent primary Glomerular Kidney Diseases (GKDs) worldwide. Although the renal biopsy currently remains the gold standard for the routine diagnosis of idiopathic GN, the invasiveness and diagnostic difficulty related with this procedure highlight the strong need for new diagnostic and prognostic biomarkers to be translated into less invasive diagnostic tools. Matrix Assisted Laser Desorption/Ionisation Mass Spectrometry Imaging (MALDI-MSI) was applied to fresh frozen bioptic renal tissue from patients with a histological diagnosis of FSGS (n=6), IgAN, (n=6) and MGN (n=7), and from controls (n=4) in order to detect specific molecular signatures of primary glomerulonephritis. MALDI-MSI was able to generate molecular signatures capable to distinguish between normal kidney and pathological GN, with specific signals (*m/z* 4025, 4048 and 4963) representing potential indicators of CKD development. Moreover, specific disease-related signatures (*m/z* 4025 and 4048 for FSGS, *m/z* 4963 and 5072 for IgAN) were detected. Of these signals, *m/z* 4048 was identified as α-1-antitrypsin (A1AT) and was shown to be localised to the podocytes within sclerotic glomeruli by immunohistochemistry. A1AT could be one of the markers of podocyte stress that is correlated with the development of FSGS due to both an excessive loss and a hypertrophy of podocytes.

ABBREVIATIONS

A1AT – α-1-antitrypsin, **CKD** – Chronic kidney disease, **eGFR** – Estimated glomerular filtration rate, **FFPE** – Formalin-fixed paraffin-embedded, **FSGS** – Focal segmental glomerulosclerosis, **GKD** – Glomerular kidney disease, **GN** – Idiopathic glomerulonephritis, **IgAN** – IgA nephropathy, **MCD** – Minimal change disease, **MGN** – Membranous glomerulonephritis, **SA** – Sinapinic acid

STATEMENT OF SIGNIFICANCE

The body of work enclosed in this manuscript presents MALDI-imaging as tool useful for detecting molecular signatures of glomerulonephritis and highlights the added value of correlating *in situ* proteomic information with urinary proteomics when attempting to identify translatable disease markers. Such molecular signatures could potentially assist in the routine diagnosis of idiopathic glomerulonephritis, where there is a need for less-invasive markers due to the potential complications and diagnostic difficulty associated with the renal biopsy. Specifically, the study employs MS-Imaging and immunohistochemistry to identify and validate one particular protein, α-1-antitrypsin, that was found to be localised in the podocytes of sclerotic glomeruli. This finding suggests that α-1-antitrypsin may be implicated in the development of sclerotic lesions and could represent a marker of podocyte stress, an early sign of glomerulonephritis progression. Several fragments of this protein were also detected in urine and were shown to be over-expressed in the urine of patients who progressed to the latter stages of Chronic Kidney Disease. Therefore, α-1-antitrypsin may represent a potential non-invasive proteomic indicator of the progression of glomerulonephritis.

1 INTRODUCTION

Glomerular kidney disease (GKD) represents the third leading cause of end-stage renal disease (ESRD) in Western countries[1]. Clinicians classify GKD in primary and secondary forms based on etiopathogenetic criteria. The former includes idiopathic glomerulonephritis (GN), such as membranous glomerulonephritis (MGN), focal segmental glomerulosclerosis (FSGS) and IgA nephropathy (IgAN), that represent the most frequent primary GKDs worldwide[2,3]. Currently, the renal biopsy remains the gold standard for routine diagnosis [4]. However, the availability of pathological renal tissue also provides a great opportunity for the research of new diagnostic and prognostic markers that are potentially transferable into less invasive diagnostic tools if they are also detectable in biological fluids such as urine or serum. For this purpose, proteomic approaches are currently very promising and, among them, Matrix-Assisted Laser Desorption/Ionisation Mass Spectrometry Imaging (MALDI-MSI) represents a potential technology that can be employed for biomarker discovery, providing the capability to match traditional morphological data related with pathology to proteomic information. Recent feasibility studies showed the possible application of MALDI-MSI in this field, showing the existence of alterations in the tissue protein profiles of MGN and minimal change disease (MCD) patients[5]. Interestingly, these modifications were observed not only in tissue areas with evident pathological alterations, but also in regions with morphologically normal appearance, thus highlighting the potentiality of MALDI-MSI in nephropathology. In this complex background, we analyzed fresh-frozen tissue from heterogeneous forms of primary GN (FSGS, IgA and MGN) by MALDI-MSI in order to investigate the potential application of this technique in GNs more deeply and explore the identification of possible new indicators of CKD progression.

2 MATERIALS AND METHODS

2.1 Materials

Conductive indium tin oxide (ITO) glass slides, Protein Calibration Standard I and Peptide Calibration Standard I were purchased from Bruker Daltonik (Bremen, Germany). Sinapinic Acid (SA), α-cyano-4-hydroxycinnamic acid (CHCA), HPLC grade acetonitrile, ethanol and trifluoroacetic acid (TFA) were purchased from Sigma-Aldrich Chemie (Buchs, Switzerland). Tissue-Tek® O.C.T. Compound was obtained from Sakura® Finetek (Alphen aan den Rijn, Netherlands). Alpha-1 antitrypsin (A1AT) polyclonal rabbit Ab was purchased from Dako (Glostrup, Denmark).

2.2 Tissue samples

The study included only primary GNs classified as idiopathic according to the strong clinical criteria presented in Table 1. Fresh-frozen biopsies taken from patients, who underwent renal biopsy with a histological diagnosis of FSGS (n=6), IgAN, (n=6) and MGN (n=7), were collected. Normal cortical biopsies (controls, n=4) corresponded to regions of kidney obtained from radical nephrectomy during tumour treatment. Control patients had no history of functional renal disease. The study was approved by the local Ethical Boards. Renal specimens were embedded in Tissue-Tek Optimal Cutting Temperature within 30 min of biopsy execution or surgical procedure.

Table 1. Clinical criteria used to determine the primitivity of MGN, FSGS and IgAN patients.

	Criteria
MGN	- Antinuclear antibodies (ANA) below a titer of 1:80 - Negativity for Anti-double stranded DNA antibodies - Absence of histological signs of lupus membranous nephritis (type V lupus nephritis) - Negative HBV and HCV serology - Negativity for malignancy
FSGS	- Serological negativity to HIV1, SV40, CMV, EBV, parvovirus B19 - No history of systemic hypertension - No renal dysgenesia/abnormalities - No history of drug abuse
IgAN	- Clinical presentation inconsistent for Henoch-Schoenlein purpura - Negative serology for HCV infection

2.3 Sample preparation

For each specimen, two 4 µm thick sections were cut and thaw-mounted on the same conductive Indium Tin Oxide (ITO) glass slide (Bruker Daltonik GmbH, Germany) and stabilised for 30 minutes in a conventional dry oven at 85°C (Tecnovetro s.r.l., Monza, Italy). The slides were then stored at -80°C until the day of analysis. Glass slides were thawed by desiccation for 30 minutes and then washed in a graded series of ethanol (70, 90 and 95%). Following the washes, they were again dried for 10 minutes via desiccation. Sinapinic acid (SA) was deposited on the slide through a sublimation apparatus (plate diameter 10 cm, S.B.L. Apparecchi Scientifici, Vimodrone, Italy) with 500 mg of SA at 145°C and 90 mTorr for 30 minutes[5]. Sublimation was followed by automated spraying of the SA (10 mg/mL in 60%/0.2%

v/v acetonitrile/TFA) using the Imageprep (Bruker Daltonik GmbH) to attain the desired matrix thickness. For the identification process, α-cyano-4-hydroxycinnamic acid (7mg/mL in 50%/0.1% v/v acetonitrile/TFA) was deposited onto consecutive sections sectioned from the previously used renal specimens using the ImagePrep automated sprayer. The matrix was removed from the tissue by washing with a 50%/0.1% v/v acetonitrile/TFA solution. The resulting solution was concentrated using a HETO vacuum concentrator (Thermo Scientific, A. De Mou, Milano, Italy) for 30 minutes, to a final volume of 20 µL. A volume of 0.8 µL was spotted onto a Ground Steel MALDI Target Plate (Bruker Daltonik GmbH, Germany), allowed to dry, and then followed by an equal volume of 7 mg/ml α-cyano-4-hydroxycinnamic acid.

2.4 Mass spectrometric analysis

For MALDI- MSI analysis, all mass spectra were acquired in linear positive mode in the mass range of *m/z* 3000 to 20000 using an UltrafleXtreme (Bruker Daltonik GmbH) MALDI-TOF/TOF MS equipped with a Smartbeam laser operating at 2kHz frequency. External calibration was performed using a mixture of standard proteins within the mass range of *m/z* 5500 to 17000 (ProtMix I, Bruker Daltonics). Images were acquired with a laser diameter of 50 µm and a rastering of 50 µm. For MALDI-MS/MS, representative mass spectra were acquired in reflectron positive mode in the mass range of *m/z* 700 to 4500. Precursor ions were selected and fragmented using the laser-induced dissociation (LID) and LIFT™ technology and an MS/MS spectra obtained from the accumulation of ~100000 laser shots. External calibration was performed using a mixture of standard peptides within the mass range of *m/z* 750 to 3500 (PepMix I, Bruker Daltonics).

2.5 Histological evaluation

Following MALDI-MSI analysis, the matrix was removed with increasing concentrations of ethanol (70% and 100%) and the slides were stained using Trichrome. The slides were then converted to digital format using a ScanScope CS

digital scanner (Aperio, Park Center Dr., Vista, CA, USA) and pathological glomerular areas of interest (Regions of Interest, ROI) were highlighted by a pathologist, which included all of the glomeruli and regions manifesting in pathological alterations related to the disease. This allowed for the direct overlap of images and the integration of proteomic and pathological information. The study only compared the profiles glomerular tufts while tubulointerstitial features were not considered for the purpose of the current investigation; specific segmental glomerular areas of fibrosis were included. Globally sclerotic areas were excluded.

2.6 Data analysis

FlexImaging 3.0 (Bruker Daltonics, Bremen, Germany) data, containing spectra of each entire measurement region, were imported into SCiLS Lab 2014 software (http://scils.de/; Bremen, Germany) after the acquisition. SCiLS was used to perform a series of pre-processing steps on the loaded spectra: baseline subtraction (TopHat algorithm) and normalisation (total ion current algorithm). A series of further steps were performed in order to generate an average (avg.) spectrum representative of the whole measurement region and of the primary GN sub-classes: peak picking (orthogonal matching pursuit algorithm), peak alignment (to align the detected ions with peak maxima) and spatial denoising (http://scils.de/; SCiLS Lab; 8.8 Spatial Denoising). Principal Component Analysis (PCA) was also performed to reduce the high complexity of the data. Finally, Receiver Operative Characteristic (ROC) analysis was performed, with an AUC of >0.8 being required, as an additional criterion to the $p<0.05$, for a peak to be considered as statistically significant. For MALDI-MS/MS spectra, baseline subtraction and smoothing were performed using FlexAnalysis3.4 (Bruker Daltonics, Bremen, Germany). All MS/MS spectra were searched against the Swiss-Prot database (Release 2015_05 of 29-Apr-15) with the Mascot 2.4 search engine (Matrix Science, London, UK). Mass tolerances were set at 2.5-3 Da for MS and 1.4 Da for MS/MS. No enzymes or any fixed post-translational modifications were set in the search parameters.

2.7 Immunohistochemistry with alpha-1-antitrypsin (A1AT) antibody

In order to confirm the proteomic identification data, a further series of formalin-fixed paraffin-embedded (FFPE) renal biopsies taken from patients with IgAN and FSGS were tested for IHC analysis. This validation group included IgAN with wide sclerosis (n=4), IgAN with a prevalent mesangioproliferative pattern without sclerosis (n=4) and FSGS (n=6). For each specimen, 3µm thick sections were cut from FFPE blocks. After deparaffinization and rehydration, slides underwent endogenous peroxidase blockage and an antigen retrieval process via EnVision Flex (DAKO). Finally, Autostainer Link 48 (Dako, Glostrup, Denmark) was used to apply the primary antibody directed against A1AT (polyclonal rabbit, Dako).

3 RESULTS

3.1 Proteomic signatures of primary GN

Initially, the average mass spectra of the entire cohort of patients affected by GN was built within the *m/z* 3,000 to 15 000 mass range. Several of the signals (*m/z*) present in the spectra had a statistically significant higher intensity ($p<0.05$ and $AUC>0.8$) in primary GN, most specifically signals at *m/z* 4025, 4048 and 4963, compared with controls (Figure 1). Moreover, when the specific protein profiles of FSGS, IgAN and MGN were compared, several signals showed different intensity (Figure 2; A-C). Among them, the intensity of the two signals at *m/z* 4025 and 4048 was significantly higher in FSGS in comparison to IgAN and MGN (AUC values of 0.84 and 0.82, respectively, Figure 2; A-C). Additionally, the specific protein profile of IgAN showed two signals at *m/z* 4963 and 5072 with a higher intensity when compared to FSGS, and a higher intensity of signals at *m/z* 5072 and 6180 when compared to MGN (Figure 2; A-C). Unsupervised PCA was performed on the entire dataset in order to further highlight any proteomic differences between FSGS, MGN and IgAN, (Figure 3a). In general, the spectra related to FSGS and IgAN presented distinct distributions, except for one IgAN case (Figure 3a). The co-registration of the proteomic findings with the histological image highlighted that the group of spectra present in this IgAN patient, that were in common with the spectra from the FSGS

cohort, were localised to a distinct group of three sclerotic glomeruli. Therefore, we proceeded with virtual micro dissection in order to export spectra from these particular glomeruli and PCA was again performed (Figure 3b). The spectra exported from these sclerotic glomeruli found within this IgAN patient showed a similar distribution to the entire FSGS cohort in the PCA score chart. In fact, they also showed similar protein profiles, thus strengthening the initial observation that MALDI-MSI has the capability to distinguish individual lesions or sub-regions of tissue even within an individual form of the studied primary GN. Interestingly, the same IgAN patient identified as more comparable with the FSGS cohort following the PCA presented a similar level of intensity of the two target signals (*m/z* 4025 and 4048) previously detected as up-regulated in FSGS patients (Figure 2, E). Upon viewing the spatial localisation of these two signals, they were again correlated with the previously histologically identified sclerotic regions (Figure 4). Furthermore, these ions also shared a specific sclerosis-related localisation within FSGS biopsies (Figure 4). More interestingly, there was also an individual patient within the MGN group that showed a higher intensity of these signals when compared to the other MGN patients (Figure 2, F). These signals were again well correlated with sclerotic areas within the tissue of this patient.

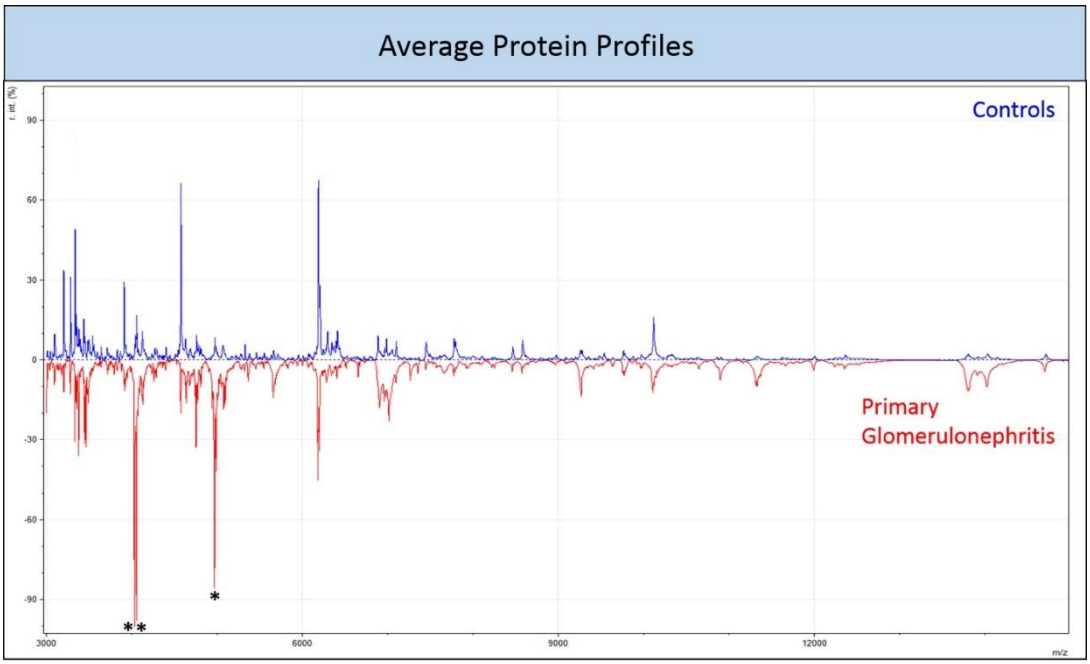

Figure 1. Average protein profiles of healthy renal tissue (top) and from patients with primary glomerulonephritis (bottom) in the m/z 3-15 000 mass range.

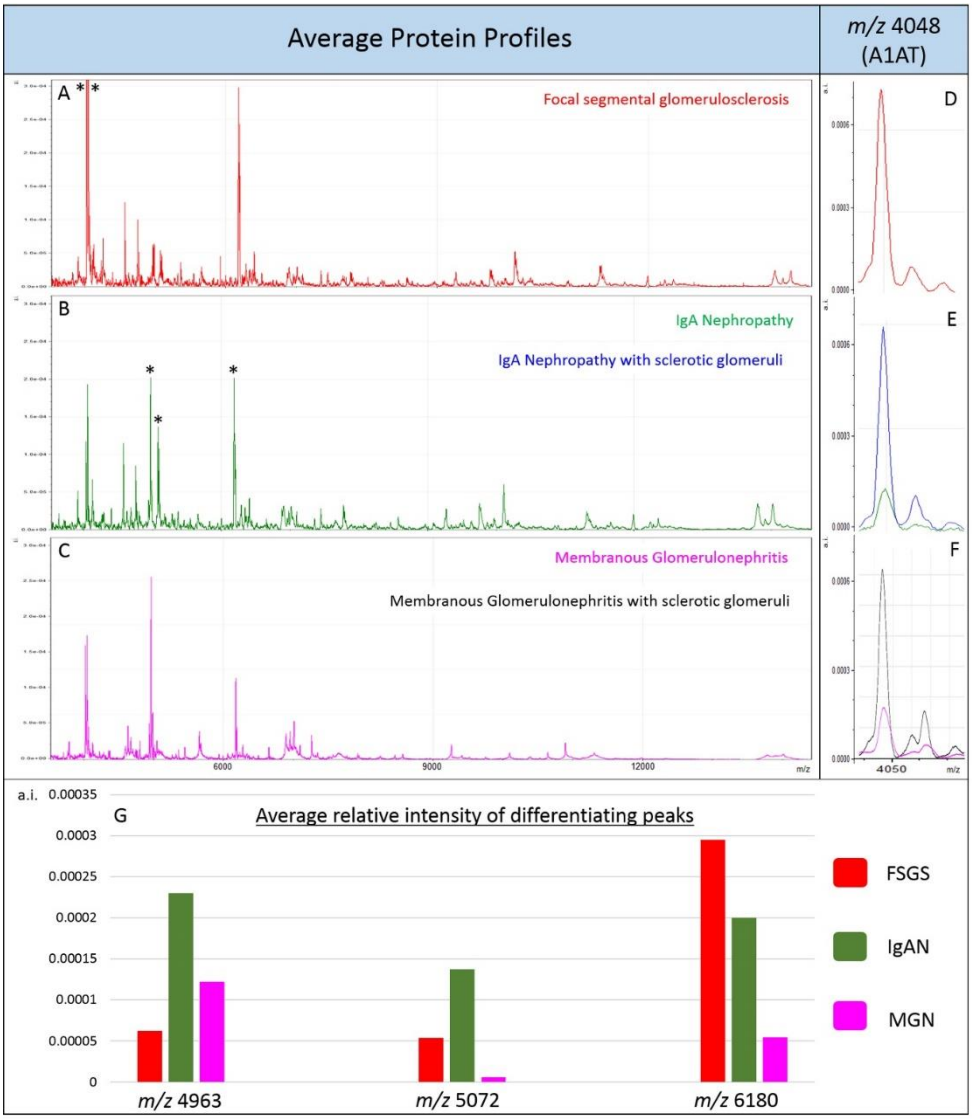

Figure 2. (A-C): Average protein profiles of patients with FSGS (A), IgAN (B) and MGN (C) in the m/ z 3-15 000 mass range with differentiating peaks (AUC>0.8) denoted by an *. (D-F): Relative intensity of m/z 4048 (A1AT) in FSGS (D), IgAN and IgAN with sclerotic glomeruli (E; green and blue, respectively) and MGN and MGN with sclerotic glomeruli (F; fuchsia and black, respectively). G: The average relative intensity for the three further differentiating peaks (m/z 4963, m/z 5072 and m/z 6180) in FSGS, IgAN and MGN.

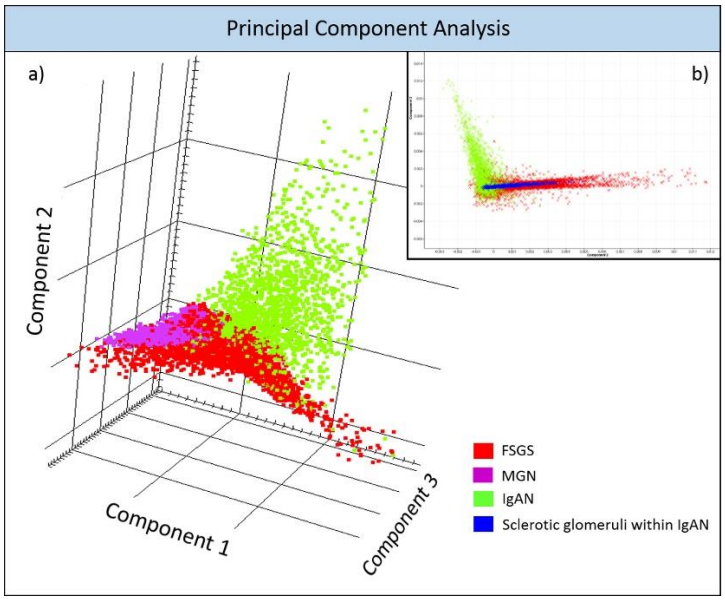

Figure 3. (a) Three-dimensional principal component analysis score chart presenting the distribution of spectra from FSGS (red), MGN (fuchsia) and IgAN (green) patients. (b) Two-dimensional principal component analysis score chart presenting the distribution of spectra from FSGS (red) and IgAN (green) patients along with the distribution of spectra virtually micro dissected from sclerotic glomeruli within an IgAN patient (blue).

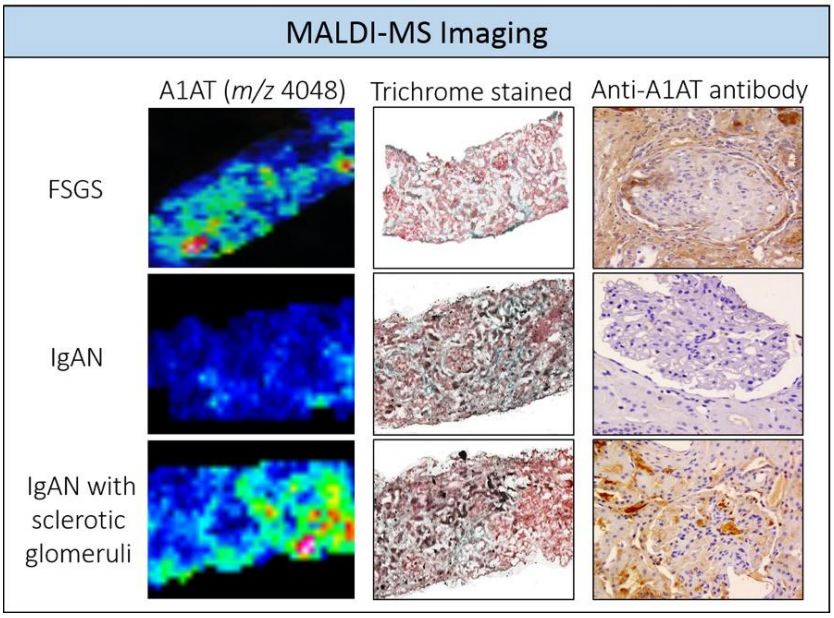

Figure 4. (Left) The molecular distribution of m/z 4048 (A1AT) in sections of bioptic renal tissue, obtained using MALDI-MSI, (centre) Trichrome stained image of the identical sections used for MALDI-MS Imaging and (right) immuno-histochemical staining with the anti-A1AT antibody from a validation set of patients. The collection of images is derived from patients with FSGS (top), IgAN (middle) and IgAN with sclerotic glomeruli (bottom).

3.2 Identification of A1AT

The two signals at *m/z* 4025 and 4048 had the capability to discriminate sclerotic glomeruli within different forms of primary GN. Therefore, their identity was investigated by acquiring MS/MS spectra by MALDI-TOF/TOF. The peptide fragments in the resulting spectrum were searched against the Swiss-Prot database with the Mascot 2.4 search engine. The signal at *m/z* 4048 was identified as a peptide fragment of α-1-antitrypsin (A1AT) (IPPEVKFNKPFVFLMIEQNTKSPLFMGKVVNPTQK) with a Mascot score of 77. The IHC staining for A1AT on renal biopsies showed a diffuse positivity among sclerotic areas of FSGS and IgAN and scant-positivity/negativity among IgAN with a prevalent mesangioproliferative pattern and controls. Interestingly, in renal

biopsies classified as “sclerotic”, there was also a strong positivity to A1AT in the cytoplasm of podocytes (Figure 4). On the contrary, the podocytes present in the renal biopsies with a mesangioproliferative pattern of IgAN and normal glomeruli were completely negative, suggesting that intraepithelial deposits of A1AT are consistent with a dysfunction of podocytes.

4 DISCUSSION

MALDI-MSI could be the ideal tool for a new approach in investigating GN, both for diagnostic and prognostic purposes. This technique has been reported to be capable of providing specific proteomic profiles for the physiological counterpart and for pathological glomeruli[5]. It can define nosological entities, such as IgAN and FSGS, through their distinctive signatures and could be potentially useful in the biological comprehension of these lesions, supporting the existence of specific molecular alterations. The characterization of the proteomic phenotype of glomeruli is mainly related to the possible clinical development of biomarkers for the prognostic stratification of patients with CKD progression. MALDI-MSI is the newest and most promising imaging method for combining protein/peptide expression with distinct localisation inside tissue. In this study, we provide additional evidence of the capability of this technology to discriminate normal kidney from pathological GN, based on specific signals (*m/z* 4025, 4048 and 4963) (Figure 1) that may represent indicators of CKD development. Moreover, specific disease-related signatures (*m/z* 4025 and 4048 for FSGS, *m/z* 4963 and 5072 for IgAN, Figure 2) were also found. MALDI-MSI showed a common proteomic profile overlap between IgAN and FSGS in sclerotic glomerular regions (Figures 3). In particular, two specific ions at *m/z* 4025 and at *m/z* 4048 were of higher intensity in the sclerotic areas of all FSGS patients as well as in the single IgA patient that presented sclerotic lesions (Figure 4).

The signal at *m/z* 4048 was identified by MALDI-TOF/TOF as the resulting peptide fragments belonged to the A1AT protein. A1AT is a major serine proteinase inhibitor

(serpin) found in human plasma. It is a glycoprotein with a broad range of activities, including the down-regulation of neutrophil elastase during the inflammatory processes. Kwak et al. recently evaluated this protein expression in renal biopsies[6] while other authors independently described its over-excretion in the urine of some patients with primary GNs, most specifically FSGS, IgAN and MCD[7-9]. The IHC staining against A1AT demonstrated its localisation in the cytoplasm of podocytes present in sclerotic glomeruli. This represented an intriguing finding related with possible epithelial dysfunction and consequent insufficient degradation of the extracellular matrix. In this setting, many studies correlated the development of FSGS both with an excessive loss[10] and a hypertrophy of podocytes[11] and A1AT could be one of the markers of podocyte stress, in addition to nephrin, Wilms tumor antigen 1 (WT1), the glomerular epithelial protein 1 (GLEPP1) and thymosin beta-4[12].

Additionally, the identification of A1AT fragment(s) in urine samples taken from GN patients have been reported[13,14]. Smaller fragments of the peptide derived from the A1AT protein that we have identified in tissue were also previously detected in urine samples taken from CKD patients. In 2010, Good *et. al* investigated the urinary peptidome of 230 patients with renal disease and compared them to 379 healthy controls. The authors detected 273 urinary peptides found to be significantly different between cases and controls. Using support vector machines, those potential biomarkers were integrated into a single classifier, called "the CKD 273 classifier", which was validated in several studies for the diagnosis and prognosis of CKD. For three of the detected differentiating ions (*m/z* 4963, 5072 and 6180), peaks of similar molecular weight were detected in the CKD 273 classifier (personal communication). However, focusing on A1AT, 18 different fragments of this protein were present in the CKD 273 classifier. All of them were up-regulated in CKD patients in comparison to the control groups. Five of these fragments partially overlapped with the A1AT fragment we identified in tissue samples. Moreover, urinary A1AT fragments were also found to be correlated with CKD progression in Schanstra *et al*. The authors of this study performed *de novo* correlation analysis to investigate which

urinary peptides were highly associated with CKD progression (high progression patients were defined on the basis of a decline in % eGFR slope/ year >-5%). Thirty-five urinary fragments of A1AT were found to be correlated with baseline eGFR and % eGFR slope/ year. Among them, four fragments partially overlapped with the A1AT fragment that we identified in tissue. Moreover, the same A1AT fragment was found to be up-represented in the urine of another cohort of patients classified as CKD progressors with respect to non-progressors (data not shown). In this setting, the combined findings from tissue MALDI-MSI and urinary peptidomics provide further agreement with studies that describe the presence of glomerulosclerosis and the aforementioned podocyte changes[10,11] as early signs of disease progression[15,16]. Thus, the consistency between tissue and urinary results suggests that A1AT should be further investigated as a putative non-invasive biomarker of CKD progression by studying both bioptic renal tissue and urine from the same patients within a very well defined cohort that is based upon carefully selected etiologies (FSGN, IgAN, etc.).

In conclusion, this study shows a promising application of MALDI-MSI in the discovery of biomarkers for the assessment of CKD progression. MALDI-MSI not only facilitates the analysis of fresh frozen specimens but also FFPE tissue, making retrospective studies possible[20]. More specifically, this technology could translate molecular knowledge obtained directly in tissue into routine clinical practice, such as the successful application of the CKD 273 classifier that is based on CE-MS tools.

Furthermore, the localisation of A1AT within the sclerotic glomeruli, as highlighted by IHC, reveals that this protein could be related with the so-called “podocyte stress theory”[17-19] and the emerging fibrogenic role of different biomarkers in glomerulosclerosis[11,12]. Due to some limitations of our study related with the small number of cases analysed, further similar studies are needed for a definitive confirmation of this hypothesis and to validate the role of A1AT in GKDs.

ACKNOWLEDGEMENTS

This work was supported by grants from the MIUR: FIRB 2007 (RBRN07BMCT_11), FAR 2010–2014; from iMODE-CKD (FP7-PEOPLE-2013-ITN) and in part by the COST Action (BM1104) Mass Spectrometry Imaging: New Tools for Healthcare Research.

CONFLICT OF INTEREST STATEMENT

The authors have no other relevant affiliation or financial involvements with any organisation or entity with a financial interest in or financial conflict with the subject matter or material discussed in the manuscript apart from those disclosed.

Claudia Pontillo is employed by Mosaiques in the course of a Marie Curie programme and she has no other relevant affiliation or financial involvements with any organisation or entity with a financial interest in or financial conflict with the subject matter or material discussed in the manuscript apart from those disclosed.

REFERENCES

1. U.S. Renal Data System. USRDS 2013 Annual Data Report: Atlas of Chronic Kidney Disease and End-Stage Renal Disease in the United States. *National Institutes of Health, National Institute of Diabetes and Digestive and Kidney Diseases*. Bethesda, MD. 2013.

2. Wyatt RJ, Julian BA. IgA Nephropathy. *N Eng J Med* 2013; **368**: 2402-2414.

3. Orth SR, Eberhard R. The Nephrotic Syndrome. *N Eng J Med* 1998; **338**: 1202-1211.

4. Pagni F, Galimberti S, Goffredo P, Basciu M, Malachina S, et al. The value of repeat biopsy in the management of lupus nephritis: an international multicentre study in a large cohort of patients. *Nephrol Dial Transplant* 2013; **28**(12): 3014-3023.

5. Mainini V, Pagni F, Ferrario F, Pieruzzi F, Grasso M, et al. MALDI imaging mass spectrometry in glomerulonephritis: feasibility study. *Histopathology* 2014; **64**: 901-906.

6. Kwak NJ, Wang EH, Heo IY, Jin DC, Cha JH, et al. Proteomic analysis of alpha-1-antitrypsin in immunoglobulin A nephropathy. *Proteomics Clain Appl* 2007; **1**(4):420-428.

7. Navarro-Muñoz M, Ibernón M, Bonet J, Pérez V, Pastor MC, et al. Uromodulin and α(1)-antitrypsin urinary peptide analysis to differentiate glomerular kidney diseases. *Kidney Blood Press Res* 2012; **35**(5): 314-325.

8. Graterol F, Navarro-Muñoz M, Ibernón M, López D, Troya MI, et al. Poor hisotlogical lesions in IgA nephropathy may be reflected in blood and urine peptide profiling. *BMC Nephrol* 2013; **14**:82. doi: 10.1186/1471-2369-14-82.

9. Pérez V, Ibernón M, López D, Pastor MC, Navarro-Muñoz M, et al. Urinary peptide profiling to differentiate between minimal change disease and focal segmental glomeurlosclerosis. *PLoS One* 2014; **9(1)**:e87731. doi: 10.1371/journal.pone.0087731.

10. Lemley KV, Lafayette RA, Safai M, Derby G, Blouch K, et al. Podocytopenia and disease severity in IgA Nephropathy. *Kidney Int* 2002; **61**:1475-1485.

11. Wiggins JE, Goyal M, Sanden SK, Wharram BL, Shedden KA, et al. Podocyte hypertrophy, "adaptation," and "decompensation" associated with glomerular enlargement and glomerulosclerosis in the aging rat: prevention by calorie restriction. *J Am Soc Nephrol* 2005; **16**(10): 2953-2966.

12. Xu BJ, Shyr Y, Liang X, Ma LJ, Donnert EM, et al. Proteomic patterns and prediction of glomerulosclerosis and its mechanisms. *J Am Soc Nephrol* 2005; **16**(10): 2967-2975.

13. Good DM, Zurbig P, Argiles A, Bauer HW, Behrens G, et al. Naturally occurring human urinary peptides for use in diagnosis of chronic kidney disease. *Mol Cell Proteomics* 2010; **9**(11): 2424-2437.

14. Schanstra JP, Zurbig P, Alkhalaf A, Argiles A, Bakker SJ, et al. Diagnosis and Prediction of CKD Progression by Assessment of Urinary Peptides. *J Am Soc Nephrol* 2015; doi: 10.1681/ASN.2014050423

15. Barton M, Tharaux PL. Endothelin and the podocyte. *Clin Kidney J* 2012; **5**: 17-27.

16. Kriz W, Lemley KV. A Potential Role for Mechanism Forces in the Detachment of Podocytes and the Progression of CKD. *J Am Soc Nephrol* 2015; **26**: 258-269.

17. Smeets B, Moeller MJ. Parietal epithelial cells and podocytes in glomerular diseases. *Semin Nephrol* 2012; **32**(4): 357-367.

18. Moeller MJ, Smeets B. Role of parietal epithelial cells in kidney injury: the case of rapidly progressing glomerulonephritis and focal and segmental glomerulosclerosis. *Nephron Exp* Nephrol 2014; **126**(2): 97-100.

19. Kretzler M. Role of podocytes in focal sclerosis: defining the point of no return. *J Am Soc nephrol* 2005 **16**(10): 2830-2832.

20. De Sio G, Smith AJ, Galli M, Garancini M, Chinello C, et al. A MALDI-Mass Spectrometry Imaging method applicable to different formalin-fixed paraffin-embedded human tissues. *Mol Biosyst* 2015; **11**(6): 1507-1514.

Chapter 4

The putative role of MALDI-MSI in the study of Membranous Nephropathy

Andrew Smith BSc[†], Vincenzo L'Imperio MD[*], Elena Ajello MD[**], Franco Ferrario MD[*], Niccolò Mosele MSc[†], Martina Stella MSc[†], Manuel Galli MSc[†], Clizia Chinello PhD[†], Federico Pieruzzi MD**, Goce Spasovski MD[#], Fabio Pagni MD[**] and Fulvio Magni PhD[†]

† Department of Medicine and Surgery, Proteomics and Metabolomics Unit, University of Milano-Bicocca, Monza, Italy

* Department of Medicine and Surgery, Pathology, University of Milano-Bicocca, San Gerardo Hospital, Italy

**Department of Medicine and Surgery, Nephrology Unit, University of Milano-Bicocca, Monza, Italy

Department of Nephrology, Medical Faculty, University of Skopje, Skopje, Macedonia

Published: *BBA Proteins and Proteomics.* 2016. 10.1016/j.bbapap.2016.11.013

ABSTRACT

Membranous Nephropathy (MN) is an immunocomplex mediated renal disease that represents the leading cause of nephrotic syndrome in adults and is one of the most frequent glomerulopathies worldwide. This glomerular disease can manifest as primary (idiopathic) or secondary and this distinction is crucial when choosing the most appropriate management of patients. In secondary cases, the best strategy consists in treating the underlying disease whereas in primary forms, the possible identification of confirmatory markers of the idiopathic etiology underlining the process is requested by clinicians. Among those currently reported, the positivity to circulating antigens (PLA2R, IgG4 and THSD7A) was demonstrated in approximately 75% of iMN patients, while approximately 1 in 4 patients with iMN still lack a putative diagnostic marker. Ultimately, the discovery of useful biomarkers to help further stratify these two different forms of glomerulopathy seems mandatory.

Here, MALDI-MSI was applied to formalin-fixed paraffin-embedded (FFPE) renal biopsies from histologically diagnosed primary and secondary MN patients (n=20) in order to evaluate the capability of this technology to detect alterations in their tissue proteome. MALDI-MSI was able to generate molecular signatures of primary and secondary MN, with one particular signal (*m/z* 1459), identified as Serine/threonine-protein kinase MRCK gamma, being over-expressed in the glomeruli of primary MN patients with respect to secondary MN. Furthermore, this proteomic approach detected a number of signals that could differentiate the different forms of iMN that were positive to PLA2R or IgG4 as well as a further set of signals (*m/z* 1094, 1116, 1381 and 1459) that distinguish these patients from those who were negative to both. These signals could potentially represent future targets to be investigated as proteomic markers for the further stratification of iMN patients.

ABBREVIATIONS

CSV – Comma separated value, **CV** – Coefficient of Variation, **ESRD** – End-stage

renal disease, **FFPE** – Formalin-fixed paraffin-embedded, **FSGS** – Focal Segmental Glomerulosclerosis, **GN** – Glomerulonephritis, **IgAN** – IgA Nephropathy, **IgG4** – Immunoglobulin G4, **iMN** – Idiopathic Membranous Nephropathy, **MCD** – Minimal Change Disease, **MN** –Membranous Nephropathy, **PCA** – Principal Component Analysis, **PLA2R** – M-type phospholipase A2 receptor, **PLS** – Partial Least Square, **ROC** – Receiver Operative Curve, **RFE** – Recursive Feature Elimination, **SVM** – Sample Vector Machine, **THSD7A** – Thrombospondin type-1 domain-containing 7A

1 INTRODUCTION

Membranous Nephropathy (MN) is an immunocomplex mediated renal disease that represents the leading cause of nephrotic syndrome in adults and is one of the most frequent glomerulopathies worldwide[1,2]. Notwithstanding its relatively low incidence rate, many cases of MN progress to end-stage renal disease (ESRD), having a clear negative impact upon the patients' quality of life and healthcare costs[3–5]. This glomerular disease can manifest as primary (idiopathic)[6] or secondary[7–10] and in the latter occurs as a result of underlying systemic conditions which can be brought about due to treatment with therapeutic agents (eg. NSAIDs), malignancies or autoimmune rheumatologic conditions. This distinction is crucial when choosing the most appropriate approach for MN patients. In secondary cases, the best strategy consists in treating the underlying disease[11,12], which results in a consequent improvement of the patient's renal condition. On the contrary, in primary forms clinicians would desire a final confirmation of the idiopathic origin of the disease to avoid improper medical investigations and to manage the more correct protocols [11–17]. For these reasons, the discovery of useful biomarkers seems mandatory[19-21]. An important step in this field has been reached by Beck et al. with the identification of circulating auto-antibodies directed against a normally expressed podocyte membrane antigen, the M-type phospholipase A2 receptor (PLA2R), which is present in at least 70% of patients with idiopathic (iMN)[18]. Recently, a further contribution to this field was provided by Tomas et al. with the description of another podocyte membrane antigen, termed thrombospondin type-1 domain-containing 7A (TSHD7A), which was able to account for a further 5% of iMN cases[19]. Alternatively, the evidence of restriction to a particular subtype of immunoglobulins (IgG4) in the context of iMN immunocomplexes and the relative absence of these antibodies in secondary forms may represent another crucial element for the discrimination of iMN subtypes[20]. Such multidisciplinary investigations into MN were traditionally based on immunological, serological and histological tools while proteomic approaches, involving LC-MS, were more recently employed. Furthermore, Matrix Assisted Laser Desorption/Ionisation Mass Spectrometry

Imaging (MALDI-MSI) has been demonstrated on renal biopsies to represent a technique capable of detecting changes within the proteome of glomeruli and tubules affected by different types of glomerulonephritis (GN) such as MN and minimal change disease (MCD) or IgA nephropathy (IgAN) [21,22,23]. This technique is now feasible with formalin-fixed paraffin-embedded (FFPE) renal tissue[24], making the collection of a greater number of patients possible.

In this preliminary study, we analysed FFPE bioptic renal tissue of MN patients aimed at investigating the potentiality of this technique to explore the proteomic alterations that may occur within the glomeruli of primary and secondary forms and to detect preliminary proteomic signatures of this frequently occurring glomerulopathy.

2 MATERIALS AND METHODS

2.1 Patient selection

Twenty patients with a biopsy proven diagnosis of MN, provided between February 2011 and February 2015 at University Milano-Bicocca, San Gerardo Hospital, Monza, Italy, were included in the study that was approved by the ethical board. MN diagnosis was performed after careful histopathological evaluation of renal biopsies. For adequacy purposes, at least 2 core biopsies were taken from each patient, containing an average of at least 10 glomeruli. The routine histological staining procedures were performed, including immunofluorescence and electron microscopy, with all these techniques being considered for the diagnosis. As inclusion criteria for the study, a strong granular parietal staining for IgG and c3 was needed as the ultrastructural confirmation of subepithelial deposits. Cases were staged in a 4-tiered scheme according to the current guidelines[22]. Patients were classified as secondary according to clinical characteristics. The remaining cases were considered to be idiopathic. Moreover, for comparative purposes, one case of focal segmental glomerulosclerosis (FSGS), one case of IgA nephropathy (IgAN), one case of Minimal Change Disease (MCD) and one normal control taken from a

region of normal kidney following total nephrectomy for renal cell carcinoma were enrolled in the study for the MALDI-MSI analysis.

2.2 Materials

Renal biopsies collected for the study underwent standard histological protocols; in particular, core biopsies were fixed for an average time of 12 hours. After the fixation phase, inclusion was performed using an automatic Tissue Processing Centre (TPC 15 Duo/Trio, Medite, MeBurgdorf, German). For every patient of the study, a 4-micron thick section from the corresponding FFPE block was mounted onto an ITO slide (Bruker Daltonik, Bremen, Germany) for MALDI-MSI analysis. 3-micron thick sections were also recruited on polarized slides for immunohistochemistry (IHC).

2.3 Immunohistochemistry

Blank sections were deparaffinised, rehydrated and then stained by the polyclonal mouse antibodies against PLA2R *(0.4 mg/ml, dilution 1:300,* Atlas Antibodies, AlbaNova University Center, Stockholm, Sweden*)* and IgG4 (*0.4 mg/ml, dilution 1:300*, AbNova*)* on a Dako Autostainer (DAKO, Glostrup, Denmark) using a 3,3'-diaminobenzidine (DAB) for PLA2R and 3-amino 9-ethyl *carbazole (3AC,* Vector Labs, DBA ITALIA S.R.L. Segrate, Italy) for IgG4 as previously described[23]. The incubation with the primary antibody in the Autostainer Link 48 (DAKO) was performed after endogenous peroxidase blockage and antigen retrieval. Cases were analysed in blind by three different nephropathologists and scored for the positivity/negativity according to the interpretation criteria shown in Figure 1. IHC results are recorded in Table 1.

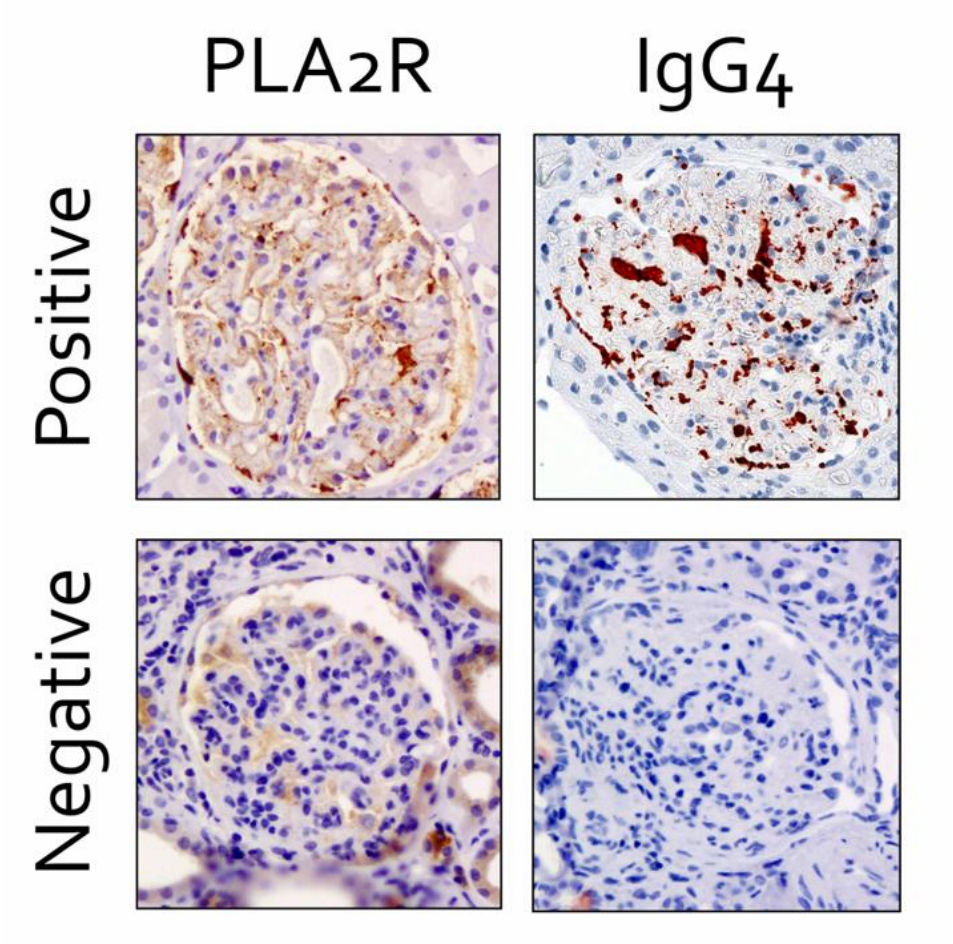

Figure 1: The positivity (top) to PLA2R (left) and IgG4 (right) was marked by the presence of coarse granular staining in a sub-epithelial fashion. On the contrary, in cases where this criterion was absent, the sample was assessed as negative (bottom).

Table 1. IHC results for each case with the relative etiology based on clinical features.

Number of patients	Pathology	Etiology	PLA2R Positivity	IgG4 Positivity
5	MN	Primary	+	-
1	MN	Primary	-	+
7	MN	Primary	+	+
2	MN	Primary	-	-
5	MN	Secondary (LES)	-	-
1	Normal Control	N/A		
1	FSGS	N/A		
1	IgAN	N/A		
1	MCD	N/A		

2.4 MALDI-MSI sample preparation

The slides were stocked at room temperature until the day of the analysis. Paraffin removal and antigen retrieval was performed as previously described[24]. Then, trypsin deposition (Sigma-Aldrich, Chemie Gmbh, Steinheim, Germany, 100 ng/µl) was performed using the iMatrix Spray (Tardo Gmbh, Subingen, Switzerland) automated spraying system and then left in a humid chamber overnight at 40°C. Finally, matrix deposition for MALDI analysis was performed by spraying α-cyano-4-hydroxycinnamic acid (10 mg/ml in 50:50 ACN:H_20 w/0.4% TFA) using the iMatrix Spray (Tardo Gmbh, Subingen, Switzerland) and an optimised method.

2.5 Mass spectrometric analysis

All the mass spectra were acquired in reflectron positive mode in the mass range of *m/z* 750 to 3500 with the UltrafleXtreme (Bruker Daltonik GmbH) MALDI-TOF/TOF MS equipped with a Smartbeam laser operating at 2kHz frequency. External calibration was performed using a mixture of standard peptides within the

mass range of *m/z* 750 to 3500 (PepMix I, Bruker Daltonics). Images were acquired with a laser diameter of 50 μm and a rastering of 50 μm. For MALDI-MS/MS, representative mass spectra were acquired in reflectron positive mode in the mass range of *m/z* 750 to 3500, using the "Random Walk" feature. This was performed in order to confirm whether the ion of interest was still present and of sufficient abundance and in order to obtain the correct mass value to be selected for dissociation. A single precursor ion was selected by using the smallest PCIS (Precursor Ion Selector) window possible and dissociated using laser-induced dissociation (LID) and LIFT™ technology, with the laser energy being set within a range of 40-70%. This process was performed until an MS/MS spectra was obtained from the accumulation of ~100000 laser shots.

After MALDI analysis, the matrix was removed by washing the tissue sections with increasing concentrations of EtOH (70% and 100%) and the slides stained with Periodic Acid-Schiff. The slides were converted to digital format using a ScanScope CS digital scanner (Aperio, Park Center Dr., Vista, CA, USA), thus allowing the direct overlap of images and the integration of proteomic and morphologic data.

2.6 Data analysis

The raw MALDI-MSI data were elaborated as previously described[23]. Briefly, FlexImaging 3.0 (Bruker Daltonics, Bremen, Germany) data, containing spectra of each entire measurement region, were imported into SCiLS Lab 2014 software (http://scils.de/; Bremen, Germany) to perform pre-processing: baseline subtraction (TopHat algorithm), normalisation (Total Ion Current algorithm). Average (avg) spectrum representative of the whole measurement region was obtained by peak picking, alignment and spatial denoising. Reproducibility of our method was evaluated based on number of peaks and Coefficient of Variation (CV) of their intensity. Principal Component Analysis (PCA) was also performed to reduce the high complexity of the data. Finally, Receiver Operative Characteristic (ROC) analysis was performed, with an AUC of ≥ 0.7 being required, as an additional criterion to the $p<0.05$, for a peak to be considered as statistically significant.

In order to perform further statistical analysis, the peak list for each MN patient was exported in comma separated value (CSV) format and imported into R (https://www.r-project.org/). Feature selection was performed using Recursive Feature Elimination (RFE), fixing the selection to a maximum number of 20 features. The algorithm recursively chooses a subset of features and evaluates the classification performances of a Partial Least Squares (PLS) classifier, which is subjected to a 5-time 10-fold cross-validation. At the end, the RFE algorithm calculates a weight (variable importance) for each feature, computed by averaging the weights for the models across all resamples, which is directly correlated with the impact that each feature has onto the classification. Finally, the best 20-feature subset is used to build a classification model using a Support Vector Machine (SVM) algorithm with Radial Basis Kernel function, which performances are evaluated by a 5-time 10-fold cross-validation.

For MALDI-MS/MS spectra, baseline subtraction and smoothing were performed using FlexAnalysis 3.4 (Bruker Daltonics, Bremen, Germany). All MS/MS spectra were searched against the Swiss-Prot database (Release 2015_05 of 29-Apr-15) with the Mascot 2.4 search engine (Matrix Science, London, UK). Mass tolerances were set at 0.2 Da for MS and 1.3 Da for MS/MS Trypsin was set as the enzyme, allowing for one partial cleavage. No fixed post-translational modifications were set in the search parameters.

3 RESULTS

3.1 MALDI-MSI reproducibility

Initially, the analytical reproducibility of the protocol applied to FFPE renal biopsies was evaluated. Three bioptic specimens from the same MN patient were analysed on three different days (Figure 2). Average mass spectra for each replicate were generated within the m/z 1000 to 2500 mass range. The number of signals detected, with a signal-to-noise ratio (S/N) of 5, in each replicate were similar, being 477, 510

and 473, respectively. Furthermore, the mean CV of every signal intensity present in the spectra were 30, 28 and 29%, respectively.

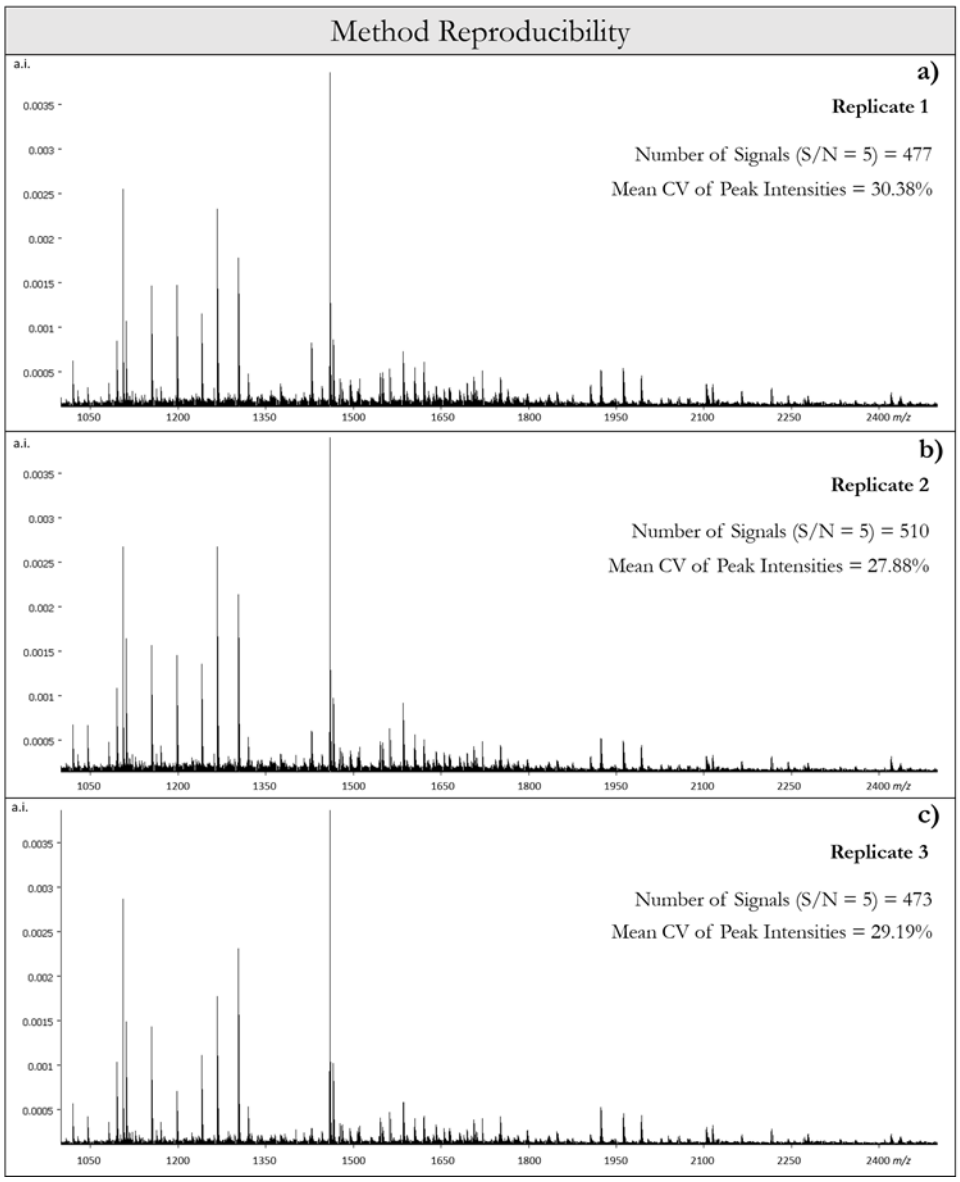

Figure 2: (A-C) Average mass spectra generated in the m/z 1000 to 2500 mass range from three bioptic specimens taken from the same patient. Relative intensity is expressed in arbitrary units (a.i.). The number of signals (S/N = 5) and Coefficient of Variation (CV) of the peak intensities for each specimen is listed on each individual spectrum.

Then, average tryptic peptide profiles from a normal control, MN and other GN (FSGS, IgAN and MCD) patients were generated within the m/z 1000 to 2000 mass range (Figure 3). The tryptic peptide profiles from the normal control, MN and other GN patients (Figure 3; a, b & c) were distinctly different, with several ions of differing intensity, indicating that alterations to the tissue proteome related with the presence of the disease could be easily detected even in average spectra obtained from the whole tissue section. On the contrary, the spectral diversity between MN and other forms of GN was not so evident (Figure 3; b & c).

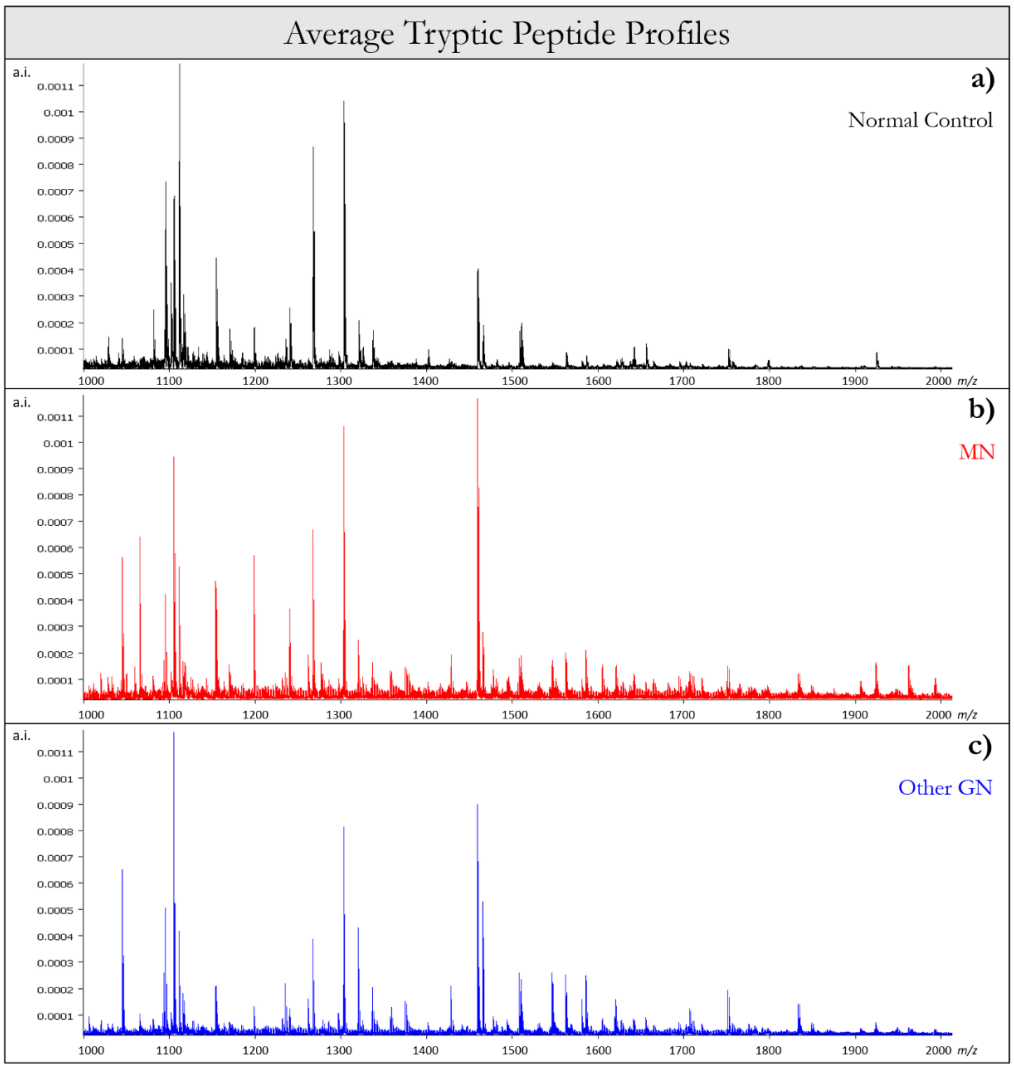

Figure 3. Average tryptic peptide profiles for (A) normal controls, (B) MN and (C) Other GN (FSGS, IgAN and MCD. in the m/z 1000 to 2000 mass range. Relative intensity is expressed in arbitrary units (a.i.).

3.2 Proteomic signatures of primary MN: Positivity to currently known antigens

15 cases were considered to be primary (idiopathic) on the base of clinical features (Table 1). Moreover, through the application of IHC, 7 were positive to both IgG4 and PLA2R, 6 were positive to either PLA2R or IgG4 and the remaining 2 cases were negative to both (double-negative).

In order to evaluate whether the tissue proteome of iMN patients was altered in correspondence with their positivity to the currently known antigens (PLA2R and IgG4), average tryptic peptide profiles were generated in the *m/z* 1000 to 2000 mass range for patients who were determined to be positive only to PLA2R and those positive to both PLA2R and IgG4 (Figure 4; a and b). Following ROC analysis performed within SCiLS Lab, three statistically significant signals were detected, *m/z* 1303, 1459 and 1923 (Figure 4 and Table 2).

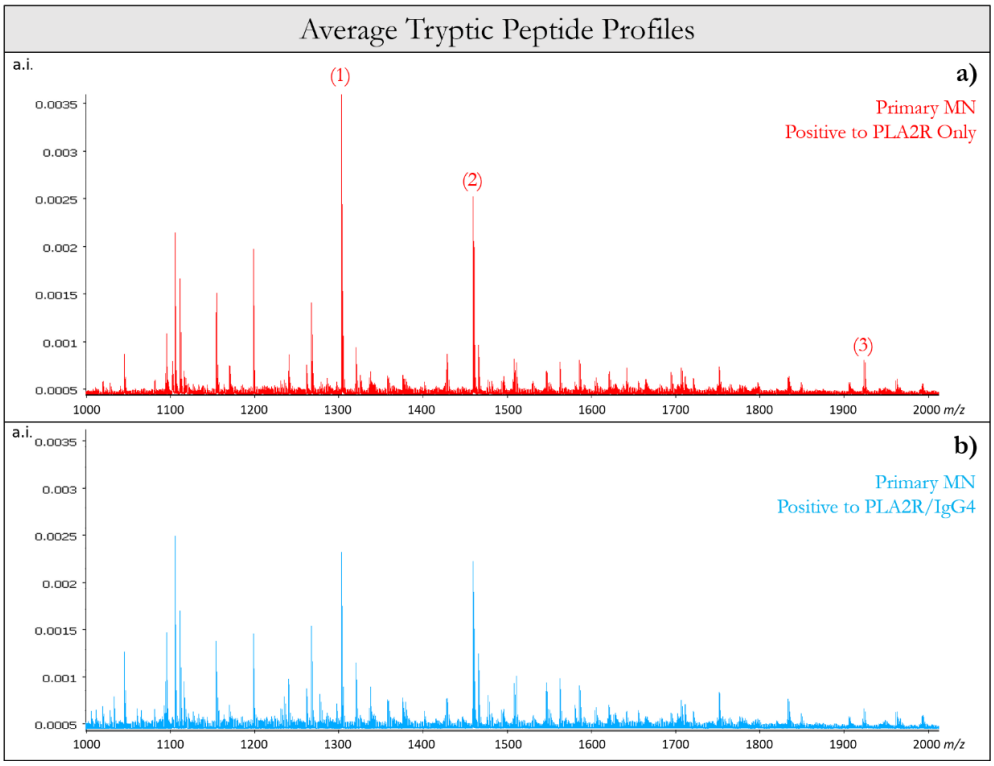

Figure 4. (A and B) Average tryptic peptide profiles for primary MN patients positive only to PLA2R (A) and primary MN patients positive to PLA2R and IgG4 (B) in the m/z 1000 to 2000 mass range. Relative intensity is expressed in arbitrary units (a.i.). Differentiating peaks (AUC≥0.7) are denoted by numbers in parentheses.

Table 2. Discriminatory ions highlighted by ROC analysis between primary MN patients positive to currently known antigens (PLA2R v PLA2R/IgG4). Numbers in parentheses denote the corresponding signals marked in Figure 4.

m/z	AUC Value	Relative Intensity Levels
(1) 1303	0.76	Up +Ve PLA2R Only
(2) 1459	0.70	Up +Ve PLA2R Only
(3) 1923	0.71	Up +Ve PLA2R Only

In order to highlight further possible proteomic indicators of iMN and to verify the discriminative power of the signals detected using ROC analysis, the peak lists from these patients were used to build a cluster of peptides with the best capability to distinguish these two groups. RFE feature selection was performed on the entire dataset and the top-ten ranked features, along with their relative weight, are listed in Table 3. Interestingly, the two top ranked features (*m/z* 1303 and 1459) were also among the three most statistically significant ions detected by ROC analysis (Table 2). Cross-validation of these features in a training model that employed a SVM algorithm with Radial Basis Kernel led to a classification accuracy of 85%.

Table 3. Top-ten weighted ions highlighted by Recursive Feature Elimination (RFE) between primary MN patients positive to currently known antigens (PLA2R v PLA2R/IgG4).

Feature (*m/z*)	Relative Weight	Rank
1303	100.00	1
1459	78.08	2
1045	45.98	3
1268	32.95	4
1111	31.46	5
1198	28.15	6
1155	25.24	7
1033	18.72	8
1277	18.16	9
1102	16.81	10

3.3 Proteomic signatures of primary MN: Negativity to currently known antigens

A preliminary investigation was also performed in order to evaluate whether further tissue proteome alterations could be observed in those patients who were negative to the currently known antigens (PLA2R and IgG4). Average tryptic peptide profiles were generated in the *m/z* 1000 to 2000 mass range for patients who were determined to be positive to one of either, or both, PLA2R and IgG4 and those who were negative to both (double negative) (Figure 5; a & b). Following ROC analysis, four statistically significant signals were detected, *m/z* 1094, 1116, 1381 and 1459 with an AUC value $\geq$0.7 (Figure 5 and Table 4). Interestingly, the ion at *m/z* 1459 was again statistically significant and presented a higher intensity in the group of patients who were double negative, with an AUC value of 0.70 than in those positive to PLA2R/IgG4.

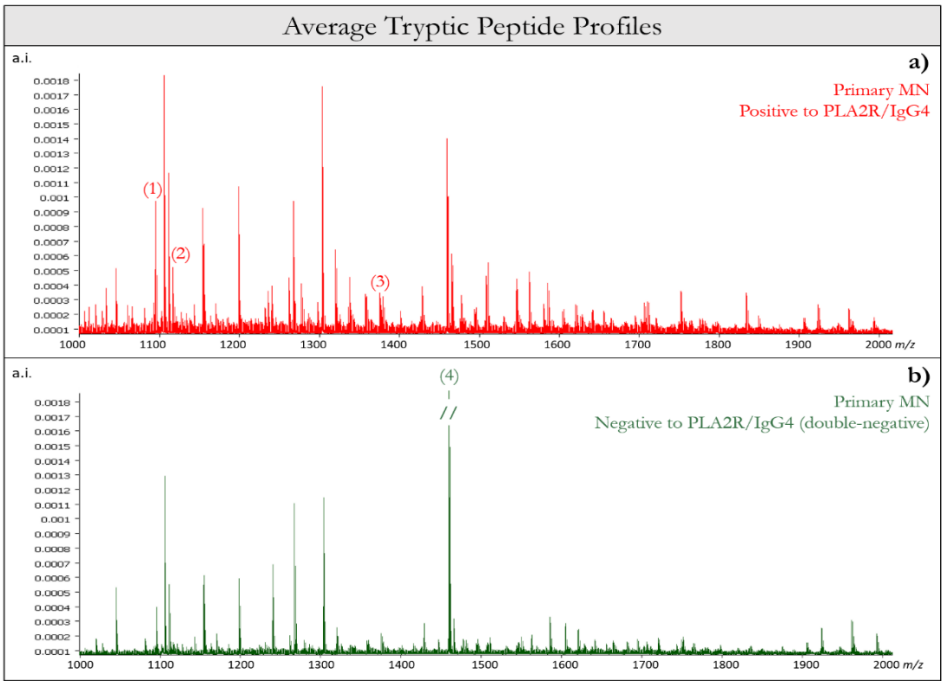

Figure 5. (A and B) Average tryptic peptide profiles for primary MN patients positive to PLA2R/IgG4 (A) and primary MN patients negative to PLA2R/IgG4 (double-negative) (B) in the m/z 1000 to 2000 mass range. Relative intensity is expressed in arbitrary units (a.i.). Differentiating peaks (AUC≥0.7) are denoted by numbers in parentheses.

Table 4. Discriminatory ions highlighted by ROC analysis when comparing primary MN patients positive to currently known antigens (PLA2R/IgG4) with those negative to currently known antigens (double-negative). Numbers in parentheses denote the corresponding signals marked in Figure 5.

m/z	AUC Value	Relative Intensity Levels
(1) 1094	0.79	Up +Ve PLA2R/IgG4
(2) 1116	0.75	Up +Ve PLA2R/IgG4
(3) 1381	0.71	Up +Ve PLA2R/IgG4
(4) 1459	0.70	Up -Ve PLA2R/IgG4 (double-negative)

The peak lists from these patients were again imported into R and RFE feature selection was performed on the entire dataset. The top-ten ranked features, along with their relative weight, are listed in Table 5. Cross-validation of these features within a training model could not be performed due to the limited number of patients within the double negative group.

Table 5. Top-ten weighted ions highlighted by Recursive Feature Elimination (RFE) when comparing primary MN patients positive to currently known antigens (PLA2R/IgG4) with those negative to currently known antigens (double-negative).

Feature (*m/z*)	Relative Weight	Rank
1459	100.00	1
1303	66.36	2
1154	29.17	3
1095	29.01	4
1240	29.00	5
1198	28.18	6
1465	27.44	7
1111	26.38	8
1105	25.54	9
1268	23.16	10

3.4 Proteomic signatures of primary and secondary MN

Firstly, unsupervised PCA was performed on the entire MN dataset in order to highlight any proteomic differences between primary and secondary forms. The Scores Plot clearly showed that spectra related to primary and secondary MGN presented distinctly different distributions (Figure 6c). Then, average tryptic peptide profiles of the entire cohort of patients affected by primary and secondary MN, respectively, were built within *the m/z* 1000 to 2000 mass range *(*Figure 6*; a & b).*

Several signals (*m/z*) had a statistically significant intensity ($p<0.05$ and AUC>0.8) when the average spectrum of primary MN was compared to that of secondary MN. Among them, the ion at *m/z* 1459 had the greatest discriminatory power between the two groups, with an AUC value >0.85. Its relative intensity was significantly higher in primary MN than in secondary MN (Figure 6d).

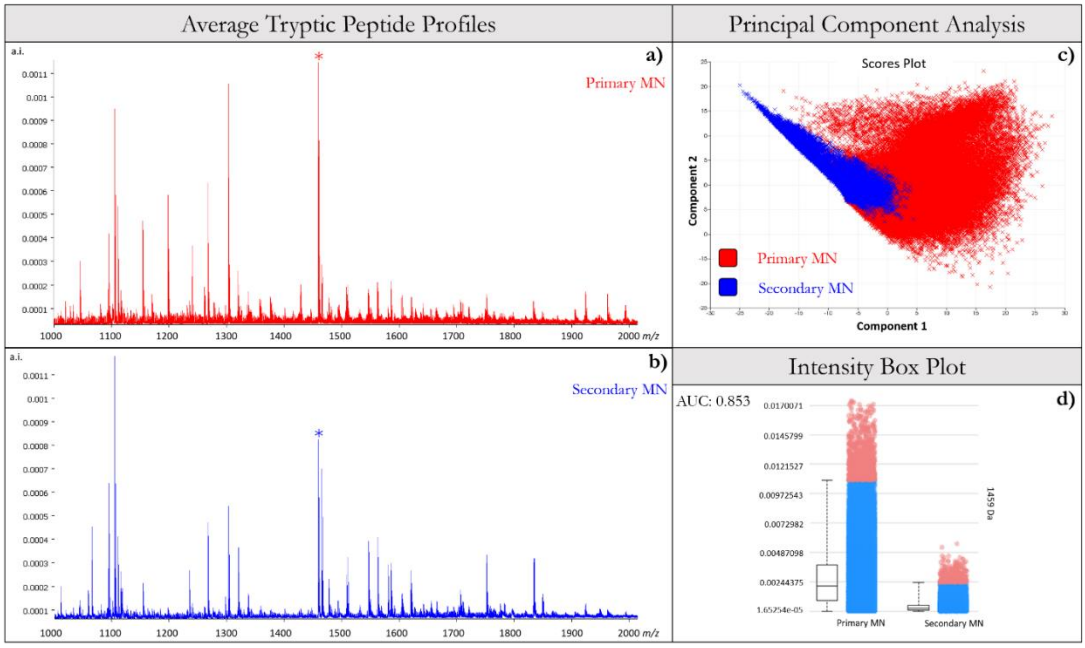

Figure 6. (A and B) Average tryptic peptide profiles for primary (A) and secondary MN (B) in the m/z 1000 to 2000 mass range. Relative intensity is expressed in arbitrary units (a.i.). The peak at m/z 1459 is denoted by an asterik. (C) Two-dimensional principal component analysis scores plot presenting the distribution of spectra from primary (Red) and secondary MN (Blue). (D) Intensity box plot indicating the relative intensity levels of m/z 1459 in primary (left bar) and secondary MN (right bar).

Given this discriminatory power, the identity of this ion was investigated by acquiring MS/MS spectra by MALDI-TOF/TOF. The signal at *m/z* 1459 was identified as a tryptic peptide fragment of Serine/threonine-protein kinase MRCK gamma (K.VIGRGAFGEVTVVR.Q) with a Mascot score of 31. Co-registration of the proteomic MALD-MSI information with the histological image highlighted that the higher relative intensity of this ion was localised to the glomeruli of iMN patients

that were affected by the disease (Figure 7a). In the secondary form, the relative intensity of the ion was far lower in glomeruli that were affected by the disease (Figure 7b). The relative intensity and isolation of the other discriminatory signals was not sufficient to obtain MS/MS spectra that could provide a positive identification.

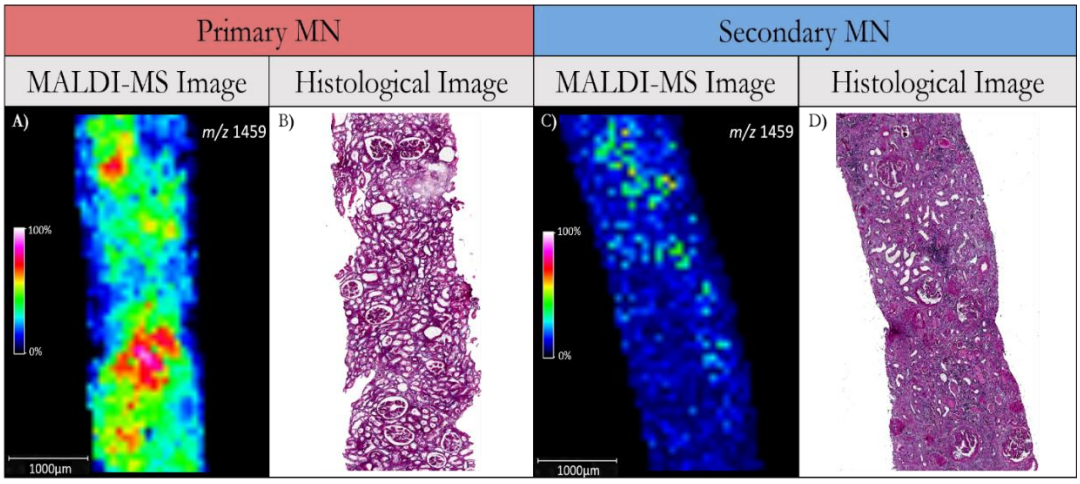

Figure 7. The molecular distribution of m/z 1459 (Serine/threonine-protein kinase MRCK gamma) obtained using MALDI-MSI in primary (A) and secondary MN (C) along with their corresponding histological image following staining with Periodic Acid-schiff (B and D).

DISCUSSION

MALDI-MSI may represent an ideal tool useful for determining proteomic indicators of MN in FFPE tissue. These indicators could then be used to more easily distinguish the primary and secondary forms of this glomerulopathy, as well as further stratify those iMN patients that are negative to the currently known antigens. This technique has already been reported to be capable of providing specific proteomic profiles for pathological glomeruli and tubules that have been affected by GN[22], as well being able to characterise particular glomerular lesions that may be associated with disease progression[23]. It is by combining this approach with the potential to analyse FFPE tissue[24] that we focused our attention on MN, investigating the potentiality of this

technique to explore the proteomic alterations that may occur within the kidney of primary and secondary MN patients with this pilot study.

Therefore, we employed a MALDI-MSI approach to analyse FFPE renal biopsies of a small cohort of patients. Initially, the analytical features of the protocol were evaluated prior to the analysis of the entire sample cohort. Three bioptic specimens from the same MN patient were analysed on three different days. Results showed a good level of reproducibility, both in terms of the number of signals as well as their intensity, in particular considering that these bioptic specimens were heterogeneous (incorporating glomerular and tubulointerstitial regions) and, thus, varying signal intensities are to be expected (Figure 2). Furthermore, the comparison of a normal subject with MN and other GN (FSGS, IgAN and MCD) patients (Figure 3) highlighted that proteomic alterations due to the presence of GN could also be detected, indicating that this approach was both robust as well as capable of extracting pathologically significant information that could be used to further categorise MN patients.

From a proteomic standpoint, those patients who were positive only to PLA2R and those who were also positive to IgG4 were distinguishable, with statistically significant signals at *m/z* 1303, 1459 (Serine/threonine-protein kinase MRCK gamma) and 1923 being of a higher intensity in those patients who were only positive to PLA2R (Figure 4 & Table 2). Employing these signals, in addition to a number of further features (*m/*z) that were selected using RFE (Table 3), a model was built using SVM with Radial Basis Kernel in a training phase. Encouraging results were observed when cross-validation was performed on this small cohort of patients (classification accuracy of 85%*)*, thus suggesting the possibility that this technology can provide clinical information for this disease. Primarily, these findings further highlighted the reliability of our approach, given that the proteomic information obtained reflected the IHC findings. More speculatively, however, these results may indicate that the immunocomplexes implicated in iMN may be driven by, or may lead to, renal tissue alterations at the molecular level.

It is on this basis of this approach that we aimed to investigate the potential of detecting proteomic alterations in those iMN patients who were negative to the currently known antigens. There were a number of statistically significant signals, *m/z* 1094, 1116, 1381 and 1459 (Serine/threonine-protein kinase MRCK gamma), that presented differing levels of intensity in patients positive to PLA2R/IgG4 and double-negative patients (Figure 5 & Table 4). Two of these signals (*m/z* 1459 and 1094) were again highlighted by RFE feature selection, further demonstrating their reliability. In this particular cohort of iMN patients, only two were double-negative, which reflects the natural occurrence of this iMN form with respect to the number of iMN patients enrolled in this study. Therefore, a greater number of double-negative iMN patients needs to be analysed before these findings could be translated in a more reliable and definitive manner. It is important to consider, however, that the tissue samples employed for the MALDI-MSI analysis were derived from the same FFPE blocks used within the diagnostic workflow and, thus, they represent scant and precious material. Notwithstanding this information, however, these findings provide a preliminary platform for more in-depth MALDI-MSI investigations and the signals detected here may represent possible proteomic signatures that could be used to further stratify this frequently occurring and difficult to correctly diagnose glomerulopathy.

Comparing primary with secondary MN, both through the means of spectral comparison and unsupervised PCA, highlighted that these forms of MN presented distinct protein signatures. The PCA score chart (Figure 6c) containing spectra from the entire cohort of primary and secondary MN patients presented distinct spectral distributions that were associated with each form. These proteomic differences were further evident in the generated average spectra (Figure 6; a & b). There were a number of signals whose relative intensity varied significantly between the two forms of MN. In particular, one ion, m/z 1459, provided the highest AUC value (0.853) when attempting to compare these two groups of patients using ROC analysis and had a much higher relative intensity in the primary MN group (Figure 6d). This signal at m/z 1459 was later identified by MALDI/TOF/TOF as a tryptic peptide fragment

of Serine/threonine-protein kinase MRCK gamma. Through the correlation of the MALDI-MSI image with its histological counter-part we were able to visualise that the highest relative intensity of this signal correlated with glomeruli that were affected by the glomerulopathy in primary MN, whereas these increased levels of intensity were not noted in the effected glomeruli in secondary MN patients (Figure 7)

Serine/threonine kinase MRCK gamma belongs to the Cell division control protein 42 binding protein (CDC42BP) family, a kinase group of proteins that has been previously studied[25]. In particular, they seem responsible for cytoskeleton re-organization, especially in the heart and skeletal muscle, since they are downstream to the Rho/Rac/Cdc42 group of kinases that are crucially involved in actin filament phosphorylation and assembly [26,27]. Although their role in glomerular cells has not been previously fully investigated, it seems that their over expression can lead to the phosphorylation of downstream proteins, altering actin dynamics with a consequent effacement of podocyte foot processes, disruption of the glomerular filtration barrier and development of nephrotic syndrome[28]. In this study, the over expression of this antigen in primary cases can be mainly related to the pathophysiology of the podocyte damage, representing the epiphenomenon of the clinical syndrome of these patients. In particular, the relatively higher presence of this antigen in idiopathic forms, as compared with secondary ones, might be explained by the presence of different pathways of glomerular dysfunction. However, a more consistent case series, including secondary cases other than lupus nephritis related MN, is required in order to investigate the role of the antigen and its relative pathogenetic meaning, as well as the reason for its different expression in the groups of MN considered.

In terms of prospective work, the primary objective should be to increase the number of samples, in particular double-negative iMN patients, in order to further investigate the preliminary proteomic signatures obtained in this initial body of work with greater statistical power. Furthermore, the identity of the ions with discriminatory capabilities, once proved, could be obtained. This would enable a greater understanding of the molecular alterations at play during the development of MN

and, potentially, provide complementary information to that already available regarding the stratification of iMN patients[18,19]. Finally, secondary cases of MN different from those related to lupus nephritis need to be analysed with this technique in order to further demonstrate the different expression of the putative ion identified here and, eventually, to find further differences that may help in the diagnostic workup.

CONCLUSION

In conclusion, MALDI-MSI was able to generate molecular signatures of primary and secondary MN, with reliable technical performances, using FFPE specimens. The positive results obtained with this proteomic approach facilitated the detection of a number of signals that could differentiate the different forms of iMN that were positive to PLA2R or IgG4 and to distinguish these patients from those who were negative to both, encouraging the prosecution of further investigations. These signals could potentially represent future targets to be investigated as proteomic markers for the further stratification of iMN patients once verified on a larger cohort of patients.

ACKNOWLEDGMENTS

The author wishes to thank all the centres that participated to the work providing bioptic material (Renal Unit, Santa Marta e Santa Venera Hospital, Acireale, Catania, Italy; Nephrology Department, Bassini Hospital, Cinisello Balsamo, Milan, Italy; Nephrology Department, ASST Lodi, Lodi, Italy) as well as Carla Scalia and Lorella Riva for their precious contribution in the sample processing and IHC staining.

The research leading to these results has received funding from the European Union's Seventh Framework Programme FP7/ 2007-2013 under grant agreement N^{o} 305739. This work was also supported by grants from the MIUR: FIRB 2007 (RBRN07BMCT_11), FAR 2012–2015; and in part by Fondazione Gigi & Pupa Ferrari Onlus.

REFERENCES

1. Black DA, Rose G, Brewer DB. Controlled trial of prednisone in adult patients with the nephrotic syndrome. *Br Med*. 1970;**3**:421-426.

2. Medawar W, Green A, Campbell E, et al. Clinical and histopathologic findings in adults with the nephrotic syndrome. *Ir J Med Sci*. 1990;**159**(5):137-140.

3. Falagas ME, Vardakas KZ,Vergidis PI. Under-diagnosis of common chronic diseases: prevalence and impact on human health. *Int J Clin Pr*. 2007;**61**:1659-1579.

4. Bethesda M. *United States Renal Data System. USRDS 2013 Annual Data Report: Atlas of Chronic Kidney Disease and End-Stage Renal Disease in the United States. National Institutes of Health. National Institute of Diabetes and Digestive and Kidney Diseases. 2013*.; 2013.

5. Obrador GT, Pereira BJG, Kausz AT. Chronic kidney disease in the United States: an underrecognized problem. *Semin Nephrol*. 2002;**22**(6):441-448.

6. Ronco P, Debiec H. Anti-phospholipase A2 receptor antibodies and the pathogenesis of membranous nephropathy. *Nephron Clin Pract*. 2014;**128**(3-4):232-237. doi:10.1159/000368588.

7. Hsu HC, Lin GH, Chang MH, Chen CH. Association of hepatitis B surface (HBs) antigenemia and membranous nephropathy in children in Taiwan. *Clin Nephrol*. 1983;**20**:121-129.

8. Slusarczyk J, Michalak T, Nazarewicz-de Mezer T, Krawczyński K.,Nowosławski A. Membranous glomerulopathy associated with hepatitis B core antigen immune complexes in children. *Am J Pathol*. 1980;**98**:29-43.

9. Takekoshi Y, Tanaka M, Shida N, Satake Y, Saheki Y, Matsumoto S. Strong association between membranous nephropathy and hepatitis-B surface antigenaemia in Japanese children. *Lancet*. 1978;**2**:1065-1068.

10. Kleinknecht C, Levy M, Gagnadoux MF, Habib R. Membranous glomerulonephritis with extra-renal disorders in children. *Med*. 1979;**58**:219-228.

11. Matsui S, Tsuji H, Takimoto Y, Ono S. Clinical improvement of membranous nephropathy after endoscopic resection of double early gastrointestinal cancers. *Clin Exp Nephrol*. 2011;**15(**2):285-288. doi:10.1007/s10157-010-0389-6.

12. Zheng XY, Wei RB, Tang L, Li P, Zheng XD. Meta-analysis of combined therapy for adult hepatitis B virus-associated glomerulonephritis. *World J Gastroenterol WJG*. 2012;**18**(8):821-832. doi:10.3748/wjg.v18.i8.821.

13. Ponticelli C, Zucchelli P, Passerini P, Cagnoli L, Cesana B, Pozzi, C, Pasquali S, Imbasciati E, Grassi C, Redaelli B, et al. A randomized trial of methylprednisolone and chlorambucil in idiopathic membranous nephropathy. *N Engl J Med*. 1989;3**20**:8-13.

14. Ponticelli C, Zucchelli P, Imbasciati E, Cagnoli L, Pozzi C, Passerini P, Grassi C, Limido D, Pasquali S, Volpini T, et al. Controlled trial of methylprednisolone and chlorambucil in idiopathic membranous nephropathy. *N Engl J Med*. 1984;**310**:946-950.

15. Ponticelli C, Zucchelli P, Passerini P, Cesana B, Locatelli F, Pasquali S, Sasdelli M, Redaelli B, Grassi C, Pozzi C, et al. A 10-year follow-up of a randomized study with methylprednisolone and chlorambucil in membranous nephropathy. *Kidney Int*. 1995;**48**:1600-1604.

16. Ponticelli, C, Zucchelli P, Passerini P, Cesana B. Methylprednisolone plus chlorambucil as compared with methylprednisolone alone for the treatment of idiopathic membranous nephropathy. The Italian Idiopathic Membranous Nephropathy Treatment Study Group. *Engl J Med*. 1992;**327**:599-603.

17. Branten AJ, Reichert LJ, Koene RA, Wetzels JF. ral cyclophosphamide versus chlorambucil in the treatment of patients with membranous nephropathy and renal insufficiency. *QJM Mon J Assoc Physicians*. 1998:359-366.

18. Beck LH, Bonegio RGB, Lambeau G, et al. M-type phospholipase A2 receptor as target antigen in idiopathic membranous nephropathy. *N Engl J Med*. 2009;**361**(1):11-21. doi:10.1056/NEJMoa0810457.

19. Tomas NM, Beck LH, Meyer-Schwesinger C, et al. Thrombospondin type-1 domain-containing 7A in idiopathic membranous nephropathy. *N Engl J Med*. 2014;**371**(24):2277-2287. doi:10.1056/NEJMoa1409354.

20. Debiec H, Ronco P. Immunopathogenesis of membranous nephropathy: an update. *Semin Immunopathol*. 2014;**36**(4):381-397. doi:10.1007/s00281-014-0423-y.

21. L'Imperio V, Smith A, Chinello C, Pagni F, Magni F. Proteomics and glomerulonephritis: A complementary approach in renal pathology for the identification of chronic kidney disease-related markers. *Proteomics Clin Appl*. 2015:371-383. doi:10.1002/prca.201500075.

22. Mainini V, Pagni F, Ferrario F, et al. MALDI imaging mass spectrometry in glomerulonephritis: Feasibility study. *Histopathology*. 2014;**64**(6):901-906. doi:10.1111/his.12337.

23. Smith A, L'Imperio V, De Sio G, et al. alpha-1-antitrypsin detected by MALDI-Imaging in the study of glomerulonephritis: its relevance in chronic kidney disease progression. *Proteomics*. 2016:1-8. doi:10.1002/pmic.201500411.

24. De Sio G, Smith AJ, Galli M, et al. A MALDI-Mass Spectrometry Imaging method applicable to different formalin-fixed paraffin-embedded human tissues. *Mol Biosyst*. 2015;**11**(6):1507-1514. doi:10.1039/c4mb00716f.

25. Talman V, Gateva G, Ahti M, Ekokoski E, Lappalainen P, Tuominen RK. Evidence for a role of MRCK in mediating HeLa cell elongation induced by the C1 domain ligand HMI-1a3. *Eur J Pharm Sci*. 2014;**55**(1):46-57. doi:10.1016/j.ejps.2014.01.002.

26. Nakamura N, Oshiro N, Fukata Y, et al. Phosphorylation of ERM proteins at ® lopodia induced by. 2000;**1**:571-582.

27. Tan I, Ng CH, Lim L, Leung T. Phosphorylation of a Novel Myosin Binding Subunit of Protein Phosphatase 1 Reveals a Conserved Mechanism in the Regulation of Actin Cytoskeleton. *J Biol Chem*. 2001;**276**(24):21209-21216. doi:10.1074/jbc.M102615200.

28. Teng B, Lukasz A, Schiffer M. The ADF/cofilin-pathway and actin dynamics in podocyte injury. *Int J Cell Biol*. 2012;2012. doi:10.1155/2012/320531.

Chapter 5

Summary, conclusions and future perspectives

1 SUMMARY

Glomerulonephritis (GN), such as membranous glomerulonephritis (MGN), focal segmental glomerulosclerosis (FSGS) and IgA nephropathy (IgAN) represent the most frequent primary Glomerular Kidney Diseases (GKDs) worldwide and are a common cause of end-stage renal disease (ESRD). Without the correct diagnosis and, ultimately, the correct selection of therapeutic treatment, the patient has a higher probability of progressing to ESRD and requiring dialysis or transplantation. Although the renal biopsy currently remains the gold standard for the routine diagnosis of idiopathic GN, the invasiveness and difficulty of diagnoses related with this procedure means that there is a strong need for the detection of diagnostic and prognostic biomarkers that can be translated into less invasive diagnostic tools. In this context, various proteomic techniques have played a crucial role in determining the molecular changes related to disease progression and early pathological glomerular modifications[1,2].

Matrix-Assisted Laser Desorption/Ionisation-Mass Spectrometry is a modern proteomic technology that is capable of detecting several different classes of compounds (proteins, lipids, drugs, etc.) directly in situ. In profiling mode (MALDI-MSP), various macro areas of tissue (e.g. tumour and normal tissue) are analysed to obtain their specific protein profiles. These protein profiles can be then compared to highlight differences. In Imaging mode (MALDI-MSI), the spatial distribution of proteins can be used to build a molecular image of the tissue. MALDI-MSI enables one to rebuild the image of the tissue, based upon the intensity of the ions and their localisation, that can be correlated with pathological alterations in patient tissue. Therefore, MALDI-MSI represents a unique tool that combines the analytical power of mass spectrometry with traditional optical microscopy. The majority of clinical MSI investigations have been performed on numerous forms of cancers; i.e. brain gliomas, breast, colon, lung, ovarian, prostate, as well as in the case of neurological disorders; i.e. Parkinson's and Alzheimer's disease[3]. Consequently, MALDI-MSI could also be the ideal tool for detecting new, specific, diagnostic markers of glomerular diseases.

The application of MALDI-MSI directly on bioptic renal tissue in order to highlight differences in protein expression among a wide range of glomerular conditions represents a new stimulating perspective in the field of nephropathology[4]. Through the correlation of molecular with histological information, along with the direct collaboration with nephropathologists, facilitates the detection of specific proteomic indicators that are directly correlated with the pathological alterations that occur within the glomeruli, or tubules, during the development of glomerulonephritis. Given the small amount of tissue made available through the bioptic procedure (renal biopsies are commonly ~10mm in length and ~3mm in diameter), correlation with the histological features represents a crucial step in the study of glomerular diseases.

The initial line of work presented in this thesis focused on the development and optimisation of a protocol that would facilitate the routine MALDI-MSI analysis of formalin-fixed paraffin-embedded (FFPE) tissue. The ultimate aim of this initial phase was to enable the utilisation of large collections of clinically annotated samples and permit the preservation of tissue specimens that were stored at room temperature for long periods of time, capabilities that are imperative in multi-centric studies where the sharing of samples between centres with different expertise is commonplace. Following in this vein, the main body of work encompassed in this thesis involved the application of MALDI-MSI to renal biopsies, both fresh-frozen and FFPE, in order to generate proteomic signatures of the most common forms of GN and to detect potential molecular markers associated with Chronic Kidney Disease (CKD) progression. The positive results obtained with this proteomic approach facilitated the detection of a number of protein signals that could differentiate the different forms of GN, both in fresh-frozen and FFPE tissue, and such signals could potentially represent future targets to be investigated as diagnostic or prognostic markers of the most common glomerular diseases.

2 CONCLUSIONS

2.1 MALDI-Mass Spectrometry Imaging method applicable to different formalin-fixed paraffin-embedded human tissues

The results presented in this work highlight that the MALDI-MSI analysis of clinical FFPE tissue specimens is feasible. Not only this, the presented protocol is highly reproducible and applicable to a wide variety of different tissue types, thus making it highly appropriate for clinically relevant studies that require the comparison between large numbers of patients. Furthermore, the maintenance of analyte localisation during the procedure is of paramount importance and indicates that when in performed in combination with next-generation MALDI-MSI instruments, high spatial resolutions (<20µm) would be achievable.

Notwithstanding the fact that the findings presented in this work would not be directly translated into direct use within the clinics, the potential to analyse FFPE samples opens up numerous doors for clinically-relevant studies. Given that FFPE is the routine fixation method within clinical centres, the potential to analyse these samples means that much larger sample cohorts can be obtained and the easy transfer of samples between multinational partners becomes feasible. This is of paramount importance when attempting to obtain statistically robust findings that can be reliable and ultimately translated into information that can be exploited within the clinics for diagnostic or prognostic purposes.

2.2 α-1-antitrypsin detected by MALDI-Imaging in the study of glomerulonephritis: its relevance in chronic kidney disease progression

In conclusion, this study shows a promising application of MALDI-MSI in the discovery of biomarkers for the assessment of CKD progression. Furthermore, it highlights the potential to correlate tissue findings with those obtained from urine using complimentary mass spectrometric techniques. This overcomes a significant obstacle with regards to obtaining results that could be translated into the clinic, as it indicates that the highly specific markers obtained through MALDI-MSI can then be detected in lowly-invasive, and inherently variable, biological samples such as urine.

More specifically, this technology could translate molecular knowledge obtained directly in tissue into routine clinical practice, such as the successful application of the CKD 273 classifier that is based on CE-MS tools[5].

Additionally, the localisation of A1AT within the sclerotic glomeruli, as highlighted by IHC, reveals that this protein could be related with the so-called "podocyte stress theory"[6-8] and the emerging fibrogenic role of different biomarkers in glomerulosclerosi[9,10]. Due to some limitations of our study related with the small number of cases analysed, further similar studies are needed for a definitive confirmation of this hypothesis and to validate the role of A1AT in GKDs. Notwithstanding this, A1AT represents a promising potential marker of GKD progression.

2.3 The putative role of MALDI-MSI in the study of Membranous Nephropathy

The application of MALDI-MSI to FFPE renal biopsies showed a good level of analytical reproducibility, both in terms of the number of signals as well as their intensity, when analytical reproducibility was evaluated. This was an important finding when regarding this particular approach, especially given the various potential sources of specimen variability, including homogeneity of the trypsin and matrix deposition as well as the length of storage following formalin-fixation and paraffin-embedding. This aspect becomes even more imperative when considering the nature of the tissue being analysed, as the limited amount of tissue provided by renal biopsy and the small dimensions of the morphological features being investigated (< 150µm) means that analyte localisation and extraction is of utmost importance.

MALDI-MSI was able to generate molecular signatures of primary and secondary MN, with one particular signal (m/z 1459), identified as Serine/threonine-protein kinase MRCK gamma, being over-expressed in the glomeruli of primary MN patients with respect to secondary MN. Furthermore, this proteomic approach detected a number of signals that could differentiate the different forms of iMN that were

positive to PLA2R or IgG4 as well as a further set of signals (m/z 1094, 1116, 1381 and 1459) that distinguish these patients from those who were negative to both. These signals could potentially represent future targets to be investigated as proteomic markers for the further stratification of iMN patients.

This preliminary study represents the first example of MALDI-MSI being applied to FFPE renal biopsies in order to study the tissue proteome of MN. The positive results obtained with this proteomic approach facilitated the detection of a number of signals that could differentiate the different forms of iMN that were positive to PLA2R or IgG4 as well as distinguish primary from secondary MN.

The work of Beck et al.[11,12] presented a large step forward in the diagnosis of MN, however, there is still the strong need for further markers that can be used to stratify primary MN patients. Detecting such molecular markers would represent a large step forward in the field of nephropathology and have a direct impact upon patient prognosis and the selection of therapeutic treatment. Although this study is in the initial phase, the preliminary results are encouraging and the line of work holds a fair degree of promise. The signals detected here could potentially represent future targets to be investigated as proteomic markers for the further stratification of iMN patients once verified on a larger cohort of patients.

3 FUTURE PERSPECTIVES

The potential of MALDI-MSI to detect disease biomarkers directly in situ is undoubted and the study of glomerular diseases using this modern proteomic technology may eventually herald an era where these findings are translated for use within a clinical context, either for diagnostic or prognostic purposes. This would be a result not only of the ability to correlate proteomic findings with morphological alterations, but also as a result of the capability to detect molecular alterations that occur before any visible morphological alterations can be noted by the pathologist[13]. However, one of the biggest limiting factors in this line of work is represented by the number of samples that can be obtained, which is particularly true for fresh-frozen samples. Without sufficiently large sample cohorts, the translation of these findings

into clinical use would be largely unrealistic and needs to be addressed as the body of work presented here begins to progress. The use of FFPE tissue begins to overcome this obstacle somewhat, and, ultimately, FFPE renal biopsies will be used in future studies in order to obtain the largest sample cohort possible and, in turn, the most statistically robust findings.

Furthermore, next generation MALDI-MSI instruments are beginning to push the boundaries related to the spatial resolution of the imaging acquisition. With such instruments, spatial resolutions of 5µm are routinely obtainable, meaning that MALDI-MSI will be able to not only analyse single cells, but also potentially delve deeper and analyse at a sub-cellular level. With regards to the study of glomerular diseases, this would mean that proteomic information from the sub-glomerular compartments could be resolved and would enable the monitoring of protein translocation throughout the glomerulus as a result of a different pathogenic state.

Further work related to the study of iMN is planned, given that the final aim of being able to correctly discriminate all primary from secondary MN patients would represent a large step forward in the field of nephropathology. Primarily, a larger sample cohort with a minimum of fifty patients, that is also better representative of the disease, will be employed. Serological information related to THSD7A positivity will also be present. Furthermore, in this planned study, a cutting-edge MALDI-MS Imaging instrument (Bruker RapifleX MALDI Tissue Typer) will be used to perform high-spatial resolution (<20µm) molecular imaging in order to build upon the findings presented in this thesis and generate more extensive proteomic classifiers of MN and its sub-classes. Additionally, an approach which involves the removal of the MALDI matrix, incorporating the analytes of interest detected in the imaging acquisition, and subsequent analysis using nanoESI-LC-MS/MS will be employed in order to obtain the identities of those proteins that are able to discriminate the different MN sub-classes[14]. These protein clusters will be used to further enhance the comprehension of the pathogenesis of MN and to, ultimately, further stratify those primary MN patients who are currently unclassifiable using traditional IHC.

These proteomic signatures will be integrated in an easy-to-use software that will provide a pixel-by-pixel classification of the renal biopsy. The final output will be a visual representation of the renal biopsy, indicating the glomeruli affected by the presence of MN, along with a final diagnosis This would represent a large step forward in terms of the diagnosis of MN and have a significant impact upon the treatment and prognosis of patients with this common glomerular disease.

REFERENCES

1. Wilkey DW, Merchant ML. Proteomic Methods for Biomarker Discovery in Urine. *Semin. Nephrol.* 2007; **27**:584–596.

2. Thongboonkerd V. Biomarker discovery in glomerular diseases using urinary proteomics. *Proteomics Clin. Appl.* 2008; **2**:1413–1421.

3. Chughtai K, Heeren RMA. Mass spectrometric imaging for biomedical tissue analysis. *Chem Rev*. 2010;110(5):3237-3277.

4. L'Imperio V, Smith A, Chinello C, Pagni F, Magni F. Proteomics and glomerulonephritis: A complementary approach in renal pathology for the identification of chronic kidney disease-related markers. *Proteomics Clin. Appl*. 2015; 371–383.

5. Schanstra JP, Zurbig P, Alkhalaf A, Argiles A, Bakker SJ, et al. Diagnosis and Prediction of CKD Progression by Assessment of Urinary Peptides. *J Am Soc Nephrol* 2015; doi: 10.1681/ASN.2014050423

6. Smeets B, Moeller MJ. Parietal epithelial cells and podocytes in glomerular diseases. *Semin Nephrol*. 2012; **32**(4): 357-367.

7. Moeller MJ, Smeets B. Role of parietal epithelial cells in kidney injury: the case of rapidly progressing glomerulonephritis and focal and segmental glomerulosclerosis. *Nephron Exp Nephrol*. 2014; **126**(2): 97-100.

8. Kretzler M. Role of podocytes in focal sclerosis: defining the point of no return. *J Am Soc Nephrol*. 2005 **16**(10): 2830-2832.

9. Wiggins JE, Goyal M, Sanden SK, Wharram BL, Shedden KA, et al. Podocyte hypertrophy, "adaptation," and "decompensation" associated with glomerular enlargement and glomerulosclerosis in the aging rat: prevention by calorie restriction. *J Am Soc Nephrol*. 2005; **16**(10): 2953-2966.

10. Xu BJ, Shyr Y, Liang X, Ma LJ, Donnert EM, et al. Proteomic patterns and prediction of glomerulosclerosis and its mechanisms. *J Am Soc Nephrol*. 2005; **16**(10): 2967-2975.

11. Beck LH, Bonegio RGB, Lambeau G, et al. M-type phospholipase A2 receptor as target antigen in idiopathic membranous nephropathy. *N Engl J Med*. 2009;**361**(1):11-21. doi:10.1056/NEJMoa0810457.

12. Tomas NM, Beck LH, Meyer-Schwesinger C, et al. Thrombospondin type-1 domain-containing 7A in idiopathic membranous nephropathy. *N Engl J Med*. 2014;**371**(24):2277-2287. doi:10.1056/NEJMoa1409354.

13. Balluff B, Frese CK, Maier SK, Schone C, Kuster B, et al. *De novo* discovery of phenotypic intratumour heterogeneity using imaging mass spectrometry. *J Pathol*. 2015;**235**(1): 3-13.

14. Heijs B, Holst S, Briaire-de Bruijn IH, van Pelt GW, de Ru AH, et al. Multimodal Mass Spectrometry Imaging of N-Glycans and Proteins from the Same Tissue Section. *Anal Chem*. *2016*; **88**(15): 7745-7753.

LIST OF PUBLICATIONS DURING PHD PERIOD

1) Galli M, Pagni F, De Sio G, Smith A, Chinello C, Stella M, L'Imperio V, Manzoni M, Garancini M, Massimini D, Mosele N, Mauri G, Zoppis I, and Magni F. **"Proteomic profiles of thyroid tumors by Mass Spectrometry-Imaging on Tissue Microarrays".** *BBA Proteins and Proteomics*. 2016. doi: 10.1016/j.bbapap.2016.11.020.
2) Smith A, L'Imperio V, Ajello E, Ferrario F, Mosele N, Stella M, Galli M, Chinello C, Pieruzzi F, Spasovski G, Pagni F, and Magni F**. "The putative role of MALDI-MS Imaging in the study of Membranous Glomerulonephritis"**. *BBA Proteins and Proteomics.* 2016. 10.1016/j.bbapap.2016.11.013
3) Chinello C, L'Imperio V, Stella M, Smith A, Bovo G, Grasso A, Raimondo F, Pitto M, Pagni F, and Magni F. **"The proteomic landscape of renal tumors".** *Expert Review of Proteomics*. 2016. Dec;13(12):1103-1120.
4) Galli M, Zoppis I, Smith A, Magni F, Mauri G. **"Machine learning approaches in MALDI-MSI: Clinical Applications".** *Expert Review of Proteomics*. 2016. Jul; 13(7):685-96.
5) Manzoni M, Bono F, Smith A, Cavenaghi G, Garavello W, and Pagni F. **"Thyreoglossal Duct Cyst with Evidence of Solid Cell Nests and Atypical Thyroid Follicles".** *Endocrine Pathology*. 2016. Jun;27(2):175-7.
6) Pagni F, De Sio G, Garancini M, Scardilli M, Chinello C, Smith AJ, Bono F, Leni D, Magni F. **"Proteomics in thyroid cytopathology: relevance of MALDI-Imaging in distinguishing malignant from benign lesions".** *Proteomics.* 2016. 2016. Jun; 16(11-12):1775-84.
7) Smith A, L'Imperio V, De Sio G, Ferrario F, Scalia C, Dell'Antonio G, Pieruzzi F, Pontillo C, Filip S, Markoska K, Granata A, Spasovski G, Jankowski J, Capasso G, Pagni F, and Magni F**. "α-1-antitrypsin detected by MALDI-Imaging in the study of glomerulonephritis: its relevance in chronic kidney disease progression"**. *Proteomics*. 2016. Jun;16(11-12):1759-66.

8) Reed H, Stanton A, Wheat J, Kelley J, Davis L, Rao W, Smith A, Owen D, and Francese S. **"The Reed-Stanton press rig for the generation of reproducible fingermarks: Towards a standardised methodology for fingermark research".** *Science and Justice.* 2016. Jan;56(1):9-17.

9) Pagni F, Galimberti S, Galbiati E, Rebora P, Pietropaolo V, Pieruzzi F, Smith AJ, and Ferrario F. **"Tubulointerstitial lesions in lupus nephritis: international multicentre study in a large cohort of patients with repeat biopsy".** *Nephrology*. 2016. Jan;21(1):35-45.

10) Chinello C, Cazzaniga M, De Sio G, Smith AJ, Grasso A, Rocco B, Signorini S, Grasso M, Bosari S, Zoppis I, Mauri G, and Magni F. **"Tumor size, stage and grade alterations of urinary peptidome in RCC".** *Journal of Translational Medicine*. 2015. Oct;13:332

11) L'Imperio V, Smith A, Chinello C, Pagni F, and Magni F. **"Proteomics and glomerulonephritis: A complimentary approach in renal pathology for the identification of chronic kidney disease-related markers".** *Proteomics Clinical Applications*. 2016. Apr;10(4):371-83.

12) Liu X, Chinello C, Musante L, Cazzaniga M, Tataruch D, Calzaferri G, Smith A, De Sio G, Magni F, Zou H, and Holthofer H. **"Intraluminal proteome and peptidome of human urinary extracellular vesicles".** *Proteomics Clinical Applications*. 2015. Jun;9(5-6):568-73.

13) Pagni F, L'Imperio V, Bono F, Garancini M, Roversi G, De Sio G, Galli M, Smith AJ, Chinello C, and Magni F. **"Proteome analysis in thyroid pathology".** *Expert review of Proteomics*. 2015. Aug;12(4):375-90.

14) De Sio G, Smith AJ, Galli M, Garancini M, Chinello C, Bono F, Pagni F, and Magni F. **"A MALDI-Mass Spectrometry Imaging method applicable to different formalin-fixed paraffin-embedded human tissues".** *Molecular Biosystems*. 2015. Jun;11(6):1507-14.

15) Chinello C, Cazzaniga M, De Sio G, Smith AJ, Gianazza E, Grasso A, Rocco F, Signorini S, Grasso M, Bosari S, Zoppis I, Dakna M, van der Burgt YE, Mauri G, and Magni F. **"Urinary signatures of Renal Cell Carcinoma**

Investigated by Peptidomic Approaches". *PLOS ONE*. 2014. Sep 9;9(9):e106684.

16) Pagni F, Jaconi M, Delitala A, Garancini M, Maternini M, Bono F, Giani A, Smith A; San Gerardo Hospital collaborators group. **"Incidental Papillary Thyroid Carcinoma: Diagnostic findings in a Series of 287 Carcinomas".** *Endocrine Pathology*. 2014. Sep;25(3):288-96.

17) Pagni F, Mainini V, Garancini M, Bono F, Vanzati A, Giardini V, Scardilli M, Goffredo P, Smith AJ, Galli M, De Sio G, and Magni F2. **"Proteomics for the diagnosis of thyroid lesions: preliminary report".** *Cytopathology*. 2014. Oct;26(5):318-24.

Book publications

---

1) Smith A, Galli M, L'Imperio V, Pagni F, and Magni F. **"Mass spectrometry imaging in the study of renal diseases".** Imaging Mass Spectrometry Methods and Protocols. *Methods in Molecular Biology, Springer. In Press.*

2) Smith A, L'Imperio V, Pangi F, and Magni F**. "Tissue MALDI-Imaging".** Integration of *omics* approaches and systems biology for clinical applications. *Wiley. In Press.*

ACKNOWLEDGEMENTS

Finding the correct words to express gratitude is not always the easiest thing to do, but I will try my utmost best...

First, and foremost, my parents. Without a doubt, I would not be the person I am today, nor in the fortunate position I find myself, without your continual support and help. I have been fortunate enough to learn the value of hard work from you, an aspect that has been valuable throughout my academic studies. You have sacrificed many things in your lives in order to support my future and to support my desire to study, and I will be forever grateful for this. There are many other words I could say, but I don't think any of them could do it justice. Simply, thank you. Truly.

The same also goes for my brother. For many years you were my idol, I looked up to every word you said and I learnt many things from you. You definitely taught me what it's like to lose whenever we played a game! Maybe that's why today I always want to win, and don't like to be second best. Once more, I wouldn't be where I am today without your guidance. You taught me how to deal with many aspects in life, and I still come to you in the most important moments. Once more, and it will never be enough, thank you.

Although you are not here Nan Nan, you always believed in me. I was not such an easy child to understand, nor am I an easy adult to understand, but you always managed to. I only wish that you were here with us now. However, I will always take a piece of you with me, and everything I have done, and will do, I do so in order to make you proud.

For all of my friends who have supported me throughout the years, listened to my pointless facts, suffered through me droning on about science, geography, or a plethora of other pointless subjects. Ryan, you have probably had to endure this the most! We've come a long way since Mr.Forder's science classes! The same goes for Dom, you have supported me throughout this period and it has been humbling to

have your support throughout university and this PhD, both in professional and personal aspects. You will always have my utmost gratitude for this, and I hope that I can offer the same for you if you decide to embark upon a PhD.

Now moving on to my time here in Italy. This was a challenge both professionally, and personally. I was fortunate enough to walk into a laboratory and work with such kind, warm-hearted individuals. Gabriele, Manuel, having both of you in the laboratory was more than I could have wished for. You have been both colleagues, as well as friends. You have been there to support me, and also give me a kick up the backside when I have needed it! The “burn her faces”, the “threw it on the grounds”, the “oh, ma guys”, are all things that will remain permanently lodged in my mind. Sincerely, working with both of you was the best working experience of my life, who wouldn’t want to wake up in a morning and go to work with their friends? I will always be grateful. Martina, although you came in to the laboratory, in let’s say “contentious circumstances”, I have been so happy and grateful that you did. Furthermore, I have to wholeheartedly admit that my initial judgement was wrong. You have been there to challenge me when needed, and that has made me better both personally and professionally. Thank you, and good luck with your project now that you finally have your samples.

“Fragalone”. I know you will be as humble as ever, and feel that you have done nothing. However, it has been far from the case. Since moving to Italy, you became my best friend, my confidant, and pretty much my right arm. I view my PhD as an experience, rather than only research activity, and you, and you alone, have been the best and most enriching part of this experience. There are many things that I have already told you, but know that your support has meant the world to me. Through you, through everything, even during some arguments, you have taught me to see life from a different perspective, to grow, to mature, and to, ultimately, become a better person. There can be no greater gift to a person. I will always love you for this.

Of course, there are many other people to acknowledge. The rest of my friends, my previous academic supervisors, those who have come into my life and then left. Each and every one of you has given me something that I use today, both in my work and in my personal life. Thank you to you all.

"I awoke this morning with devout thanksgiving for my friends, the old and the new"